ROMA TRE
UNIVERSITÀ DEGLI STUDI

Scuola Dottorale di Ingegneria - Sezione IMI

XXIII Ciclo

An Innovative Decomposition of the Velocity Field with the Corresponding Generalized Bernoulli Theorem for Viscous Flows

Cecilia Leotardi

A.A. 2010-2011

Docente guida: Prof. Luigi Morino

Coordinatore: Prof. Edoardo Bemporad

To my dearly beloved Davide & Sofia

Acknowlegments

I want first to thank Prof. Luigi Morino, my advisor. In the years of our knowledge you helped me to see science and life, in their full depth. You enlightened me through your enthusiasm and your brilliant intuitions.

A special mention to Prof. Umberto Iemma, I made my first steps in the world of research with you, and I will never forget it.

I also thank Giovanni Bernardini, your support turned out to be essential.

Thanks to Jacopo Serafini, Matteo Diez and Lorenzo Burghignoli, my room mates, for the insightful discussions and for the help provided.

Sharing my doctoral studies and what is more, life, has been an absolute dream. Thank you, my dear Ale.

Contents

Chapter 1

Introduction

The present dissertation addresses methods and consequent implementations of a unified formulation for unsteady aerodynamics and aeroacoustics. Specifically, the methodology is based upon the use of boundary integral representations for the primitive variables, including a decomposition of the velocity field, which provides an innovative tool for the integrated analysis of aerodynamics and aeroacoustics, from both the conceptual and the computational points of view.

The primary objective of the analysis presented in the following is to provide a validation of a method in proposed by Morino, in Ref. [1], for the unified analysis of aerodynamics and aeroacoustics, and by him referred to as the *natural velocity decomposition* (see Section 2.2.1 and following). Specifically, within the aerodynamics context, we obtain a validation for the limited case of two-dimensional incompressible Navier-Stokes equations, whereas, within the aeroacoustics context, we address an application of three-dimensional compressible Navier-Stokes formulation for the evaluation of the power spectral density of the field pressure, as a first step towards approaching Navier-Stokes flow fields.

1.1 State of the art

In this section we outline a review of the state of art on boundary integral formulations for aerodynamics, along with application to aeroacoustics. It is certainly not exhaustive, as it pertains the studies investigated in this work.

Initially boundary integral methods for steady and unsteady aerodynamics aimed to model quasi-potential fields and the problem was formulated in terms of the velocity potential $\phi(\mathbf{x})$, such

that $\nabla\phi(\mathbf{x}) = \mathbf{v}(\mathbf{x})$.[1] The boundary integral formulation for quasi-potential unsteady compressible flows, introduced by Morino [2], is relevant here because of its close relationship with the studies presented in this work. This formulation was implemented and assessed (for reviews, see, for instance, Refs. [3], [4], [5] and [6]). Its extension to aeroacoustics provides a unified formulation for aerodynamics and aeroacoustics (see Refs. [4] and [6]).

More relevant to the present work, the formulation was later extended to rotational fields, Ref. [9], through the introduction of a decomposition of the field velocity, $\mathbf{v}(\mathbf{x}, t)$, into two terms, an irrotational one, $\mathbf{v}_{\mathrm{P}}(\mathbf{x}, t) = \nabla\varphi(\mathbf{x}, t)$, and a rotational one, $\mathbf{w}(\mathbf{x}, t)$:

$$\mathbf{v}(\mathbf{x}, t) = \mathbf{v}_{\mathrm{P}}(\mathbf{x}, t) + \mathbf{w}(\mathbf{x}, t) \tag{1.1}$$

where $\mathbf{w}$ is any particular solution of the equation

$$\nabla \times \mathbf{w} = \boldsymbol{\zeta} \tag{1.2}$$

where $\boldsymbol{\zeta} = \nabla \times \mathbf{v}$ denotes the vorticity.

The standard approach used to exploit such a problem is to obtain the vorticity $\boldsymbol{\zeta}$ from its own evolution equation and then to obtain the rotational portion of the velocity field such as to satisfy Eq. 1.2. In other words, with this approach the rotational contribution $\mathbf{w}$, and hence the velocity $\mathbf{v}$, is determined once $\boldsymbol{\zeta}$ (non-primitive variable) is obtained. Thus, all the methodologies based upon this approach may be referred to, collectively, as *non–primitive–variable potential/vorticity decompositions*, or simply as *potential/vorticity decompositions*. Each decomposition differs by how $\mathbf{w}$ is obtained from $\boldsymbol{\zeta}$.[2] It should be pointed out that this class of decompositions is, actually, quite wide. In particular, it includes the well-known *Helmholtz decomposition* in which the vortical velocity contribution, $\mathbf{w}$, is expressed as the curl of vector potential field $\boldsymbol{\psi}$ (see Serrin, Ref. [7]). Using this approach, as noted by Morino in Ref. [8], a problem arises while addressing unsteady viscous compressible flow fields. Indeed, both the potential vector and the scalar potential, are governed by Poisson equation, whereas compressible flows have a wave equation behavior. Therefore, the sound propagation phenomenon is hidden by the use of this decomposition.

[1] We recall that a flow around a boundary surface $\mathcal{S}$ is called *quasi-potential*, if it is irrotational everywhere, except for the points that come in contact with $\mathcal{S}$. These points form a surface defined inviscid wake, $\mathcal{S}_{\mathrm{W}}$, which is a surface of tangential discontinuity for the velocity. Note that the d'Alembert paradox does not apply to quasi-potential flows.

[2] Note that, whereas for a given $\mathbf{w}(\mathbf{x}, t)$ the corresponding vorticity field $\boldsymbol{\zeta}(\mathbf{x}, t)$ is unique, for a given $\boldsymbol{\zeta}(\mathbf{x}, t)$ the reconstructed $\mathbf{w}(\mathbf{x}, t)$ is not unique. Indeed, two $\mathbf{w}(\mathbf{x}, t)$ reconstructed by different approaches differ by a potential field.

1.2 Why using such an approach?

In order to underline the features provided with the approach followed, we briefly describe the methodology applied. The novel decomposition, formally akin to the ones introduced in Refs. [9], [10], [11] and [12], reads again as $\mathbf{v} = \nabla\varphi + \mathbf{w}$ (as in Eq. 1.1), but its prominent aspect pertains the fact that now the rotational portion of the velocity field, $\mathbf{w}$, is defined through its own differential equation.[3] In other words, contrary the ones in Refs. [9], [10], [11] and [12], the methodology does not require the solution of the evolution equation for the vorticity. In this sense, this approach may be considered as a *primitive-variable decomposition.*

As mentioned above, this formulation was introduced in Ref. [1] and has been obtained as a consequence of the straight-forward application of the standard boundary integral formulation to the system of equations that govern the phenomenon, in particular the continuity and the Navier-Stokes equations for the case of incompressible Navier-Stokes flows (see Eqs.2.4 and 2.5). Because of this type of decomposition stems naturally from the boundary integral equation approach, in Ref. [1] it is referred to as the *natural velocity decomposition*. This approach is complicated and unwarranted here. For, at the end of the day, the only relevant aspect is the choice for the equation governing the rotational portion of the velocity field. Thus, in this thesis, we introduced the equation for $\mathbf{w}$ simply as a convenient choice, and refer to Ref. [1] to see that it is a direct consequence of the straightforward application to the Navier-Stokes equations of the standard boundary integral equation methodology for systems of linear partial differential equations.

For incompressible viscous fields[4] the governing equation for $\mathbf{w}$ resulting from the primitive-variable boundary integral formulation is $\mathrm{D}\mathbf{w}/\mathrm{D}t + \left(\mathbf{w}\cdot\nabla\right)\mathbf{v}_{\mathrm{P}} = \nu\,\nabla^2\mathbf{w}$, where $\mathrm{D}/\mathrm{D}t := \partial/\partial t + \mathbf{v}\cdot\nabla$ denotes the *material time derivative*, whereas ν is dynamic viscosity coefficient.

As a result we obtain some significant contribution to the overall scope of the analysis performed in this work. Since we describe events modelled by homogeneous initial conditions (for instance, start from rest), we may claim that $\mathbf{w}$, and consequently the vorticity, are bounded in a thin region and are negligible outside the vortical region.[5] Moreover an extension of the Bernoulli theorem for incompressible viscous flows is achieved combining Navier-Stokes equations with the velocity field decomposition, yielding the so-called *generalized Bernoulli theorem for viscous in-*

[3] Details of the formulations used in Refs. [9], [10], [11] and [12] are given in Section 2.7.

[4] Let us consider external problem as, in first instance, the attention in this work pertains aerodynamic problems.

[5] This is true also for the decomposition introduced in Refs. [9], [10], [11] and [12].

compressible fields $\dot{\varphi} + p/\rho + \frac{1}{2}\, v_{\mathrm{P}}^2 - \nu\nabla^2\varphi = const.$

Besides we may observe that both in the $\mathbf{w}$ evolution equation and in the equation for the velocity potential, φ, pressure does not appear. Therefore this states that velocity field evaluation is independent from the relative pressure field. Instead, we may intend pressure field arising from velocity field and it may be evaluated through the generalized Bernoulli theorem as a post-process.

In the end, with regards to computational resources and high costs in terms computational time the numerical solution of the Navier-Stokes equations is clearly simplified. For, in the process of computing the velocity $\mathbf{v}$, we have that

- the evaluation of the pressure is not required,
- the computational domain for the equation for $\mathbf{w}$ is limited to the vortical region, if the boundary integral equation method is used for the solution of the equation for φ.

Therefore, the novel formulation has all the advantages of non-primitive-variable approaches,[6] but it does not present any of the disadvantages, such as imposing the solenoidality of $\boldsymbol{\zeta}$, as well as reconstructing $\mathbf{w}$ from $\boldsymbol{\zeta}$ without introducing discontinuities, and the fact that the boundary condition needed is for $\boldsymbol{\zeta}$, whereas that available is for $\mathbf{v}$.

It should be pointed out that very similar results regarding the natural velocity decomposition are obtained also for compressible (inviscid and viscous) fields. Specifically, a generalized Bernoulli theorem is also obtained for compressible Navier-Stokes fields, Eq. 3.43.

1.3 Structure of the work

Chapter 2 addresses the problem of incompressible unsteady Navier-Stokes flow fields. We present the theoretical formulation, along with its numerical discretization and its validation. Chapter 3 presents a limited application of the extension to compressible flows of the aeroacoustics formulation of Ref. [1]; specifically, we show how to evaluate the power spectral density of the pressure at any given point in the field in terms of the power spectral density of the pressure on the boundary, using the same *natural velocity decomposition*. Theoretical, numerical formulation and numerical results are addressed. In chapter 4 we outline some concluding remarks and suggestions for future improvements.

[6] Indeed, the vorticity evolution equation does not contain the pressure and is limited to the vortical region.

In addition, we have two appendices. In order to motivate these, we note that the present work, in particular, the material addressed in Chapters 2 and 3, may be seen in framework a of optimal design, specifically within the context of an algorithm of multidisciplinary optimization for conceptual design of civil aircraft, which is the ultimate objective of the work presented here. In order to illustrate this connection, Appendix B describes the MDO algorithm used, along with some of the results obtained, in particular in the module pertaining aeroacoustics (which is the area where the MDO group at Roma Tre University has recently concentrated the effort). Of particular interest is the issue of multi-level optimization, whereby models of different level of sophistication and complexity are combined, so as to achieve the accuracy of the more sophisticated models, without a major increase of the required computational time, with respect to the simpler model formulation. Thus, the formulations introduced in Chapter 2 and 3, while of interest on their own merit even as stand-alone analysis, have been developed for a possible inclusion - as high level models - in the MDO analysis, provided of course that further analysis confirms the validity of the methodology for more general cases (and its robustness). Each task handled may be seen as a module, with increasing accuracy, while modelling aerodynamics and aeroacoustics. In addition, in Appendix A, we present an analysis on steady transonic flows, once again through boundary integral representation with a novel approach while evaluating nonlinear terms. This activity is to be seen as a necessary preliminary activity, before the *natural velocity decomposition* may be utilized to take into account the vorticity generated by the shock.

Chapter 2

Incompressible Navier-Stokes Equations

In this chapter we present the theoretical formulation used to address incompressible unsteady Navier-Stokes flow fields. Moreover we describe the its discretization along with the validations performed. In the end we outline some interesting remarks.

2.1 Incompressible Navier–Stokes fields

Consider an incompressible unsteady Navier-Stokes flow field around a solid object which is in arbitrary motion with respect to a frame of reference rigidly connected to the undisturbed air, in the following referred to as the airframe.

The flow field region is denoted by $\mathcal{V}$ whereas its boundary is $\mathcal{S} = \partial\mathcal{V}$. These kinds of fields are governed by

- continuity equation;
- Navier-Stokes equation.

Assuming that the forces per unit volume are negligible, these equations read

$$\nabla \cdot \mathbf{v} = 0 \tag{2.1}$$

$$\frac{\partial \mathbf{v}}{\partial t} + \mathbf{v} \cdot \nabla \mathbf{v} + \nabla \wp = \nu \nabla^2 \mathbf{v} \tag{2.2}$$

where, for convenience, we have introduced

$$\wp = (p - p_\infty)/\rho \tag{2.3}$$

whereas ν indicates the the dynamic viscosity coefficient, here assumed to be a constant.

Performing a separation between nonlinear and linear terms one obtains

$$\nabla \cdot \mathbf{v} = 0 \tag{2.4}$$

$$\frac{\partial \mathbf{v}}{\partial t} - \nu \nabla^2 \mathbf{v} + \nabla \wp = \mathbf{f} \tag{2.5}$$

where

$$\mathbf{f} = -\mathbf{v} \cdot \nabla \mathbf{v} \tag{2.6}$$

To complete the problem described by the above equations, we introduce the appropriate conditions, which are:

- The classical no–slip boundary condition on the boundary surface $\mathcal{S}$

$$\mathbf{v}(\mathbf{x}, t) = \mathbf{v}_{\text{B}}(\mathbf{x}, t) \qquad (\mathbf{x} \in \mathcal{S}) \tag{2.7}$$

  with $\mathbf{v}_{\text{B}}(\mathbf{x}, t)$ prescribed.

- The boundary conditions at infinity

$$\mathbf{v}(\mathbf{x}, t) = \mathbf{0} \quad \text{and} \quad \wp(\mathbf{x}, t) = 0 \qquad (\|\mathbf{x}\| \to \infty) \tag{2.8}$$

- The initial conditions that, for simplicity, we assume to be homogenous

$$\mathbf{v}(\mathbf{x}, 0) = \mathbf{0} \qquad (\mathbf{x} \in \mathcal{V}) \tag{2.9}$$

2.2 The formulation for the velocity

The approach used in this dissertation is outlined here. As reported in the previous section the system of equations of interest is given by Eqs. 2.4 and 2.5.

Considering $\mathbf{f}$ as a prescribed term, akin to the acoustic analogy introduced by Lighthill [14], Eqs. 2.4 and 2.5 define a system of linear, non-homogenous, partial differential equations, with constant coefficient. This fact is exploited here.

2.2.1 Velocity field decomposition

The velocity field is given, according to what mentioned in the introduction, as the sum of two different terms:

- an irrotational one;
- its complement, the rotational one.

Its expression reads again as (Eq. 1.1)

$$\mathbf{v}(\mathbf{x},t) = \nabla\varphi(\mathbf{x},t) + \mathbf{w}(\mathbf{x},t) = \mathbf{v}_{\text{P}}(\mathbf{x},t) + \mathbf{w}(\mathbf{x},t) \qquad (\mathbf{x} \in \mathcal{V}) \tag{2.10}$$

where $\mathbf{v}_{\text{P}} = \nabla\varphi(\mathbf{x},t)$ is the potential velocity component. Moreover, Eq. 2.10 implies $\nabla \times \mathbf{w} = \boldsymbol{\zeta} := \nabla \times \mathbf{v}$. Therefore $\mathbf{w}(\mathbf{x},t)$ is in direct relationship with the vorticity $\boldsymbol{\zeta} := \nabla \times \mathbf{v}$, and hence will be referred to as the *rotational contribution* to the velocity field.

As mentioned in Chapter 1, in this work the novel and exact velocity field decomposition of Morino, Ref. [1], is analyzed, and the corresponding numerical formulation is presented. Such a decomposition has this convenient feature, that $\mathbf{w} = \mathbf{0}$ in the irrotational region, defined here as the region where $\boldsymbol{\zeta}$ is negligible.

Substituting the expression of the velocity decomposition, Eq. 2.10, in the Navier-Stokes equation, Eq. 2.5, and using

$$-\mathbf{f} = \mathbf{v}\cdot\nabla\mathbf{v} = \mathbf{v}\cdot\nabla\mathbf{w} + \mathbf{w}\cdot\nabla\mathbf{v}_{\text{P}} + \nabla\frac{\|\mathbf{v}_{\text{P}}\|^2}{2} \tag{2.11}$$

one obtains

$$\nabla\left(\dot{\varphi} + \frac{\|\mathbf{v}_{\text{P}}\|^2}{2} + \wp - \nu\nabla^2\varphi\right) + \frac{\partial\mathbf{w}}{\partial t} + \mathbf{v}\cdot\nabla\mathbf{w} + \mathbf{w}\cdot\nabla\mathbf{v}_{\text{P}} - \nu\nabla^2\mathbf{w} = \mathbf{0} \tag{2.12}$$

2.2.2 Equation for $\mathbf{w}$

It is apparent that it may be highly convenient to chose $\mathbf{w}$ so that both two terms in parenthesis vanish. This choice yields (the first term in Eq.2.12 is addressed in Subsection 2.3)

$$\frac{\partial\mathbf{w}}{\partial t} + \mathbf{v}\cdot\nabla\mathbf{w} + \mathbf{w}\cdot\nabla\mathbf{v}_{\text{P}} - \nu\nabla^2\mathbf{w} = \mathbf{0} \tag{2.13}$$

which represents the rotational evolution equation (the solution of Eq.2.13 must be completed by imposing the appropriate boundary and initial conditions, which are discussed below).

As already pointed out in Chapter 1, in Ref. [1] Eq. 2.13 is obtained as a direct consequence of the straightforward application to the Navier-Stokes equations of the standard boundary integral equation methodology for systems of linear partial differential equations. Also, the rotational contribution of the velocity field $\mathbf{w}$ is obtained directly from its own evolution equation, thereby rendering unnecessary the evaluation of $\boldsymbol{\zeta}$, as widely used in non-primitive-variable decompositions, such as the Helmholtz decomposition. Thus, the decomposition should be considered as a *primitive-variable decomposition*.

Boundary and initial conditions

The solution of Eq. 2.13 is provided once the suitable boundary and initial conditions are imposed. The conditions used in this work are

- The boundary condition on the boundary surface $\mathcal{S}$
  - the normal component of the rotational portion of velocity vanishes

$$\mathbf{w} \cdot \mathbf{n} = 0 \qquad (\mathbf{x} \in \mathcal{S}) \tag{2.14}$$

  - the tangent component is consequently determined by projection of Eq. 2.7 onto the tangent direction

$$\mathbf{v} \cdot \mathbf{t} = \mathbf{v}_{\text{P}} \cdot \mathbf{t} + \mathbf{w} \cdot \mathbf{t} = \mathbf{v}_{\text{B}} \cdot \mathbf{t} \tag{2.15}$$

    Therefore

$$\mathbf{w} \cdot \mathbf{t} = \mathbf{v}_{\text{B}} \cdot \mathbf{t} - \mathbf{v}_{\text{P}} \cdot \mathbf{t} \tag{2.16}$$

- The boundary conditions at infinity[1]

$$\mathbf{w}(\mathbf{x}, t) = \mathbf{0} \qquad (\|\mathbf{x}\| \to \infty) \tag{2.17}$$

- The initial condition, here assumed to be homogenous (see Eq. 2.9)

$$\mathbf{w}(\mathbf{x}, 0) = \mathbf{0} \tag{2.18}$$

[1]Note that $\mathbf{w}(\mathbf{x}, t)$ tends to zero exponentially at infinity. This allows to limit the computational domain to a relatively small region, essentially equal to the irrotational region (here defined as the region where the vorticity is negligible).

2.2.3 Equation for φ

Combining continuity equation, Eq. 2.4 with the expression for the velocity decomposition, Eq. 2.10, one obtains

$$\nabla^2\varphi = \sigma := -\nabla \cdot \mathbf{w} \tag{2.19}$$

whose solution is determined by imposing the following boundary conditions

- Velocity normal component on the body surface $\mathbf{x} \in \mathcal{S}$ (see Eq. 2.7)

$$\mathbf{v} \cdot \mathbf{n} = \nabla\varphi \cdot \mathbf{n} + \mathbf{w} \cdot \mathbf{n} = \mathbf{v}_{\text{B}} \cdot \mathbf{n} \tag{2.20}$$

  which using Eq. 2.14 implies, in terms of potential φ,

$$\frac{\partial\varphi}{\partial n} = \mathbf{v}_{\text{B}} \cdot \mathbf{n} := \chi \qquad (\mathbf{x} \in \mathcal{S}) \tag{2.21}$$

- Potential φ evanescent at infinity, which in the airframe reads

$$\varphi \to 0 \qquad (\|\mathbf{x}\| \to \infty) \tag{2.22}$$

Equation 2.19, along with its boundary conditions may be conveniently solved by boundary integral method. Boundary integral methods are based on the fundamental solution $G(\mathbf{x}, \mathbf{y})$, which is - for Laplacian operator - defined by

$$\nabla^2 G = \delta(\mathbf{x} - \mathbf{y}) \qquad (\mathbf{x} \in \mathcal{R}^3) \tag{2.23}$$

whose solution, in three dimensions, is $G(\mathbf{x}, \mathbf{y}) = -1/4\pi\|\mathbf{x} - \mathbf{y}\|$. Multiplying Eq. 2.19 by G and Eq. 2.23 by φ, subtracting and integrating over $\mathcal{V}$, and imposing the boundary condition, Eq. 2.21, and that at infinity, Eq. 2.22, one obtains the boundary integral formulation - here adopted - which reads

$$\varphi(\mathbf{x}) = \oint_{\mathcal{S}} \left(\chi G - \varphi \frac{\partial G}{\partial n} \right) \mathrm{d}\mathcal{S}(\mathbf{y}) + \int_{\mathcal{V}_{\mathbf{w}}} G\sigma \mathrm{d}\mathcal{V}(\mathbf{y}) \qquad (\mathbf{x} \in \mathcal{V}) \tag{2.24}$$

The relationship in Eq. 2.24 is a boundary integral representation for φ, in the field, in terms of φ and $\partial\varphi/\partial n$ on $\mathcal{S}$ and of σ in $\mathcal{V}_{\mathbf{w}}$, with $\mathcal{V}_{\mathbf{w}}$ denoting the region where $\mathbf{w} \neq \mathbf{0}$. The evaluation of the unknown φ in the entire domain requires the knowledge of φ and its normal derivative $\partial\varphi/\partial n = \chi$ on the body surface and of σ in rotational area $\mathcal{V}_{\mathbf{w}}$.

Note that $\chi = \partial\varphi/\partial n$ on the body surface is known from the boundary condition, Eq. 2.21. In addition, σ in rotational area $\mathcal{V}_{\mathbf{w}}$ may be obtained once the equation for $\mathbf{w}$ has been solved. However, we do not have φ on the body surface. In order to solve this problem, we consider the limit of Eq. 2.24 as $\mathbf{x} \in \mathcal{V}$ tends to $\mathbf{x} \in \mathcal{S}$. This yields (see Ref. [4])

$$\frac{1}{2}\varphi(\mathbf{x}) = \oint_{\mathcal{S}} \left(\chi G - \varphi \frac{\partial G}{\partial n} \right) \mathrm{d}\mathcal{S}(\mathbf{y}) + \int_{\mathcal{V}_{\mathbf{w}}} G\sigma \mathrm{d}\mathcal{V}(\mathbf{y}) \qquad (\mathbf{x} \in \mathcal{S}) \tag{2.25}$$

The relationship in Eq. 2.24 represents a compatibility relationship between: (1) the values of φ, calculated on $\mathcal{S}$ the body surface, (2) the values of $\partial\varphi/\partial n$ also on $\mathcal{S}$, and (3) the values of σ in $\mathcal{V}$. However, $\partial\varphi/\partial n$ on $\mathcal{S}$ is known from the boundary condition, Eq. 2.21, whereas σ in $\mathcal{V}$ may be calculated once $\mathbf{w}$ has been evaluated; thus, Eq. 2.24 is a *boundary integral equation* relating φ on $\mathcal{S}$ to $\partial\varphi/\partial n$ on $\mathcal{S}$ and σ in $\mathcal{V}$.

It should be underlined that, once Eq. 2.24 has been solved (namely, once the potential φ on $\mathcal{S}$ has been obtained), the corresponding potential velocity is evaluated by taking the gradient of Eq. 2.24, to obtain

$$\mathbf{v}_{\mathrm{P}}(\mathbf{x}) = \oint_{\mathcal{S}} \left(\chi \nabla_{\mathbf{x}} G - \varphi \nabla_{\mathbf{x}} \frac{\partial G}{\partial n} \right) \mathrm{d}\mathcal{S}(\mathbf{y}) + \int_{\mathcal{V}} \nabla_{\mathbf{x}} G\sigma \mathrm{d}\mathcal{V}(\mathbf{y}) \qquad (\mathbf{x} \in \mathcal{V}) \tag{2.26}$$

It should be noted again that the calculation of φ, by the representation in Eq. 2.24, implies the knowledge of the rotational contribution of the rotational portion of velocity, $\mathbf{w}$, whose expression is derived as using Eq. 2.13.

2.3 Generalized Bernoulli theorem

Combining Eqs. 2.12 and 2.13 yields

$$\nabla \left(\dot{\varphi} + \frac{\|\mathbf{v}_{\mathrm{P}}\|^2}{2} + \wp - \nu\nabla^2\varphi \right) = 0 \tag{2.27}$$

This implies that the term in parenthesis (first integral of Eq. 2.27) is constant. This constant is obtained from the conditions at infinity, Eqs. 2.22 and 2.8, to yield

$$\dot{\varphi} + \frac{\|\mathbf{v}_{\mathrm{P}}\|^2}{2} + \wp - \nu\nabla^2\varphi = 0 \tag{2.28}$$

which represents a generalization of the Bernoulli theorem to incompressible viscous flows.

It should be noted that this expression is similar to that for the incompressible potential flows - recall that the Bernoulli theorem for incompressible potential flow field reads

$$\dot{\varphi} + \frac{\|\mathbf{v}\|^2}{2} + \frac{p}{\rho} = \frac{p_\infty}{\rho}. \tag{2.29}$$

The difference is due to the term $-\nu\nabla^2\varphi$, whose evaluation does not represent any problem, since $\nabla^2\varphi = \sigma$.

2.4 Numerical Formulation

The theoretical formulation presented applies both to three-dimensional and two-dimensional problems. Since numerical validations have been performed only on two dimensional cases, the corresponding numerical formulation described in the following refers only to two-dimensional flow fields.

As pointed out in the preceding chapter, Eqs. 2.24 and 2.25 give, respectively, the boundary integral representation and the boundary integral equation for φ. They may be combined

$$E(\mathbf{x})\varphi(\mathbf{x}) = \oint_{\mathcal{C}} \left(\chi G - \varphi \frac{\partial G}{\partial n} \right) \mathrm{d}s(\mathbf{y}) + \int_{\mathcal{A}_\mathbf{w}} G\,\sigma\,\mathrm{d}\mathcal{A}(\mathbf{y}) \qquad (\mathbf{x} \in \mathcal{A}_\mathbf{w}) \tag{2.30}$$

where

$$E(\mathbf{x}) = \begin{cases} 1 & \text{if } \mathbf{x} \in \mathcal{A}_\mathbf{w} \\ \dfrac{1}{2} & \text{if } \mathbf{x} \in \mathcal{C} \end{cases} \tag{2.31}$$

whereas $\mathcal{C}$ is the body contour and $\mathcal{A}_w$ represent the portion of the flow field in which the rotational component of the velocity is not negligible.[2] It is worth noting that in two dimensions the expression of the fundamental solution is

$$G(\mathbf{x}, \mathbf{y}) = \frac{1}{2\pi} \ln \|\mathbf{x} - \mathbf{y}\| \tag{2.32}$$

Akin to the three dimensional case, the representation in Eq. 2.30 allows the evaluation of φ in the field whenever φ and χ on $\mathcal{C}$ as well as σ in $\mathcal{A}_\mathbf{w}$ are known. As pointed out above, χ is prescribed from the boundary condition, Eq. 2.21, whereas σ may be obtained from $\mathbf{w}$. Thus, we need to evaluate φ on $\mathcal{C}$. In the limit, if $\mathbf{x}$ tends to $\mathcal{C}$, Eq. 2.30 yields to a compatibility relationship

[2] Note that $\mathcal{C}$ is the two-dimensional equivalent of $\mathcal{S}$, and $\mathcal{A}_\mathbf{w}$ is the two dimension equivalent of $\mathcal{V}_\mathbf{w}$.

between φ and χ on $\mathcal{C}$ as well as σ in $\mathcal{A}_{\mathbf{w}}$. This corresponds to an integral equation in which the only unknown is φ on $\mathcal{C}$.[3]

The velocity field may then be obtained by taking the gradient of Eq. 2.30 to yield

$$\nabla_{\mathbf{x}}\varphi(\mathbf{x}) = \oint_{\mathcal{C}_B} \left(\chi \nabla_{\mathbf{x}} G - \varphi \nabla_{\mathbf{x}} \frac{\partial G}{\partial n} \right) \mathrm{d}s(\mathbf{y}) + \int_{\mathcal{A}_{\mathbf{w}}} \sigma \, \nabla_{\mathbf{x}} G \, \mathrm{d}\mathcal{A}(\mathbf{y}) \qquad (\mathbf{x} \in \mathcal{A}) \tag{2.33}$$

2.4.1 Velocity potential discretization

The numerical approach implemented and here outlined is the *boundary element method*, which corresponds to the discretized form of boundary integral equation method.

Equation 2.30 is approximated as follows

$$\varphi(\mathbf{x}) = \sum_{j=1}^{N_B} \varphi_j p_j(\mathbf{x}) \tag{2.34}$$

$$\chi(\mathbf{x}) = \sum_{j=1}^{N_B} \chi_j p_j(\mathbf{x}) \tag{2.35}$$

where $p_j(\mathbf{x})$ represent the suitable global interpolation functions over $\mathcal{C}$, whereas $\varphi_j = \varphi(\mathbf{x}_j)$ and $\chi_j = \chi(\mathbf{x}_j)$, with $\mathbf{x}_j$ being the interpolation nodes. In addition,

$$\sigma(\mathbf{x}) = \sum_{j=1}^{N_A} \sigma_j q_j(\mathbf{x}) \tag{2.36}$$

where $q_j(\mathbf{x})$ represent again suitable global interpolation functions over $\mathcal{A}_{\mathbf{w}}$.[4]

This yields the discretized form of the boundary integral representation for any point in the field

$$\varphi(\mathbf{x}) = \sum_{j=1}^{N_B} B_j(\mathbf{x}) \chi_j + \sum_{j=1}^{N_B} C_j(\mathbf{x}) \varphi_j + \sum_{j=1}^{N_A} H_j(\mathbf{x}) \sigma_j \tag{2.37}$$

where

$$B_j(\mathbf{x}) = \int_{\mathcal{C}} p_j(\mathbf{y}) \, G(\mathbf{x}, \mathbf{y}) \, \mathrm{d}s(\mathbf{y}) \tag{2.38}$$

$$C_j(\mathbf{x}) = \int_{\mathcal{C}} p_j(\mathbf{y}) \, \frac{\partial G(\mathbf{x}, \mathbf{y})}{\partial n} \, \mathrm{d}s(\mathbf{y}) \tag{2.39}$$

$$H_j(\mathbf{x}) = \int_{\mathcal{A}} q_j(\mathbf{y}) \, G(\mathbf{x}, \mathbf{y}) \, \mathrm{d}\mathcal{A}(\mathbf{y}) \tag{2.40}$$

[3] The methodology is exactly the same as that presented for the three-dimensional case.

[4] The same interpolation functions are used for the description of the geometry (isoparametric scheme). The local interpolation functions for $p_j(\mathbf{x})$ are given as a combination of Hermite polynomials (see the subsubsection on interpolation functions). The local interpolation functions for $q_j(\mathbf{x})$ are bi-linear.

The boundary integral equation discretization should be completed, so as to have as many equation as unknowns. The procedure used is the so-called the collocation method in which Eq.2.37 is satisfied at N_B prescribed points, known as collocation points. In this work these coincide with the nodes of the elements under consideration, so that $E(\mathbf{x}) = 1/2$. The corresponding discretized form of the boundary integral equation reads

$$\frac{1}{2}\varphi_k = \sum_{j=1}^{N_B} B_{kj}\chi_j + \sum_{j=1}^{N_B} C_{kj}\varphi_j + \sum_{j=1}^{N_A} H_{kj}\sigma_j \tag{2.41}$$

where $B_{kj} = B_j(\mathbf{x}_k)$, $C_{kj} = C_j(\mathbf{x}_k)$ and $H_{kj} = H_j(\mathbf{x}_k)$.

The above expression represents a system of linear algebraic equations in which the unknowns φ_j may be easily calculated. Once φ is evaluated on the body contour its value in the flow field can be obtained, directly, using Eq. 2.37.

It is worth repeating that the evaluation of the potential φ is possible only after the rotational portion of the velocity $\mathbf{w}$ and hence its divergence σ have been calculated.

On the interpolation functions

In Eqs. 2.34, 2.35 and 2.36 the shape functions $p_j(\mathbf{x})$ and $q_j(\mathbf{x})$ are still unspecified. Here, we present the choice for these functions. Let us begin with $q_j(\mathbf{x})$. For these, as mentioned above, a locally bi-linear interpolation is used.

Next, consider the $p_j(\mathbf{x})$. For these, we choose interpolation functions that are locally cubic. The main reason for this is to remove singularities that would appear in the discretized representation for $\mathbf{v}$, if lower orders were to be considered, thereby making it impossible to use collocation points that coincide with nodes of the elements, at least as far as the evaluation of $\mathbf{v}_{\mathrm{P}}(\mathbf{x})$ is concerned.[5] Specifically, we want the $p_j(\mathbf{x})$ to be continuous with their derivatives. The easiest way to obtain this is by using, locally, the third-order Hermite interpolation functions. However, this introduces new unknowns - the derivative of φ and χ - at the nodes. These are eliminated by expressing the derivatives in term of their finite-difference approximations differences.[6]

Let us go into details. The expression for φ is obtained using the Hermite (third-order) inter-

[5]Discontinuities in the intensity of the doublet integral yield a vortex singularity, whereas discontinuities in the derivative of the intensity of the doublet integrals, or in the intensity of the source integrals yield a so-called jet singularity.

[6]We use centered differences, except at the trailing-edge, where forward/backward differences are used.

polation

$$\varphi(\xi) = M_-(\xi)\varphi^+ + M_+(\xi)\varphi^- + N_-(\xi)\varphi_\xi^+ + N_+(\xi)\varphi_\xi^- \tag{2.42}$$

where φ^+, φ^-, φ_ξ^+ and φ_ξ^- represent the value of the potential perturbation and of its derivative in the vertices of the element.

The interpolating functions are the Hermite polynomials, which assuming $\xi \in [-1 : 1]$, are given by the following expressions

$$M_-(\xi) = \frac{1}{4}(2 - 3\xi + \xi^3) \tag{2.43}$$

$$M_+(\xi) = \frac{1}{4}(2 + 3\xi - \xi^3) \tag{2.44}$$

$$N_-(\xi) = \frac{1}{4}(1 - \xi - \xi^2 + \xi^3) \tag{2.45}$$

$$N_+(\xi) = \frac{1}{4}(-1 - \xi + \xi^2 + \xi^3) \tag{2.46}$$

They are depicted in Fig. 2.1.

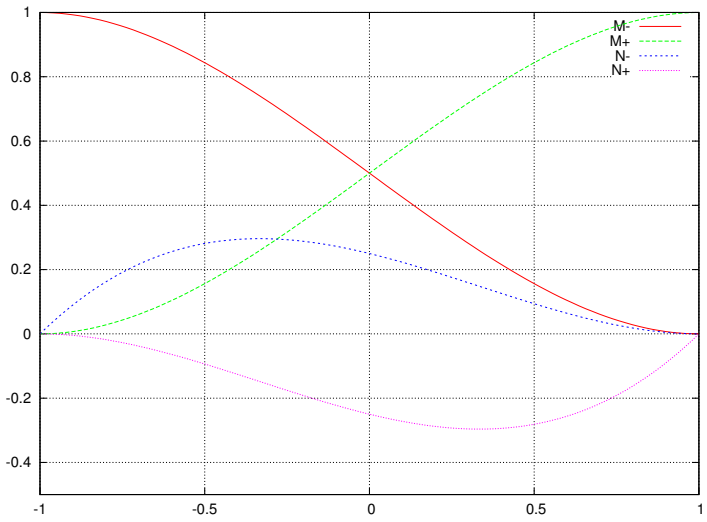

Figure 2.1: Hermite polynomials

As pointed out above, according to this scheme, in order to perform the interpolation the knowledge of its derivative is requested as well. To avoid the consequent increase in the number of unknowns, the derivatives may be expressed by means of an appropriate finite-difference scheme,

involving both the value of φ on the nodes of the panel observed and its value on the nodes of the contiguous elements. According to the scheme depicted in Fig. 2.2 Eq. 2.42 yields

$$\varphi(\xi) = M_-(\xi)\varphi^+ + M_+(\xi)\varphi^- + N_-(\xi)\frac{\varphi_2 - \varphi_0}{\Delta\xi} + N_+(\xi)\frac{\varphi_3 - \varphi_1}{\Delta\xi} \tag{2.47}$$

where

$$\Delta\xi = 2 \tag{2.48}$$

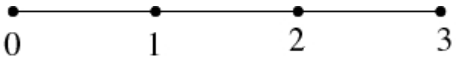

Figure 2.2: Body contour panel representation 2

Indicating by $\mathbf{p}$ the Hermite polynomials vector, whose expression is

$$\mathbf{p} = \mathbf{A}\boldsymbol{\xi} = \frac{1}{4}\begin{bmatrix} 2 & -3 & 0 & 1 \\ 2 & 3 & 0 & -1 \\ 1 & -1 & -1 & 1 \\ -1 & -1 & 1 & 1 \end{bmatrix}\begin{pmatrix} 1 \\ \xi \\ \xi^2 \\ \xi^3 \end{pmatrix} \tag{2.49}$$

Eq. 2.47 reads (local interpolation)

$$\varphi(\xi) = \mathbf{p}^T\begin{pmatrix} \varphi_1 \\ \varphi_2 \\ \frac{\varphi_2-\varphi_0}{2\Delta\xi} \\ \frac{\varphi_3-\varphi_1}{2\Delta\xi} \end{pmatrix} = (\mathbf{A}\boldsymbol{\xi})^T\begin{bmatrix} 0 & 1 & 0 & 0 \\ 0 & 0 & 1 & 0 \\ -\frac{1}{2\Delta\xi} & 0 & \frac{1}{2\Delta\xi} & 0 \\ 0 & -\frac{1}{2\Delta\xi} & 0 & \frac{1}{2\Delta\xi} \end{bmatrix}\begin{pmatrix} \varphi_0 \\ \varphi_1 \\ \varphi_2 \\ \varphi_3 \end{pmatrix} = \boldsymbol{\xi}^T\mathbf{A}^T\mathbf{T}\boldsymbol{\varphi} \tag{2.50}$$

A similar expression may be used to approximate the function $\chi(\mathbf{x})$.

Then, the contour integral coefficient B_{kj} and C_{kj} may be calculated by Gaussian quadrature.

Next, consider the interpolation used for the double integrals. The source intensity σ is approximated by bi-linear shape functions. This interpolation is also used for the geometry, so that the surface element is described as an hyperbolic paraboloid through the vertices of the panel. In order

to define the position of any point P a local coordinate system (ξ, η) is introduced. Its position is defined by

$$\mathbf{x}_P = \mathbf{p}_0 + \xi\mathbf{p}_1 + \eta\mathbf{p}_2 + \xi\eta\mathbf{p}_3 \qquad \begin{matrix} \xi \in [-1,1] \\ \eta \in [-1,1] \end{matrix}$$

whereas the vertices position is defined by

$$\mathbf{x}_{s_\xi, s_\eta} = \mathbf{p}_0 + s_\xi\mathbf{p}_1 + s_\eta\mathbf{p}_2 + s_\xi s_\eta\mathbf{p}_3$$

where $s_\xi = \pm 1$ and $s_\eta = \pm 1$. Performing an inversion of the previous equation one obtains the link between the vectors $\mathbf{p}_0, \mathbf{p}_1, \mathbf{p}_2, \mathbf{p}_3$ and the location of the vertices:

$$\begin{aligned}
\mathbf{p}_0 &= \frac{1}{4}(\mathbf{x}_{++} + \mathbf{x}_{+-} + \mathbf{x}_{-+} + \mathbf{x}_{--}) \\
\mathbf{p}_1 &= \frac{1}{4}(\mathbf{x}_{++} + \mathbf{x}_{+-} - \mathbf{x}_{-+} - \mathbf{x}_{--}) \\
\mathbf{p}_2 &= \frac{1}{4}(\mathbf{x}_{++} - \mathbf{x}_{+-} + \mathbf{x}_{-+} - \mathbf{x}_{--}) \\
\mathbf{p}_3 &= \frac{1}{4}(\mathbf{x}_{++} - \mathbf{x}_{+-} - \mathbf{x}_{-+} + \mathbf{x}_{--})
\end{aligned}$$

By means of these relationships the element is completely defined.

Moreover, it is possible to define both the covariant base vectors

$$\mathbf{g}_1 = \frac{\partial \mathbf{x}}{\partial \xi} = \mathbf{p}_1 + \eta\mathbf{p}_3 \tag{2.51}$$

$$\mathbf{g}_2 = \frac{\partial \mathbf{x}}{\partial \eta} = \mathbf{p}_2 + \xi\mathbf{p}_3 \tag{2.52}$$

its relative unit normal

$$\mathbf{n} = \frac{\mathbf{g}_1 \times \mathbf{g}_2}{\| \mathbf{g}_1 \times \mathbf{g}_2 \|} \tag{2.53}$$

In addition, we need to define the contravariant base vectors, as

$$\mathbf{g}_\alpha \cdot \mathbf{g}^\beta = \delta_\alpha^\beta \tag{2.54}$$

and the Jacobian of the transformation, $\mathbf{x} = \mathbf{x}(\xi^\alpha)$, from curvilinear to Cartesian coordinates:

$$J = \frac{\partial(x_1, x_2)}{\partial(\xi^1, \xi^2)} = \|\mathbf{g}_1 \times \mathbf{g}_2\| \tag{2.55}$$

Then, the surface integral coefficient H_{kj} may be calculated by Gaussian quadrature.

Evaluation of σ and the numerical scheme implemented

The term $\sigma = -\mathrm{div}\mathbf{w}$ has been evaluated, in the two dimensional case, according to the curvilinear-coordinate expression for the divergence of a generic vector $\mathbf{b}$, as follows

$$\mathrm{div}\mathbf{b} = \frac{1}{J}\frac{\partial(Jb^\alpha)}{\partial\xi^\alpha} = \frac{1}{J}\frac{\partial(Jb^1)}{\partial\xi^1} + \frac{1}{J}\frac{\partial(Jb^2)}{\partial\xi^2} \tag{2.56}$$

where $b^\alpha = \mathbf{b}\cdot\mathbf{g}^\alpha$, with $\alpha = 1, 2$.

Accordingly, indicating with the subscript 0 the point in which the term σ has to be calculated, we have, for each field node (but not for the boundary nodes),

$$-J\sigma)\big|_0 = \frac{1}{2\Delta\xi^1}(Jw^1\big|_3 - Jw^1\big|_1) + \frac{1}{2\Delta\xi^2}(Jw^2\big|_2 - Jw^2\big|_4) \tag{2.57}$$

where the subscripts 1, 2, 3, 4 represent, respectively, the points depicted in Figure 2.3.

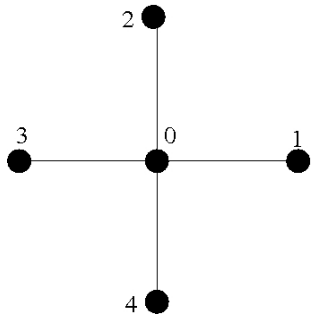

Figure 2.3: Node numbering scheme to evaluate σ in the flow field

Conversely, to evaluate the same quantity, σ, on the body contour surface, a forward finite difference scheme has been implemented, so that

$$\left.\frac{\partial(Jw^\alpha)}{\partial\xi^\alpha}\right| = \frac{1}{2\Delta\xi^1}(Jw^1|_3 - Jw^1|_1) + \frac{1}{2\Delta\xi^2}(-Jw^2|_4 + 4Jw^2|_2 - 3Jw^2|_0) \tag{2.58}$$

where again $w^\alpha = \mathbf{w}\cdot\mathbf{g}^\alpha$ ($\alpha = 1, 2$).

Discretization of the potential velocity contribution, $\mathbf{v}_{\mathrm{P}}$

Once the potential φ has been obtained, the potential portion of the velocity field $\mathbf{v}_{\mathrm{P}} = \nabla\varphi$ is obtained from the finite-difference approximation of the expression of the gradient, namely

$$\mathrm{grad}u = \frac{\partial u}{\partial\xi^1}\mathbf{g}^1 + \frac{\partial u}{\partial\xi^2}\mathbf{g}^2 \tag{2.59}$$

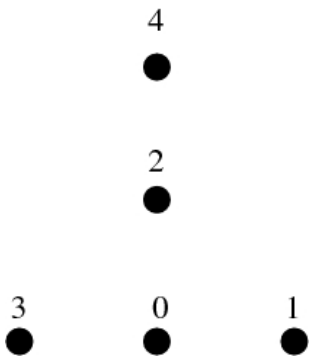

Figure 2.4: Node numbering scheme to evaluate σ on the body contour

2.4.2 Evaluation of the rotational velocity contribution, $\mathbf{w}$

Here we present the methodology used for the numerical solution of the equation for the rotational portion of the velocity field, Eq. 2.13, which may be written as

$$\frac{\partial \mathbf{w}_0}{\partial t} = \mathbf{f}_0 \tag{2.60}$$

where

$$\mathbf{f}_0 \;=\; [\nu \nabla^2 \mathbf{w}]_0 - [\mathbf{v} \cdot \nabla \mathbf{w}]_0 - [\mathbf{w} \cdot \nabla \mathbf{v}_{\mathrm{P}}]_0 \tag{2.61}$$

where the subscript 0 identifies the field point in which the term $\mathbf{f}$ has to be evaluated (Eq. 2.60 is used only in the field points, not on the boundary).

All the space derivatives are approximated by centered differences. The details for the evaluation of $[\nabla^2 \mathbf{w}]_0$, $[\mathbf{v} \cdot \nabla \mathbf{w}]_0$ and $[\mathbf{w} \cdot \nabla \mathbf{v}_{\mathrm{P}}]_0$ are presented below.

The time-dependent solution has been performed by using explicit integration schemes (both the Runge-Kutta and the Euler explicit method have been utilized).

Evaluation of $\nabla^2 \mathbf{w}$

The term $\nabla^2 \mathbf{w} = \mathrm{div}\,\mathrm{grad} \mathbf{w}$ has been evaluated by using $\nabla^2 = \mathrm{divgrad}$, along with the two-dimensional expressions for the divergence Eq. 2.56 and gradient Eq. 2.59. This yields, for the Laplacian of a generic function $u(\xi^1, \xi^2)$,

$$\nabla^2 u = \mathrm{div}\,\mathrm{grad}\, u = \frac{1}{J} \frac{\partial}{\partial \xi^\alpha} \left(J g^{\alpha\beta} \frac{\partial u}{\partial \xi^\beta} \right) \tag{2.62}$$

where the contravariant components of the metric tensor, $g^{\alpha\beta}$, are defined by

$$g^{\alpha\beta} g_{\beta\gamma} = \delta^{\alpha}_{\gamma} \tag{2.63}$$

Hence, we have

$$\nabla^2 \mathbf{w} = \frac{1}{J} \frac{\partial}{\partial \xi^{\alpha}} \left(J g^{\alpha\beta} \frac{\partial \mathbf{w}}{\partial \xi^{\beta}} \right) \tag{2.64}$$

Specifically, we use

$$\begin{aligned}
\nabla^2 \mathbf{w}\big|_0 &= \frac{1}{J_0} \left[\frac{1}{2} (\hat{g}_1^{11} + \hat{g}_0^{11})(\mathbf{w}_1 - \mathbf{w}_0) - \frac{1}{2} (\hat{g}_3^{11} + \hat{g}_0^{11})(\mathbf{w}_0 - \mathbf{w}_3) \right] \frac{1}{(\Delta\xi^1)^2} \\
&+ \frac{1}{J_0} \left[\hat{g}_1^{12} (\mathbf{w}_6 - \mathbf{w}_5) - \hat{g}_3^{12} (\mathbf{w}_7 - \mathbf{w}_8) \right] \frac{1}{4\Delta\xi^1 \Delta\xi^2} \\
&+ \frac{1}{J_0} \left[\hat{g}_2^{21} (\mathbf{w}_6 - \mathbf{w}_7) - \hat{g}_4^{21} (\mathbf{w}_5 - \mathbf{w}_8) \right] \frac{1}{4\Delta\xi^1 \Delta\xi^2} \\
&+ \frac{1}{J_0} \left[\frac{1}{2} (\hat{g}_2^{22} + \hat{g}_0^{22})(\mathbf{w}_2 - \mathbf{w}_0) - \frac{1}{2} (\hat{g}_4^{22} + \hat{g}_0^{22})(\mathbf{w}_0 - \mathbf{w}_4) \right] \frac{1}{(\Delta\xi^2)^2}
\end{aligned} \tag{2.65}$$

where $\hat{g}^{\alpha\beta} = J g^{\alpha\beta}$ and the subscripts 1, 2, 3, 4, 5, 6, 7, 8 represent, respectively, the points depicted in Figure 2.5

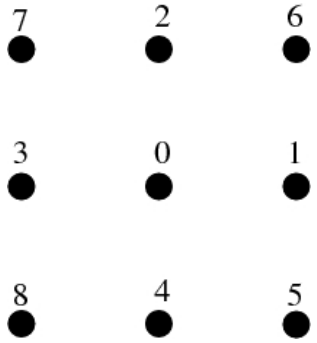

Figure 2.5: Node numbering scheme to evaluate $\nabla^2 \mathbf{w}$ in the flow field

Evaluation of $[\mathbf{v} \cdot \nabla \mathbf{w}]_0$ and $[\mathbf{w} \cdot \nabla \mathbf{v}_{\mathrm{P}}]_0$

The term $[\mathbf{v} \cdot \nabla \mathbf{w}]_0$ and $[\mathbf{w} \cdot \nabla \mathbf{v}_{\mathrm{P}}]_0$ have been evaluated, using a finite different scheme, as follows (the related computational grid scheme is the one depicted in Fig. 2.3)

$$\begin{aligned}
\mathbf{v} \cdot \nabla \mathbf{w}|_0 &= \left[(w_x + v_{P_x}) g_x^1 + (w_y + v_{P_y}) g_y^1 \right]_0 \frac{\mathbf{w}|_3 - \mathbf{w}|_1}{2\Delta\xi^1} \\
&+ \left[(w_x + v_{P_x}) g_x^2 + (w_y + v_{P_y}) g_y^2 \right]_0 \frac{\mathbf{w}|_2 - \mathbf{w}|_4}{2\Delta\xi^2}
\end{aligned} \tag{2.66}$$

where g_x^α and g_y^α denote the $x-$ and $y-$components of $\mathbf{g}^\alpha$. Similarly,

$$\mathbf{w} \cdot \nabla \mathbf{v}_{\mathrm{P}}|_0 = \left[w_x g_x^1 + w_y g_y^1 \right]_0 \frac{\mathbf{v}_{\mathrm{P}}|_3 - \mathbf{v}_{\mathrm{P}}|_1}{2\Delta\xi^1} + \left[w_x g_x^2 + w_y g_y^2 \right]_0 \frac{\mathbf{v}_{\mathrm{P}}|_2 - \mathbf{v}_{\mathrm{P}}|_4}{2\Delta\xi^2} \tag{2.67}$$

2.5 Validation

As stated in the introduction, the main objective of this dissertation is the validation of the scheme, and its assessment in terms of accuracy and efficiency. Therefore we have numerically simulated two-dimensional steady-state incompressible flows and we have compared the results achieved against some reference data available in literature.

2.5.1 Flow around a cylinder

The first test case pertains the numerical simulation of a uniform flow around a circular cylinder, having diameter D. Extensive results are available in literature and a comparison is shown in Figs. 2.6 and 2.7. Specifically, in Fig. 2.6, the distance of the singular point from the cylinder (that is, the dimensionless length of the recirculation bubble) along the x-axis in terms of Reynolds number, $Re := u_\infty D/\nu$, is depicted.

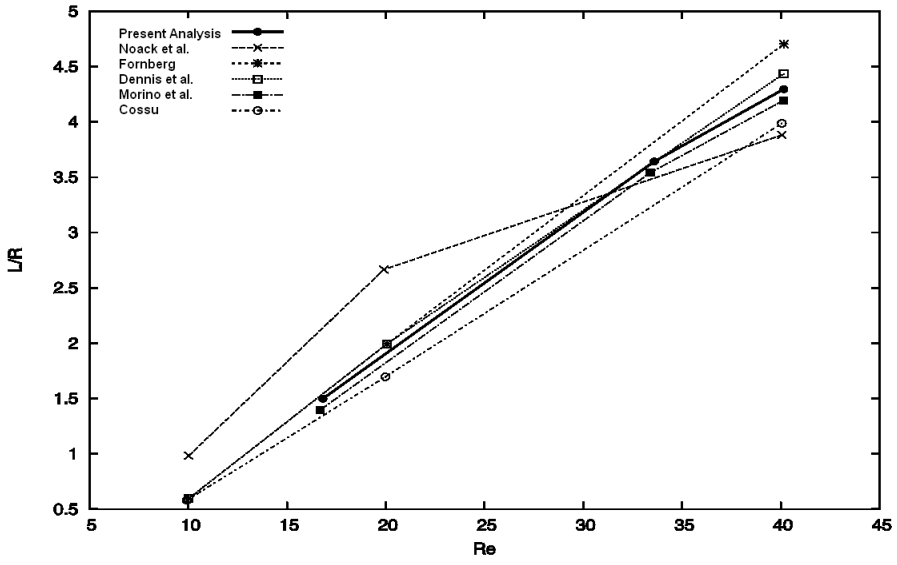

Figure 2.6: Recirculation bubble length *vs* Reynolds number

As shown in Fig. 2.6 the agreement between present results and other numerical ones, see Dennis and Chang, Fornberg, Cossu and Morino *et al.*, Refs. [15], [16] and [17], is very good, whereas the agreement with Noack *et al.*, Ref. [18], is good only in a subspace of the range investigated.

Hence a comparison between experimental data, numerical data and the present analysis has been conducted. In Fig. 2.7 the separation point angle as a function of Reynolds number is compared. The reference experimental data are by Thom and Grove *et al.*, Refs. [19] and [20], whereas the numerical ones are by Cossu, Ref. [21], and are obtained through the application of the Biot-Savart low and by Morino *et al.* and are determined by the formulation addressed in Ref. [12]. We

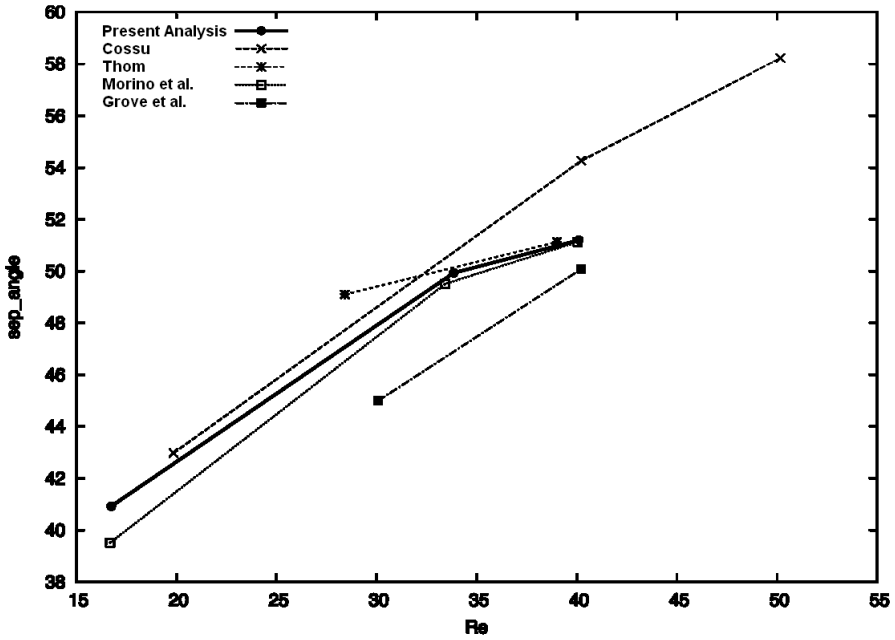

Figure 2.7: Separation angle *vs* Reynolds number

can observe that the agreement is again satisfactory. It should be noted that we performed these tests using the same discretization used in Ref. [12], that is 100 elements in ξ-direction and 20 in η-direction, to emphasize that, all other things being equal, the results are in good agreement.

2.5.2 Flow around an airfoil

Moreover, we performed an analysis on a symmetric Joukowsky airfoil in uniform flow, having chord c at an angle of attack $\alpha = 3°$. The Reynolds number is $Re = 40$. Again the results are compared with the ones of Morino *et al.*, Ref. [12], and with the one of Cossu and Morino, Ref. [17]. In Fig. 2.8 we compare $v^1(0.25, \eta)$, namely the quarter-chord contravariant component of the velocity velocity, as a function of η.

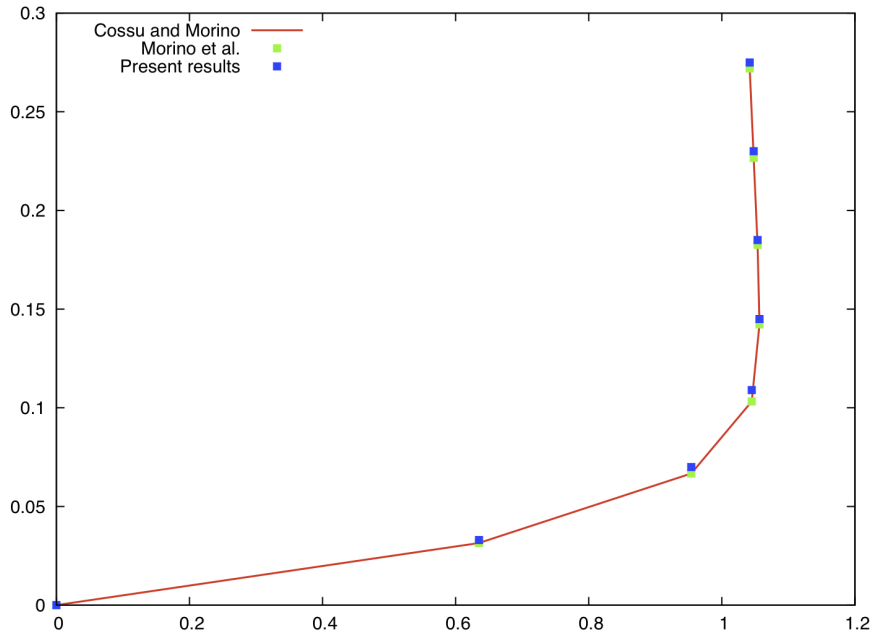

Figure 2.8: Velocity contravariant component at $\xi = .25$, Re=40 and $\alpha = 3°$.

Again the results are in good agreement. In order to validate the pressure evaluation as well, Fig. 2.9 shows a comparison between present results, in terms of pressure coefficient along the airfoil boundary and those obtained using a commercial code (i.e. FLUENT 5.5).[7]

[7]These results obtained via FLUENT have been already compared with the ones of Morino *et al.*, obtained through the formulation presented in Ref. [12].

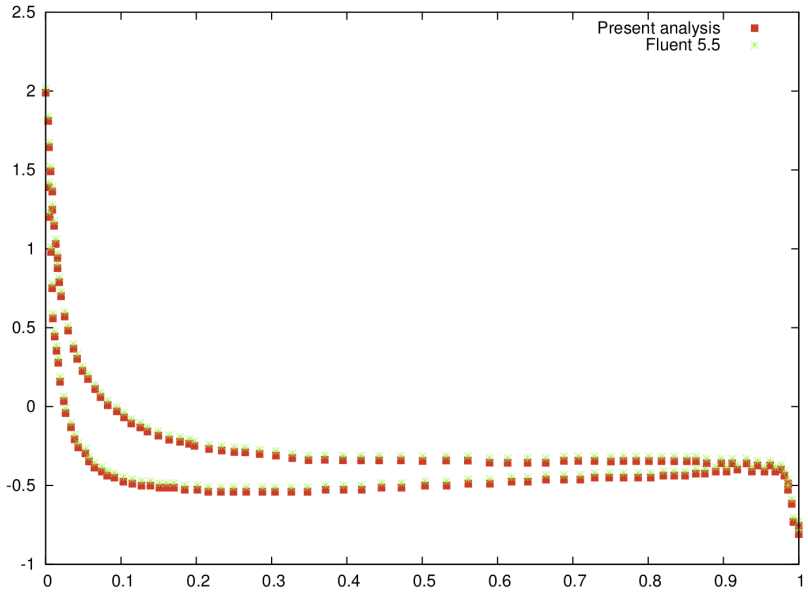

Figure 2.9: Wall pressure coefficient, Re=40 and $\alpha = 3°$.

2.5.3 Comments

In conclusion, we outline the major advantages concerning the formulation presented above.

It should be underlined that following the approach already introduced velocity evaluation is completely independent with respect to pressure evaluation.

With respect to the use of boundary integral methods, assuming the decomposition presented in Section 2.2.1, we obtain that the overall problem requires a solution analysis limited to the vortical region,[8] and the boundary conditions at infinity are automatically taken into account by the boundary integral representation.[9] Moreover, solving $\mathbf{w}$ evolution equation allows to avoid imposing either the solenoidality of $\mathbf{v}$ for the incompressible Navier-Stokes equations or that of $\boldsymbol{\zeta}$ for the vorticity transport equation.

[8] As pointed out in the introduction the rotational contribution of velocity, $\mathbf{w}$, vanishes exponentially at infinity.

[9] This is particularly advantageous in the compressible case since *non-reflecting* boundary conditions are avoided.

2.6 A comparison with the Lighthill viscous-flow correction

In Eq. 2.14, we have imposed, as one of the boundary conditions for $\mathbf{w}$, that $\mathbf{w} \cdot \mathbf{n} = 0$, for $\mathbf{x} \in \mathcal{S}$. In the original problem, the boundary condition on the body surface is simply $\mathbf{v}(\mathbf{x}, t) = \mathbf{v}_{\text{B}}(\mathbf{x}, t)$, for $\mathbf{x} \in \mathcal{S}$, Eq. 2.7. The need for a fourth boundary condition (namely, Eq. 2.14) is due to the fact that the problems for $\mathbf{w}$ and φ have been separated (had the two problems been treated together Eq. 2.7 would have sufficed).

In this work the fourth boundary condition implemented is the one in Eq. 2.14. This choice (that $\mathbf{w} \cdot \mathbf{n} = 0$, Eq. 2.14) is arbitrary and was made here merely for the simplicity of the implementation. Another possible choice is, for instance,

$$\nabla \cdot \mathbf{w} = 0 \qquad\qquad (\mathbf{x} \in \mathcal{S}) \tag{2.68}$$

In order to understand the implications of this choice, in this section we present a comparison of the formulation with the viscous-flow correction by Lighthill, Ref. [13]. Indeed, the formulation presented above is in a strict relationship to the Lighthill *equivalent source* method.[10] For the sake of completeness, such a method is briefly reviewed here.

2.6.1 The Lighthill equivalent source method

This approach, widely used to estimate the effect due to the presence of boundary layers while modelling potential flows, is implemented by modifying the potential boundary condition $\partial\phi/\partial n = \chi_{\text{B}}$ in

$$\frac{\partial \phi}{\partial n} = \chi_{\text{B}} + \chi_{\text{E}}, \tag{2.69}$$

where χ_{E} represents the *equivalent source* term, whose expression reads

$$\chi_{\text{E}} = \frac{-1}{\|\mathbf{g}_1 \times \mathbf{g}_2\|} \frac{\partial}{\partial \xi^\alpha} \int_0^{\xi^3_\delta} \left[J \left(v^\alpha - v^\alpha_{\text{E}} \right) \right] \mathrm{d}\xi^3, \tag{2.70}$$

being v^α_{E} the contravariant components of $\mathbf{v}_{\text{E}}$ which is the "*irrotational and solenoidal continuation*" of the velocity $\mathbf{v}$.[11] This expression is equivalent to the equivalent-source term of Lighthill.

[10] Otherwise known as the *transpiration velocity* method and connected to the *displacement thickness* method, also by Lighthill, Ref. [13].

[11] It should be pointed out that $\mathbf{v}$ is irrotational and solenoidal outside the vortical region (i.e. outside the boundary layer) therefore $\mathbf{v}_{\text{E}}$ is its continuation in the vortical region.

2.6.2 The comparison

In this subsection, we analyze both boundary conditions, Eqs. 2.14 and 2.68, within the context of the equivalent-source method by Lighthill, Ref. [13].

To begin with, note that, as shown by Morino, in Ref. [1], the solution for the velocity, $\mathbf{v}$, does not depend on the choice of the fourth boundary condition (although $\mathbf{w}$ and $\mathbf{v}_{\text{P}}$ are affected by it). Nonetheless, the comparison is useful to clarify the decomposition.

In particular, we will show that both boundary conditions yield formulations that are close to the Lighthill *equivalent source* method. Thus, further analysis of this issue is warranted, again to be supported by computational experimentation.

The comparison for $\mathbf{w}\cdot\mathbf{n}=0$ on $\mathcal{S}$

Assuming the vortical region to be thin (as in the Lighthill work), for $\mathbf{x}$ distant $\mathcal{S}$, G may be assumed to be constant across the vortical layer. This yields the following boundary integral representation for the velocity potential φ

$$E(\mathbf{x},t)\,\varphi(\mathbf{x},t)=\oint_{\mathcal{S}}\left(\left(\chi_{\text{B}}+\chi_{\text{N}}\right)G-\varphi\,\frac{\partial G}{\partial n}\right)\mathrm{d}\mathcal{S}(\mathbf{y}) \tag{2.71}$$

where

$$\chi_{\text{N}}=\frac{1}{\|\mathbf{g}_1\times\mathbf{g}_2\|}\int_0^{\xi^3_\delta} J\,\sigma_\varphi\,\mathrm{d}\xi^3 \tag{2.72}$$

being $\mathrm{d}\mathcal{V}=J\,\mathrm{d}\xi^1\,\mathrm{d}\xi^2\,\mathrm{d}\xi^3$ and $\mathrm{d}\mathcal{S}=\|\mathbf{g}_1\times\mathbf{g}_2\|\,\mathrm{d}\xi^1\,\mathrm{d}\xi^2$. Hence, as $\sigma=-\nabla\cdot\mathbf{w}$ and $\mathbf{w}=\mathbf{v}-\mathbf{v}_{\text{P}}$, we have[12]

$$\chi_{\text{N}}=\frac{-1}{\|\mathbf{g}_1\times\mathbf{g}_2\|}\,\frac{\partial}{\partial\xi^\alpha}\int_0^{\xi^3_\delta} J\left(v^\alpha-v^\alpha_{\text{P}}\right)\mathrm{d}\xi^3 \tag{2.73}$$

Although the two expressions in Eqs. 2.73 and 2.70 are similar, the two are conceptually different as v^α_{E} is solenoidal whereas v^α_{P} is not solenoidal.

The comparison for $\nabla\cdot\mathbf{w}=0$ on $\mathcal{S}$

The fact that $\sigma=-\nabla\cdot\mathbf{w}=0$ on $\mathcal{S}$ (and at the outer boundary of $\mathcal{A}_{\mathbf{w}}$) yields that σ might be negligible in the vortical region, an assumption to be verified by numerical investigations. Assuming

[12]Note that $\int_0^{\xi^3_\delta}\frac{\partial(Jw^3)}{\partial\xi^3}\,\mathrm{d}\xi^3$ vanishes. If $\xi^3=0$, $\mathbf{w}\cdot\mathbf{n}=0$ implies $w^3=0$, and if $\xi^3\geq\xi^3_\delta$, we have $\mathbf{w}=\mathbf{0}$.

that this is the case, the boundary integral representation for φ reads

$$E(\mathbf{x},t)\,\varphi(\mathbf{x},t) = \oint_{\mathcal{S}} \left(\frac{\partial \varphi}{\partial n}\, G - \varphi\, \frac{\partial G}{\partial n} \right) \mathrm{d}\mathcal{S}(\mathbf{y}). \tag{2.74}$$

Thus, corresponding boundary condition is no longer given by Eq. 2.14; correspondingly, the boundary condition for φ is no longer given by Eq. 2.21 - we have to go back to Eq. 2.20, namely

$$\frac{\partial \varphi}{\partial n} = \chi_{\mathrm{B}} - \mathbf{w}\cdot\mathbf{n}. \tag{2.75}$$

We underline that

$$J\,w^3 = \frac{\partial}{\partial \xi^\alpha} \int_0^{\xi^3_\delta} J\left(v^\alpha - v^\alpha_{\mathrm{P}}\right) \mathrm{d}\xi^3, \tag{2.76}$$

equivalent to Eq. 2.73, since $-\|\mathbf{g}_1 \times \mathbf{g}_2\|\,\chi_{\mathrm{N}} = \|\mathbf{g}_1 \times \mathbf{g}_2\|\,\mathbf{w}\cdot\mathbf{n} = \mathbf{w}\cdot\mathbf{g}_1\times\mathbf{g}_2 = J\,w^3$. Now $\mathbf{v}_{\mathrm{E}}$ and $\mathbf{v}_{\mathrm{P}}$ are conceptually equivalent (both are solenoidal fields).

2.7 A review of the past work

Here, we present a very brief overview of the decomposition used in Refs. [9], [10], [11] and [12]), where the decomposition falls within the class of direct-integration decompositions, in which Eq. 1.2 is solved by direct integration. Using the expression for the curl in curvilinear coordinates, Eq. 1.2 may be rewritten as

$$J\zeta^1 = \frac{\partial w_3}{\partial \xi^2} - \frac{\partial w_2}{\partial \xi^3} \qquad J\zeta^2 = \frac{\partial w_1}{\partial \xi^3} - \frac{\partial w_3}{\partial \xi^1} \qquad J\zeta^3 = \frac{\partial w_2}{\partial \xi^1} - \frac{\partial w_1}{\partial \xi^2} \tag{2.77}$$

where J is the Jacobian of the transformation $\mathbf{x} = \mathbf{x}(\xi^\alpha)$, ζ^j are the contravariant components of $\boldsymbol{\zeta} = \zeta^j \mathbf{g}_j$, whereas w_k are the covariant components of $\mathbf{w} = w_k \mathbf{g}^k$. This equation may be solved by choosing, arbitrarily but legitimately,

$$w_3(\xi^1,\xi^2,\xi^3) = 0. \tag{2.78}$$

Hence, recalling that $\boldsymbol{\zeta} = \mathbf{0}$ at infinity, the first two equations in Eq. 2.77 may be integrated to yield the following particular solution for Eq. 1.2:

$$w_1(\xi^1,\xi^2,\xi^3) = -\int_{\xi^3}^{\infty} J\,\zeta^2(\xi^1,\xi^2,\breve{\xi}^3)\,\mathrm{d}\breve{\xi}^3 \tag{2.79}$$

$$w_2(\xi^1,\xi^2,\xi^3) = \int_{\xi^3}^{\infty} J\,\zeta^1(\xi^1,\xi^2,\breve{\xi}^3)\,\mathrm{d}\breve{\xi}^3 \tag{2.80}$$

$$w_3(\xi^1,\xi^2,\xi^3) = 0 \tag{2.81}$$

Equation 2.79 is the key of formulation used in the past (Refs. [9], [10], [11] and [12]). The integration is performed along a ξ^3-line, which is either in the direction of the flow, or in a direction normal to the boundary. Thus, it is apparent that, in either case, $\mathbf{w} = \mathbf{0}$ in much of the region where $\boldsymbol{\omega} = \mathbf{0}$ (indeed, for attached flows, it vanishes in all the region where $\boldsymbol{\omega} = \mathbf{0}$).

Next, consider the direction of integration ξ^3. In the scheme used in Ref. [9], the direction of integration is somewhat aligned with the direction of the flow. On the other hand, in Ref. [10] they are directed along the normal to the boundary. It is apparent that, in either approach, for attached high-Reynolds-number flows (for which the rotational region is a very thin layer around the surface of the body), $\mathbf{w}$ obtained from Eq. 2.79 vanishes in the whole irrotational region, that is, the volume $\mathcal{W}$ where $\mathbf{w} \neq \mathbf{0}$ coincides with the rotational region. Thus, recalling Eq. 1.1, we have, in the whole irrotational region, $\mathbf{v} = \nabla\varphi$. Hence, the Bernoulli theorem may be used to evaluate the pressure there.

However, both of these approaches yield discontinuities in the $\mathbf{w}$ field (and hence in $\mathbf{v}_{\mathrm{P}}$), which fact renders the formulations non–user–friendly. In order to overcome this drawback, a combination of the two approaches is introduced in Ref. [11], and implemented in Ref. [12], where the field $J\boldsymbol{\zeta}$ is decomposed into symmetric and anti–symmetric fields, with the appropriate coordinate of integration applied to each. This eliminates the discontinuities in the $\mathbf{w}$ and $\mathbf{v}_{\mathrm{P}}$ fields.

Chapter 3

Towards a compressible formulation

In this chapter, we present a first step towards extending to compressible flow fields the formulation introduced in the Chapter 2. Here, we shift the emphasis towards acoustics. We present the theoretical formulation, and use it to show that the power spectral density of the field pressure is related directly to the power spectral density of the boundary pressure. Numerical results are presented a compared to available experimental data.

A closely related problem was addressed in Refs. [23] and [24], for the limited case of incompressible flows, using the potential/vorticity decomposition outlined in Section 2.7.[1] They provide a formulation for the evaluation of the power spectral density of the pressure at any given set of points *in the irrotational region*, in terms of the power spectral density of the *transpiration velocity* at the boundary points: this is a quantity that they define in terms of the vorticity and is closely related to the *equivalent source* by Lighthill [25] (see Section 2.6). The implication is that the direct relationship exists only if the vortical region (boundary layer and wake) is thin, namely for attached high-Reynolds-number flows.

However, experimental data available does not pertain the power spectral density of the transpiration velocity, but the power spectral density of the boundary pressure. In addition, the limitation to incompressible fields is inadequate for studying aeroacoustics. Both limitations are removed in Ref. [22], which presents a compressible flow formulation that shows how the power spectral density of the pressure at any given set of points *in the irrotational region* is related to the power

[1] Note that the potential/vorticity decomposition illustrated in Section 2.7 may be used for compressible flows as well. Also, as pointed out there, that decomposition has also the distinguishing feature that the rotational-velocity contribution vanishes in much of the irrotational region.

spectral density of the pressure at the boundary points. However, this work is still based upon the potential/vorticity decomposition outlined in Section 2.7; this is the reason why the field points must be located in the irrotational region, so as to allow one to use the Bernoulli theorem.

Here, the formulation is based upon the *natural velocity decomposition*. Hence, we no longer have the limitation that the field points be located in the irrotational region, because one may use the generalization of the Bernoulli theorem (Eqs. 3.10, or 3.43, depending upon the equation governing $\mathbf{w}$ that one chooses). Thus, the objective of the analysis presented here is the evaluation of the power spectral density of the pressure at any given set of points in the field in terms of the power spectral density of the pressure at the boundary points.

Specifically, we first introduce a formulation for the evaluation of the Fourier transform of the pressure at any given point (either in the field or on the boundary) in terms of the Fourier transform of the *transpiration velocity*. Then, the relationship boundary-pressure *vs* transpiration velocity is inverted and combined with the relationship field-pressure *vs* transpiration velocity to yield the desired formulation for the evaluation of the Fourier transform of the pressure at any given point in the field in terms of the power spectral density of the pressure on the boundary. The relationship regarding the power spectral density follows from the Wiener-Khintchine theorem.

3.1 Compressible-flow formulation

In this section we present the compressible-flow formulation. Consider the governing equations (continuity, Navier-Stokes and entropy): these are given by

$$\frac{\mathrm{D}\rho}{\mathrm{D}t} + \rho\,\nabla\cdot\mathbf{v} = 0 \tag{3.1}$$

$$\rho\,\frac{\mathrm{D}\mathbf{v}}{\mathrm{D}t} + \nabla p = \mathrm{Div}\mathbf{D} \tag{3.2}$$

$$\rho\,\vartheta\,\frac{\mathrm{D}S}{\mathrm{D}t} = \mathbf{D}:\mathbf{V} + \kappa\,\nabla^2\vartheta, \tag{3.3}$$

where ϑ is the temperature, S is the entropy, $\mathbf{D}$ is the strain rate tensor, and $\mathbf{V}$ is the viscous stress tensor.

Combining the Navier-Stokes equations, Eq. 3.2, with

$$\mathrm{d}h = \vartheta\mathrm{d}S + \mathrm{d}p/\rho \tag{3.4}$$

and with $\mathrm{D}\mathbf{v}/\mathrm{D}t = \partial\mathbf{v}/\partial t + \mathbf{v}\cdot\nabla\mathbf{v}$ one obtains, using Eq. 2.11

$$\frac{\partial \mathbf{v}}{\partial t} + \mathbf{v}\cdot\nabla\mathbf{v} = -\nabla h + \vartheta\nabla S + \frac{1}{\rho}\mathrm{Div}\mathbf{V} \tag{3.5}$$

3.1.1 Natural velocity decomposition

Let us introduce again the natural velocity decomposition

$$\mathbf{v} = \mathbf{v}_{\mathrm{P}} + \mathbf{w}, \qquad \text{with } \mathbf{v}_{\mathrm{P}} = \nabla\varphi. \tag{3.6}$$

Combining with the Navier-Stokes equation, as given in Eq. 3.5, yields

$$\nabla\left(\frac{\partial\varphi}{\partial t} + \frac{1}{2}v_{\mathrm{P}}^2 + h\right) + \frac{\mathrm{D}\mathbf{w}}{\mathrm{D}t} + \mathbf{w}\cdot\nabla\mathbf{v}_{\mathrm{P}} + \vartheta\nabla S + \frac{1}{\rho}\mathrm{Div}\mathbf{V} = \mathbf{0} \tag{3.7}$$

Akin to what we did in Chapter 2, it is convenient to define $\mathbf{w}$ so as to satisfy the following equation[2]

$$\frac{D\mathbf{w}}{Dt} + \mathbf{w}\cdot\nabla\mathbf{v}_{\mathrm{P}} - \vartheta\nabla S - \frac{1}{\rho}\mathrm{Div}\mathbf{V} = \mathbf{0} \tag{3.8}$$

Correspondingly, we have

$$\nabla\left(\dot{\varphi} + \frac{v_{\mathrm{P}}^2}{2} + h\right) = 0 \tag{3.9}$$

which yields, in the airframe, a generalized Bernoulli theorem for the Navier-Stokes equations

$$\dot{\varphi} + \frac{v_{\mathrm{P}}^2}{2} + h = h_\infty \tag{3.10}$$

Next, let us introduce the ideal-gas equation of state

$$\rho\, h^{-1/(\gamma-1)}\, \mathrm{e}^{S/R} = \text{constant} \tag{3.11}$$

Then, we have

$$\frac{1}{\rho}\frac{\partial\rho}{\partial h}\Big|_S = \frac{1}{(\gamma-1)\,h} = \frac{1}{\gamma R\,\vartheta} =: \frac{1}{a^2} \qquad \text{and} \qquad \frac{1}{\rho}\frac{\partial\rho}{\partial S}\Big|_h = \frac{-1}{R}, \tag{3.12}$$

[2]Here, we have a minor variation with respect to the formulation of Ref. [1]. Specifically, we use the formulation for compressible Euler flows, and - akin to the acoustic analogy of Lighthill [14] - we include all the viscous terms in the equation for $\mathbf{w}$. This issue is addressed in greater depth in Section 3.5, which presents a comparison with the compressible Navier-Stokes flows of Ref. [1], where the viscosity and entropy terms related to φ are included in the Bernoulli theorem term.

where a is called the *speed of sound* and R is the ideal-gas constant. Combining Eq. 3.10 with the non-conservative form of the continuity equation, Eq. 3.1, and using Eq. 3.12, one obtains[3]

$$\nabla^2\varphi \,+\, \nabla\cdot\mathbf{w} = -\frac{1}{\rho}\frac{D\rho}{Dt} = -\frac{1}{a^2}\frac{Dh}{Dt} + \frac{1}{R}\frac{DS}{Dt} = \frac{1}{a^2}\frac{D}{Dt}\left(\dot{\varphi} + \frac{v_{\mathrm{P}}^2}{2}\right) + \frac{1}{R}\frac{DS}{Dt} \tag{3.13}$$

Combining and recalling that $a^2 = \gamma R\vartheta$, one obtains

$$\nabla^2\varphi - \frac{1}{c^2}\frac{\partial^2\varphi}{\partial t^2} = \sigma \tag{3.14}$$

where $c = a_\infty$, whereas σ comprises all the so–called source terms, including the viscous terms, which are linear, and which in aeroacoustics are typically included in the source terms.

In a body frame of reference,[4] we have

$$\nabla^2\varphi - \frac{1}{c^2}\left(\frac{\partial}{\partial t} + U_\infty\frac{\partial}{\partial t}\right)^2\varphi = \sigma \tag{3.15}$$

Note that this equation is formally equivalent to that for full-potential flows.[5] Thus, we may use the boundary integral representation for the full-potential flows, which is obtained under the assumption of homogenous initial conditions (start from rest) and homogenous boundary condition at infinity. This yields (see for instance Ref. [4])

$$E(\check{\mathbf{x}})\varphi(\check{\mathbf{x}},t) = \oint_{\check{\mathcal{S}}}\left[\frac{\partial\varphi}{\partial\check{n}}\check{G} - \varphi\frac{\partial\check{G}}{\partial\check{n}} + \dot{\varphi}\check{G}\frac{\partial\hat{\theta}}{\partial\check{n}}\right]^{\check{\theta}}\mathrm{d}\check{\mathcal{S}}(\check{\mathbf{y}}) + \int_{\check{\mathcal{V}}_{\mathrm{F}}}\left[\check{G}\sigma\right]^{\check{\theta}}\mathrm{d}\check{\mathcal{V}}(\check{\mathbf{y}}) \tag{3.16}$$

where $E(\mathbf{x},t)$ is given by Eq. 2.31, whereas $\check{}$ denotes the Prandtl-Glauert space, having coordinates $\check{x}_1 = x_1/\beta$, $\check{x}_2 = x_2$ and $\check{x}_3 = x_3$; specifically, $\check{G} = -1/4\pi\check{r}$, with $\check{r} = \|\check{\mathbf{x}} - \check{\mathbf{y}}\|$, and $[...]^{\check{\theta}} = [...]_{\tau=t-\check{\theta}}$, where $\check{\theta} = [M(\check{y}_1 - \check{x}_1) + \check{r}]/\beta c$, whereas $\hat{\theta} = [M(\check{x}_1 - \check{y}_1) + \check{r}]/\beta c$.

If the vortical region, $\check{\mathcal{V}}$, which encompasses boundary layer and wake, is sufficiently thin, we may "compress" the source distribution over $\check{\mathcal{V}}$ into a source layer over the boundary surface $\check{\mathcal{S}}_{\mathrm{B}}$ (see Ref. [10] for a more refined analysis, involving a sequence of integration by parts). In order to exploit this fact, let us introduce a curvilinear coordinate system, ξ^α, where ξ^1 and ξ^2 are over the surfaces $\check{\mathcal{S}}_{\mathrm{B}}$ and $\check{\mathcal{S}}_{\mathrm{W}}$, whereas the coordinate ξ^3 is such that: (i) $\xi^3 = 0$ coincides with the surface $\mathcal{S}_{\mathrm{B}}$, and (ii) $\partial/\partial\xi^3 = \partial/\partial\check{n}$, for $\xi^3 = 0$. Specifically, using $\mathrm{d}\check{\mathcal{V}} = \check{J}\,\mathrm{d}\xi^1\,\mathrm{d}\xi^2\,\mathrm{d}\xi^3$ and $\mathrm{d}\check{\mathcal{S}} = \sqrt{\bar{a}}\,\mathrm{d}\xi^1\,\mathrm{d}\xi^2$, we have

$$\int_{\check{\mathcal{V}}}[\sigma\,\check{G}]^{\check{\theta}}\,\mathrm{d}\check{\mathcal{V}}(\check{\mathbf{y}}) \simeq \oint_{\check{\mathcal{S}}_{\mathrm{B}}}[\check{\chi}_{\mathrm{B}}\,\check{G}]^{\check{\theta}}\,\mathrm{d}\check{\mathcal{S}}(\mathbf{y}) + \int_{\check{\mathcal{S}}_{\mathrm{W}}}[\check{\chi}_{\mathrm{W}}\,\check{G}]^{\check{\theta}}\,\mathrm{d}\check{\mathcal{S}}(\check{\mathbf{y}}) \tag{3.17}$$

[3] See Ref. [1] for further details.

[4] That is, a frame that moves with velocity $-U_\infty\mathbf{i}$ with respect to the undisturbed air.

[5] The only difference being the definition of σ.

with

$$\check{\chi}_{\mathrm{B}} = \frac{1}{\sqrt{\check{a}}} \int_0^{\xi^3_\delta} \check{J}\, \sigma \, \mathrm{d}\xi^3 \tag{3.18}$$

(where ξ^3_δ denotes the value of ξ^3 just outside the boundary layer), and a similar definition for $\check{\chi}_{\mathrm{W}}$. Thus, Eq. 3.16 may be approximated as

$$\begin{aligned} E(\check{\mathbf{x}})\varphi(\check{\mathbf{x}},t) &= \oint_{\check{\mathcal{S}}_{\mathrm{B}}} \left[(\check{\chi}+\check{\chi}_{\mathrm{B}})\check{G} - \varphi \frac{\partial \check{G}}{\partial \check{n}} + \dot{\varphi}\check{G}\,\frac{\partial \hat{\theta}}{\partial \check{n}} \right]^{\check{\theta}} \mathrm{d}\check{\mathcal{S}}(\check{\mathbf{y}}) \\ &+ \oint_{\check{\mathcal{S}}_{\mathrm{W}}} \left[\check{\chi}_{\mathrm{W}}\check{G} - \varphi \frac{\partial \check{G}}{\partial \check{n}} + \dot{\varphi}\check{G}\,\frac{\partial \hat{\theta}}{\partial \check{n}} \right]^{\check{\theta}} \mathrm{d}\check{\mathcal{S}}(\check{\mathbf{y}}) \end{aligned} \tag{3.19}$$

Equation 3.19 is the *key* to the approach presented here. Indeed, Eq. 3.19 allows one to evaluate φ anywhere in the field, if φ, $\check{\chi}$ and $\check{\chi}_{\mathrm{B}}$ over $\check{\mathcal{S}}_{\mathrm{B}}$, as well as $\Delta\varphi$ and χ_{W} over $\check{\mathcal{S}}_{\mathrm{W}}$ are known. However, φ on $\check{\mathcal{S}}_{\mathrm{B}}$ is not known. Thus, first one must obtain an equation for evaluating φ on $\check{\mathcal{S}}_{\mathrm{B}}$. Akin ti the incompressible flow case, this is obtained by letting $\check{\mathbf{x}}$ tend $\check{\mathcal{S}}_{\mathrm{B}}$. In this case, Eq. 3.19 corresponds to a compatibility condition between φ and $\check{\chi}+\check{\chi}_{\mathrm{B}}$ over $\check{\mathcal{S}}_{\mathrm{B}}$, as well as $\Delta\varphi$ and $\check{\chi}_{\mathrm{W}}$ over $\check{\mathcal{S}}_{\mathrm{W}}$. This compatibility condition is an integral equation that allows one to evaluate φ over $\check{\mathcal{S}}_{\mathrm{B}}$ from $\check{\chi}+\check{\chi}_{\mathrm{B}}$ over $\check{\mathcal{S}}_{\mathrm{B}}$, as well as $\Delta\varphi$ and $\check{\chi}_{\mathrm{W}}$ over $\check{\mathcal{S}}_{\mathrm{W}}$. In other words, the solution for φ in the field, is obtained in two steps. In the first one, $\mathbf{x}$ denotes a generic point on the surface $\check{\mathcal{S}}_{\mathrm{B}}$. In this case, Eq. 3.19 corresponds to an integral equation for φ on $\check{\mathcal{S}}_{\mathrm{B}}$. Once φ on $\check{\mathcal{S}}_{\mathrm{B}}$ has been evaluated, we consider the second step, that which yields φ in the field: now, $\mathbf{x}$ denotes a generic point in the field, and Eq. 3.19 corresponds to an integral representation for φ in $\check{\mathcal{V}}$.

This formulation may be treated akin to that for incompressible flows. In particular, the approximation used in Eq. 3.17 may be used to approximate the volume with a surface integral, thereby defining the transpiration velocity for unsteady compressible flows.

The application of the above results to the problem under consideration here (that it, how to obtain the pressure in the field given the pressure on the body) is addressed later. Indeed, in order to show this, it is convenient first to discretize the problem.

3.2 Numerical formulation

Here we present the discretization of Eq. 3.19 used in this work. Contrary to what we did in Chapter 2, here we use a zeroth order discretization (namely a piecewise constant approximation).

Specifically, let $\mathcal{S}_{\rm B}$ be divided into $N_{\rm B}$ surface elements, $\mathcal{S}_j^{\rm B}$ ($j = 1, \ldots, N_{\rm B}$), and $\mathcal{S}_{\rm W}$ into $N_{\rm W}$ surface elements, $\mathcal{S}_n^{\rm W}$ ($n = 1, \ldots, N_{\rm B}$). Next, introduce a piece–wise constant approximation for $\varphi(\mathbf{x}, t)$, namely

$$\varphi(\mathbf{x}, t) = \varphi_j(t) \qquad\qquad (\mathbf{x} \in \mathcal{S}_j^{\rm B}) \tag{3.20}$$

The same type of approximation is used for the other variables. Next, we restrict our attention to the sound generated by a turbulent boundary layer, for a wing in uniform translation. In this case, $\check{\chi}$ is time independent. In view of the linearity of the operator, let us concentrate on the unsteady portion of the flow. Let

$$\hat{\varphi}_j(\omega) = \mathfrak{F}[\varphi_j^{\rm U}(t)] \tag{3.21}$$

denote the Fourier transform of the unsteady portion of φ. This yields, in the Fourier domain,

$$E_k\, \hat{\varphi}_k = \sum_{h=1}^{N_{\rm B}} \hat{B}_{kh}^{\rm B}\, \hat{\chi}_h^{\rm B} + \sum_{h=1}^{N_{\rm B}} \hat{C}_{kh}^{\rm B}\, \hat{\varphi}_h + \sum_{n=1}^{N_{\rm W}} \hat{B}_{kn}^{\rm W}\, \hat{\chi}_n^{\rm W} + \sum_{n=1}^{N_{\rm W}} \hat{C}_{kn}^{\rm W}\, \Delta\hat{\varphi}_n \tag{3.22}$$

where

$$\begin{aligned} \hat{C}_{kh}^{\rm B}(\omega) &= \left(C_{kh}^{\rm B} + \imath\, \omega\, D_{kh}^{\rm B}\right) e^{-\imath\, \omega\, \theta_{kh}} \qquad & \hat{B}_{kh}^{\rm B}(\omega) &= B_{kh}^{\rm B}\, e^{-\imath\, \omega\, \theta_{kh}} \\ \hat{C}_{kn}^{\rm W}(\omega) &= \left(C_{kn}^{\rm W} + \imath\, \omega\, D_{kn}^{\rm W}\right) e^{-\imath\, \omega\, \theta_{kn}} \qquad & \hat{B}_{kn}^{\rm W}(\omega) &= B_{kn}^{\rm W}\, e^{-\imath\, \omega\, \theta_{kn}} \end{aligned} \tag{3.23}$$

respectively denoting with $B_{kh}^{\rm B}$, $C_{kh}^{\rm B}$, and $D_{kh}^{\rm B}$ source, doublet and ratelet integral coefficients on the body,

$$B_{kh}^{\rm B} = \int_{\mathcal{S}_h} \check{G}(\check{\mathbf{x}}_k, \check{\mathbf{y}})\, \mathrm{d}\mathcal{S}(\mathbf{y}) \tag{3.24}$$

$$C_{kh}^{\rm B} = \int_{\mathcal{S}_h} \frac{\partial \check{G}(\check{\mathbf{x}}_k, \check{\mathbf{y}})}{\partial \check{n}}\, \mathrm{d}\mathcal{S}(\mathbf{y}) \tag{3.25}$$

$$D_{kh}^{\rm B} = \int_{\mathcal{S}_h} \check{G}(\check{\mathbf{x}}_k, \check{\mathbf{y}}) \frac{\partial \hat{\theta}}{\partial \check{n}}\, \mathrm{d}\mathcal{S}(\mathbf{y}) \tag{3.26}$$

Similarly, $B_{kh}^{\rm W}$, $C_{kh}^{\rm W}$, and $D_{kh}^{\rm W}$ denote the corresponding wake coefficients.

On the wake we have that (see Refs. [4] and [1])

$$\Delta\hat{\varphi}_n(t) = \Delta\hat{\varphi}_n^{\rm TE}(t - \theta_n^{\rm C}), \tag{3.27}$$

where $\theta_n^{\rm C}$ is the convection time required for a wake point to be convected from the trailing edge point $\mathbf{x}_n^{\rm TE}$ to the corresponding wake point $\mathbf{x}_n^{\rm W}$. In addition,

$$\Delta\hat{\varphi}_n^{\rm TE}(t) = \sum_{j=1}^{N_{\rm B}} S_{nj}\, \hat{\varphi}_j(t), \tag{3.28}$$

(where $[S_{nj}]$ is a suitable matrix, introduced to implement the trailing–edge condition, that $\Delta\varphi$ equals $\varphi_{\mathsf{upper}} - \varphi_{\mathsf{lower}}$). Similar considerations apply for χ_{W} (since the convection of χ_{W} is connected with that of $\mathbf{w}$, which in turn is connected with that of $\boldsymbol{\zeta}$). In addition, combining Eqs. 3.27 and 3.28, and taking the Fourier transform, one obtains

$$\Delta\hat{\varphi}_n = e^{-\imath\omega\theta_n^{\mathrm{C}}}\,\Delta\hat{\varphi}_n^{\mathrm{TE}} = e^{-\imath\omega\theta_n^{\mathrm{C}}}\sum_{j=1}^{N_{\mathrm{B}}} S_{nj}\,\hat{\varphi}_j \tag{3.29}$$

As mentioned above, similar considerations are used for χ_{W}, so that

$$\hat{\chi}_n^{\mathrm{W}} = e^{-\imath\omega\theta_n^{\mathrm{C}}}\sum_{j=1}^{N_{\mathrm{B}}} S_{nj}\,\hat{\chi}_j \tag{3.30}$$

Next, recall that the solution for φ in the field is obtained in two steps. In the first one, $\mathbf{x}$ denotes the generic point on the surface $\mathcal{S}_{\mathrm{B}}$; in this case, Eq. 3.19 corresponds to an integral equation for φ on $\mathcal{S}_{\mathrm{B}}$. In the second step, $\mathbf{x}$ denotes a specific point in the field, and Eq. 3.19 corresponds to an integral representation for φ in $\mathcal{V}$.

Consider the first step, the use of Eq. 3.19 as an integral equation. In this case, the collocation points $\mathbf{x}_k$ are located on the surface $\mathcal{S}_{\mathrm{B}}$: $\mathbf{x}_k \in \mathcal{S}_{\mathrm{B}}$ $(k = 1, \ldots, N_{\mathrm{B}})$. Thus, φ on the left side is evaluated on $\mathcal{S}_{\mathrm{B}}$, where $E_k = 1/2$. Then, Eq. 3.22 yields

$$\left[\frac{1}{2}\mathsf{I} - \mathsf{C}_{\mathrm{BB}} - \mathsf{C}_{\mathrm{BW}}\,\mathsf{R}\,\mathsf{S}\right]\hat{\boldsymbol{\varphi}}_{\mathrm{B}} = \left[\mathsf{B}_{\mathrm{BB}} + \mathsf{B}_{\mathrm{BW}}\,\mathsf{R}\,\mathsf{S}\right]\hat{\boldsymbol{\sigma}} \tag{3.31}$$

where, for instance, $\mathsf{C}_{\mathrm{BB}} = \left[\left(C_{kh}^{\mathrm{B}} + \imath\,\omega\,D_{kh}^{\mathrm{B}}\right)e^{-\imath\,\omega\,\theta_{kh}}\right]$, with $\mathbf{x}_k$ located in $\mathcal{S}_{\mathrm{B}}$ $(k = 1, \ldots, N_{\mathrm{F}})$. In addition, $\mathsf{S} = \left[S_{nj}\right]$, whereas the retarded–time matrix R is given by

$$\mathsf{R} = \mathrm{Diag}\left[e^{-\imath\omega\theta_n^{\mathrm{C}}}\right] \tag{3.32}$$

Next, consider the second step (integral representation). In this case, the collocation points $\mathbf{x}_k$ are located in the fluid volume, $\mathcal{V}$: $\mathbf{x}_k \in \mathcal{V}$ $(k = 1, \ldots, N_{\mathrm{F}}$, with N_{F} arbitrary). Thus, φ on the left hand side is evaluated in $\mathcal{V}$, and $E_k = 1$. Then, Eq. 3.22 yields

$$\hat{\boldsymbol{\varphi}}_{\mathrm{F}} = \left[\mathsf{C}_{\mathrm{FB}} + \mathsf{C}_{\mathrm{FW}}\,\mathsf{R}\,\mathsf{S}\right]\hat{\boldsymbol{\varphi}}_{\mathrm{B}} + \left[\mathsf{B}_{\mathrm{FB}} + \mathsf{B}_{\mathrm{FW}}\,\mathsf{R}\,\mathsf{S}\right]\hat{\boldsymbol{\sigma}} = \mathsf{Q}\,\hat{\boldsymbol{\sigma}} \tag{3.33}$$

with apparent definitions of the symbols. For instance, the elements of the matrix $\mathsf{C}_{\mathrm{FB}} = (C_{kh}^{\mathrm{B}} + \imath\,\omega\,D_{kh}^{\mathrm{B}})\,e^{-\imath\,\omega\,\theta_{kh}}$, with $\mathbf{x}_k$ located in $\mathcal{V}$ $(k = 1, \ldots, N_{\mathrm{F}})$; also, the matrix Q is obtained by expressing $\hat{\boldsymbol{\varphi}}$ in terms of $\hat{\boldsymbol{\sigma}}$, by using Eq. 3.31.

Next, consider the pressure in the field.[6] The generalized Bernoulli theorem, Eq. 3.10, may be linearized to yield, $p - p_\infty = -\rho_\infty \dot{\varphi}$, or, in the body frame of reference, $p - p_\infty = -\rho_\infty(\dot{\varphi} + U_\infty \partial\varphi/\partial x)$. Thus, we have, by taking the Fourier transform of the unsteady portion and using Eq. 3.33,

$$\hat{\mathsf{p}}_{\mathrm{F}} = -\imath\,\omega\,\rho_\infty\,\hat{\boldsymbol{\varphi}}_{\mathrm{F}} - \rho_\infty U_\infty\,\mathsf{Q}'\,\hat{\boldsymbol{\sigma}} = \mathsf{H}_{\mathrm{F}}\,\hat{\boldsymbol{\sigma}} \tag{3.34}$$

where $\mathsf{H}_{\mathrm{F}} = -\imath\omega\rho_\infty\mathsf{Q} - \rho_\infty U_\infty \mathsf{Q}'$, whereas Q' has an expression similar to that for Q, except for the fact that we take the derivative with respect to x of the integrands of each coefficient, before setting $\mathbf{x} = \mathbf{x}_k$.

Following a similar procedure, one obtains the corresponding expression for the pressure on the boundary, which may be expressed as

$$\hat{\mathsf{p}}_{\mathrm{B}} = \mathsf{H}_{\mathrm{B}}\,\hat{\boldsymbol{\sigma}} \tag{3.35}$$

Combining Eqs. 3.34 and 3.35, we finally obtained the desired relationship between the field pressure and the boundary pressure

$$\hat{\mathsf{p}}_{\mathrm{F}} = \mathsf{H}_{\mathrm{F}}\mathsf{H}_{\mathrm{B}}^{-1}\hat{\mathsf{p}}_{\mathrm{B}} = \mathsf{H}\hat{\mathsf{p}}_{\mathrm{B}} \tag{3.36}$$

3.3 Power–spectral–density analysis

In this section, we use the fact that, for the Wiener-Khintchine theorem, the power spectral density S_u of a function $u(t)$ may be expressed as

$$\mathsf{S}_u = \lim_{T\to\infty} \frac{1}{T}\,\hat{u}_{_T}^*\,\hat{u}_{_T} \tag{3.37}$$

where * denotes complex conjugate, whereas $\hat{u}_{_T}$ denotes the Fourier transform of $u_{_T}(t)$, where $u_{_T}(t) = u(t)$ for $t \in (-T, T)$, and $u_{_T}(t) = 0$ otherwise:

$$\hat{u}_{_T}(\omega) := \mathfrak{F}\big[u_{_T}(t)\big] := \int_{-T}^{T} u(t)\,e^{-\imath\omega t}\,\mathrm{d}t \tag{3.38}$$

For a vector function $\mathsf{v}(t)$, the power spectral density S_v is a matrix, which may be expressed as (still for the Wiener-Khintchine theorem)

$$\mathsf{S}_\mathsf{v} = \lim_{T\to\infty} \frac{1}{T}\,\hat{\mathsf{v}}_{_T}^*\,\hat{\mathsf{v}}_{_T}^{\mathsf{T}} \tag{3.39}$$

[6] Note that this is the main advantage of using the natural velocity decomposition formulation, with respect to the formulation of Ref. [22], where the Bernoulli theorem applies only in the non-vortical region.

Using Eq. 3.36, we have

$$\mathsf{S}_{\mathsf{p}_{\mathrm{F}}} = \mathsf{H}^{*}\, \mathsf{S}_{\mathsf{p}_{\mathrm{B}}}\, \mathsf{H}^{\mathsf{T}} \tag{3.40}$$

which is the desired relationship between the power spectral density matrix $\mathsf{S}_{\mathsf{p}_{\mathrm{F}}}$ of the pressure at N_{V} arbitrary points in the whole field and the power spectral density matrix $\mathsf{S}_{\mathsf{p}_{\mathrm{B}}}$ of the pressure at N_{B} points on $\mathcal{S}_{\mathrm{B}}$. The expression in Eq. 3.40 allows one to evaluate the field–pressure PSD from the boundary–pressure PSD, thereby providing a link between two sets of experimental data (PSD of field pressure and PSD of surface pressure), often considered independent.

3.4 Numerical results

In order to obtain a preliminary validation of the formulation presented above, the matrix H has been evaluated for a turbulent flow past a rectangular wing with a NACA 5510 airfoil. Specifically, a comparison in terms of field-pressure PSD has been performed with respect to the experimental data of Ref. [26] (of course, the power spectral density on the wing surface used as an input is also that available from the same experimental data). In the test case considered, the geometrical angle of attack is equal to $\alpha = 5^{\circ}$, the undisturbed uniform flow speed is $U_0 = 70$m/s, whereas the chord length is $c = .2$m. The resulting Mach number is $M = 0.2052$, whereas Reynolds number is $Re \approx 950,000$. It should be noted that the experimental data are two-dimensional, whereas the analysis is three-dimensional, on a wing of aspect ratio of 10.

Both the wing and wake mid–surface have been divided in elements, as depicted in Fig. 3.1. Specifically, in the stream-wise direction, 7 elements are used over the wing and 70 over the wake (the wake is conveniently assumed to be 10 times longe as the chord), whereas 19 elements are used in span-wise direction, over both the wing and wake (for a total of 7x19 elements over the top of the wing right side and 70x19 elements over the wake right side).

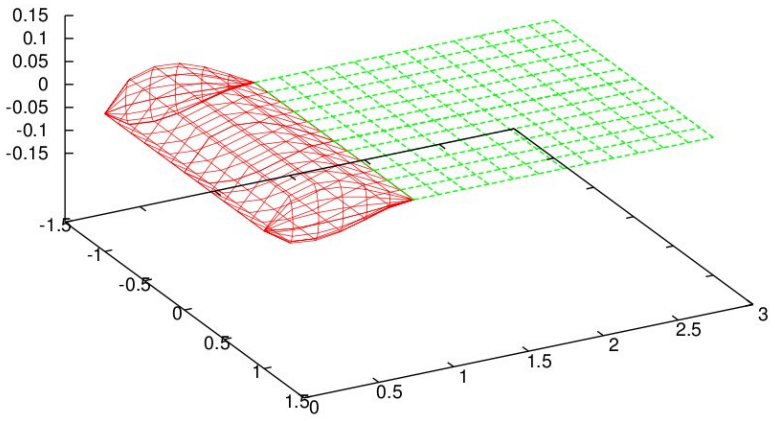

Figure 3.1: Wing and mid-surface wake discretization.

Then, the piecewise constant approximation described in Section 3.2 has been adopted to compute the matrix H relating the field–pressure PSD to the boundary–pressure PSD. In particular, the field point considered is placed on the suction side, at 5 chord away from the airfoil chord-line, the distance being measured on a direction orthogonal to the chord-line itself.

The matrix H has then been applied to the pressure PSD at the elements of the boundary, as available from the experimental measurements of Ref. [26]. First, we present an analysis of the effect of compressibility. This is presented in Fig. 3.2, where the PSD of the field pressure is depicted for $M = 0.0$ and $M = 0.2052$, which represents the experimental Mach number. We see that this effect, while small, is not negligible.

Thus, we present the comparison with the experimental results only for this Mach number. These are shown in Fig. 3.3 which depicts the numerical PSD of the field pressure, along with the PSD of the signal recorded by a far-field microphone placed at hte corresponding field point (Ref. [26]). The agreement is quite satisfactory.

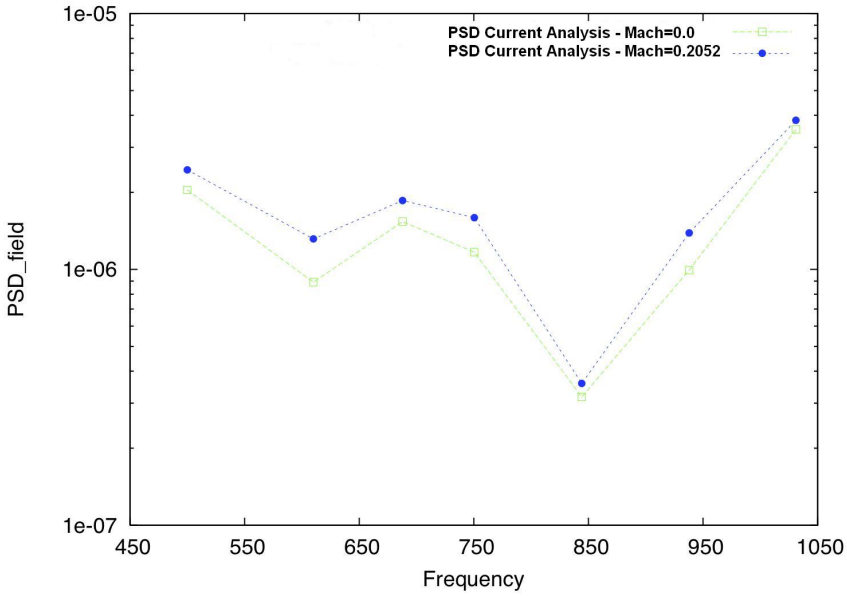

Figure 3.2: Effect of compressibility.

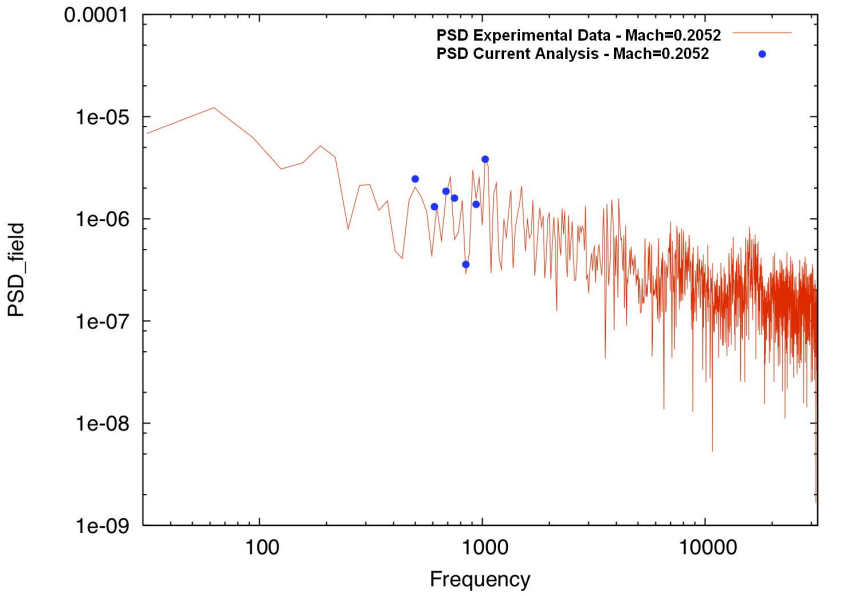

Figure 3.3: Power Spectral Density of pressure in the field for the selected range of frequencies.

3.4.1 Comments

A formulation that allows one to obtain the PSD of the pressure at N_{F} arbitrary points in the field from the PSD of the pressure on the boundary surface has been presented. This provides a link between two sets of experimental data (PSD of field pressure and PSD of surface pressure), which are often considered independent. This link must be necessarily satisfied (provided of course that the key assumption that the vortical region be thin is satisfied). The validation against experimental data is encouraging.

It should be noted that the matrix relating, in Fourier domain, the surface pressure vector to the surface potential vector is singular for $\omega = 0$ (indeed, in this case, adding constant to φ does not affect the pressure); thus, one might expect elimination of figures at low frequencies. In addition, the boundary element method requires smaller and smaller elements as the frequency increases; thus, one might expect an excessive truncation error for high frequencies. Thus, the analysis is presented for a limited range of frequencies. These issues require additional investigations.

3.5 A critique

It may be noted, that as pointed out in Section 3.1, the viscous terms are included in the source term (akin to the acoustic analogy of Lighthill [14]). This, however, appears questionable, in view of the fact that the viscosity in included in the analysis of the turbulent boundary layers, and hence it should be included in the propagation of sound. This issue is addressed in Ref. [1], where it is shown that the effect of the viscosity on the sound propagation is negligible. For the sake of completeness, such an analysis is outlined here. Again, the derivation presented here is streamlined, by assuming directly the governing equation for $\mathbf{w}$ (instead of deriving it, as in Ref. [1], as a necessary consequence of the boundary integral formulation for the compressible Navier-Stokes equations).

Let us introduce again the natural velocity decomposition, $\mathbf{v} = \mathbf{v}_{\text{P}} + \mathbf{w}$, with $\mathbf{v}_{\text{P}} = \nabla\varphi$, Eq. 3.6. Combining with the Navier-Stokes equation, yields

$$\nabla\left(\frac{\partial\varphi}{\partial t} + \frac{1}{2}v_{\text{P}}^2 + h - \vartheta_\infty S - \frac{4}{3}\nu\nabla^2\varphi\right) + \frac{\mathrm{D}\mathbf{w}}{\mathrm{D}t} + \mathbf{w}\cdot\nabla\mathbf{v}_{\text{P}} - \nu\nabla^2\mathbf{w} - \frac{1}{3}\nu\nabla\nabla\cdot\mathbf{w} - (\vartheta - \vartheta_\infty)\nabla S = \mathbf{0} \tag{3.41}$$

It is apparent that considerable advantages are obtained by choosing that $\mathbf{w}$ be governed by the

following equation:[7]

$$\frac{\mathrm{D}\mathbf{w}}{\mathrm{D}t} + \mathbf{w}\cdot\nabla\mathbf{v}_{\mathrm{P}} = \nu\,\nabla^2\mathbf{w} + \frac{1}{3}\,\nu\,\nabla\,\nabla\cdot\mathbf{w} + (\vartheta-\vartheta_\infty)\,\nabla S \tag{3.42}$$

Combining with Eq. 3.41, one obtains, as an unavoidable consequence, the *generalization of the Bernoulli theorem for compressible Navier-Stokes fields*

$$\frac{\partial\varphi}{\partial t} + \frac{1}{2}v_{\mathrm{P}}^2 + h - \vartheta_\infty S - \frac{4}{3}\,\nu\,\nabla^2\varphi = h_\infty - \vartheta_\infty S_\infty \tag{3.43}$$

or

$$\frac{\partial\varphi}{\partial t} + \wp - \frac{4}{3}\,\nu\,\nabla^2\varphi = 0 \tag{3.44}$$

where

$$\wp = h - h_\infty - \mathtt{S} + \frac{1}{2}\,v_{\mathrm{P}}^2 \qquad\qquad \text{with} \qquad \mathtt{S} = \vartheta_\infty\big(S - S_\infty\big) \tag{3.45}$$

It should be emphasized again that this equation stems directly from the choice for the governing equation for $\mathbf{w}$, Eq. 3.42.

Next, we want to obtain the equation for φ. In order to obtain this, we need to recast the continuity equation and the entropy transport equation into a more convenient form.

Consider first the entropy evolution equation. Using $h = c_p\vartheta$, we have

$$\frac{\partial\mathtt{S}}{\partial t} - \frac{\kappa}{\rho c_p}\,\nabla^2\big(\wp + \mathtt{S}\big) = h_\infty\, f_4, \tag{3.46}$$

with

$$h_\infty\, f_4 = -(\vartheta-\vartheta_\infty)\,\mathrm{D}_t S - \vartheta_\infty\,\mathbf{v}\cdot\nabla S + \frac{1}{\rho}\,\mathbf{D}:\mathbf{V} - \frac{\kappa}{\rho c_p}\nabla^2\frac{v^2}{2}. \tag{3.47}$$

Next, in order to obtain more compact expressions, set

$$\breve{a} = \frac{1}{c^2} \qquad \breve{b} = \frac{1}{h_\infty} = (\gamma-1)\,\breve{a} \qquad \breve{\nu} = \frac{1}{3}\,\nu \qquad \breve{q} = \frac{\breve{b}\,\kappa}{\rho\, c_p} = \frac{\breve{b}\,\nu}{\mathrm{Pr}} = \frac{1}{\mathrm{Pr}}\,\frac{\nu}{h_\infty}, \tag{3.48}$$

where $\mathrm{Pr} = \mu\, c_p/\kappa$ denotes the Prandtl number. Multiplying Eq. 3.46 by $\breve{b}$, we have

$$\breve{b}\,\frac{\partial\mathtt{S}}{\partial t} - \breve{q}\,\nabla^2(\wp + \mathtt{S}) = f_4. \tag{3.49}$$

[7] As for incompressible flows, in Ref. [1] Eq. 3.42 is introduced not as a convenient choice, but as a natural consequence of the boundary integral formulation of the Navier-Stokes equations.

Finally. combing with the Bernoulli theorem, so as to eliminate $\wp$, and setting

$$\mathtt{S}_*(\mathbf{x},t) := \mathtt{S}(\mathbf{x},t) + 4\,\breve{\nu}\,\nabla^2\varphi(\mathbf{x},t), \tag{3.50}$$

we have

$$\frac{\partial \mathtt{S}}{\partial t} - \frac{4}{3}\,\nu\,\nabla^2\mathtt{S}_* = \frac{1}{\breve{b}}\,f_4 = -(\vartheta-\vartheta_\infty)\,\mathrm{D}_t S - \vartheta_\infty\,\mathbf{v}\cdot\nabla S + \frac{1}{\rho}\,\mathbf{D}:\mathbf{V} - \frac{\kappa}{\rho c_p}\nabla^2\frac{v^2}{2}. \tag{3.51}$$

Next, consider the continuity equation. Using Eq. 3.12, the continuity equation reads

$$\frac{1}{a^2}\,\frac{\mathrm{D}h}{\mathrm{D}t} - \frac{1}{R}\,\frac{\mathrm{D}S}{\mathrm{D}t} + \nabla\cdot\mathbf{v} = 0. \tag{3.52}$$

Separating linear and nonlinear terms, setting

$$c^2 = a_\infty^2 = \gamma\,R\,\vartheta_\infty = (\gamma-1)h_\infty, \tag{3.53}$$

and noting that $1/R\vartheta_\infty - 1/c^2 = (\gamma-1)/c^2 = 1/h_\infty$, Eq. 3.52 may be written as

$$\frac{1}{c^2}\,\frac{\partial \wp}{\partial t} - \frac{1}{h_\infty}\,\frac{\partial \mathtt{S}}{\partial t} + \nabla\cdot\mathbf{v} = f_0', \tag{3.54}$$

where $\mathtt{S} = \vartheta_\infty(S - S_\infty)$, Eq. 3.45, whereas

$$f_0' = -\left(\frac{1}{a^2} - \frac{1}{c^2}\right)\mathrm{D}_t h - \frac{1}{c^2}\,\mathbf{v}\cdot\nabla h + \frac{1}{R}\,\mathbf{v}\cdot\nabla S + \frac{1}{c^2}\,\frac{\partial}{\partial t}\frac{v^2}{2} \tag{3.55}$$

comprises all the nonlinear terms. Next, combining the continuity equation, Eq. 3.54 with the entropy transport equation Eq. 3.49, so as to eliminate $\partial\mathtt{S}/\partial t$, we have

$$\breve{a}\,\frac{\partial \wp}{\partial t} - \breve{q}\,\nabla^2(\wp + \mathtt{S}) + \nabla\cdot\mathbf{v} = f_0, \tag{3.56}$$

with $f_0 = f_0' + f_4$, or (using Eqs. 3.55 and 3.47, as well as $1/R - \breve{b}\,\vartheta_\infty = 1/\gamma\,R$)

$$\begin{aligned} f_0 = &-\left(\frac{1}{a^2} - \frac{1}{c^2}\right)\mathrm{D}_t h - \frac{1}{c^2}\,\mathbf{v}\cdot\nabla h + \frac{1}{c^2}\,\frac{\partial}{\partial t}\frac{v^2}{2} \\ &-\frac{1}{h_\infty}\left[(\vartheta-\vartheta_\infty)\,\mathrm{D}_t S - \frac{\mathbf{D}:\mathbf{V}}{\rho} + \frac{\kappa}{\rho c_p}\nabla^2\frac{v^2}{2}\right] + \frac{1}{\gamma\,R}\,\mathbf{v}\cdot\nabla S. \end{aligned} \tag{3.57}$$

We are now in a position to derive the equation for φ. This may be obtained by combining the continuity equation, Eq. 3.56), with the velocity decomposition, Eq. 3.6), the equation for $\mathtt{S}$ (Eq. 3.50), and the Bernoulli theorem (Eq. 3.44). This yields

$$-\left(\breve{a}\,\frac{\partial}{\partial t} - \breve{q}\,\nabla^2\right)\left(\frac{\partial}{\partial t}\,\varphi - 4\,\breve{\nu}\,\nabla^2\varphi\right) + \breve{q}\,\nabla^2\big(4\,\breve{\nu}\,\nabla^2\varphi - \mathtt{S}_*\big) + \nabla^2\varphi + \nabla\cdot\mathbf{w} = f_0, \tag{3.58}$$

or

$$\nabla^2\varphi - \frac{1}{c^2}\,\ddot{\varphi} + \frac{2\,\alpha}{c^2}\,\nabla^2\dot{\varphi} = \sigma_\varphi, \tag{3.59}$$

where

$$\alpha = \left(\frac{1}{2}\breve{q} + 2\breve{a}\breve{\nu}\right) c^2 = \frac{2}{3}\gamma\nu, \tag{3.60}$$

and $\sigma_\varphi = f_0 - \nabla\cdot\mathbf{w} + \breve{q}\,\nabla^2\mathtt{S}_*$. Note that the terms with $\nabla^4\varphi$ cancel each other out.

Thus,

$$\varphi(\mathbf{x},t) = \int_0^t \int_{\mathbb{R}^3} \sigma_\varphi(\mathbf{y},\tau)\,Q(\mathbf{x}-\mathbf{y},t-\tau)\,\mathrm{d}\mathcal{V}(\mathbf{y})\,\mathrm{d}\tau, \tag{3.61}$$

where $Q(\mathbf{x},t)$ is the (causal) fundamental solution for the operator in Eq. 3.59, with $\mathbf{y} = \mathbf{0}$ and $\tau = 0^+$:

$$\nabla^2 Q - \frac{1}{c^2}\big(\ddot{Q} - 2\,\alpha\nabla^2\dot{Q}\big) = \delta(\mathbf{x}-\mathbf{y})\,\delta(t-\tau), \tag{3.62}$$

with the initial conditions $Q(\mathbf{x},0) = \dot{Q}(\mathbf{x},0) = 0$, whereas the boundary condition is $Q = 0$ at infinity.

Note that (as shown in detail in Subsubsection 3.5.1) Q is well approximated by Q_{A}, with Q_{A} given

$$Q_{\text{A}}(\mathbf{x},t) = \frac{-1}{4\pi r}\,\delta_\alpha(t,r), \tag{3.63}$$

where $r = \|\mathbf{x}\|$, whereas $\delta_\alpha(t,r)$ is given by Eq. 3.72 and, for $r \neq 0$, tends to $\delta(t - r/c)$ as α and tends to zero, where it is also shown that the difference between Q and Q_{A} is of order ν^2 and hence is very small, see Footnote 8).

Equation for φ, with $\mathbf{x} \in \mathcal{V}$

Next, consider the boundary integral representation for φ. As usual, introduce the function $\hat{\varphi}(\mathbf{x},t) = E(\mathbf{x},t)\,\varphi(\mathbf{x},t)$, where $E(\mathbf{x},t) = 1$ for $\mathbf{x} \in \mathcal{V}$ and $E(\mathbf{x},t) = 0$ otherwise (Eq. 2.31. Using Eq. 3.59 yields the desired generalization of the wave equation with $\mathbf{x} \in \mathbb{R}^3$:

$$\nabla^2\hat{\varphi} - \frac{1}{c^2}\,\frac{\partial^2\hat{\varphi}}{\partial t^2} + \frac{2\,\alpha}{c^2}\,\frac{\partial}{\partial t}\nabla^2\hat{\varphi} = \hat{\sigma}_\varphi(\mathbf{x},t) \qquad \big(\mathbf{x} \in \mathbb{R}^3\big), \tag{3.64}$$

with

$$\hat{\sigma}_\varphi(\mathbf{x},t) = E\,\sigma_\varphi + \nabla E\cdot\nabla\varphi + \nabla\cdot(\varphi\,\nabla E) - \frac{1}{c^2}\left[\dot{E}\,\dot{\varphi} + (\varphi\,\dot{E})^{\cdot}\right] \\ + \frac{2\,\alpha}{c^2}\left[\dot{E}\,\nabla^2\varphi + \nabla E\cdot\nabla\dot{\varphi} + \nabla\dot{E}\cdot\nabla\varphi + \nabla\cdot(\dot{\varphi}\,\nabla E) + \nabla\cdot(\varphi\,\nabla\dot{E})\right]. \tag{3.65}$$

Then, in analogy with Eq. 3.61, we have $E\,\varphi = \int_0^t \int_{\mathbb{R}^3} \hat{\sigma}_\varphi\, Q\,\mathrm{d}\mathcal{V}(\mathbf{y})\,\mathrm{d}\tau$, or

$$\begin{aligned} &E(\mathbf{x},t)\,\varphi(\mathbf{x},t) \\ &= \int_0^{t^+}\!\!\int_{\mathbb{R}^3} \Big(E\sigma_\varphi + \nabla_{\mathbf{y}}E\cdot\nabla_{\mathbf{y}}\varphi + \nabla_{\mathbf{y}}\cdot(\varphi\,\nabla_{\mathbf{y}}E) - \frac{1}{c^2}\left[\dot{E}\,\dot{\varphi} + (\varphi\,\dot{E})^{\cdot}\right]\Big) Q\,\mathrm{d}\mathcal{V}(\mathbf{y})\,\mathrm{d}\tau \\ &+ \frac{2\,\alpha}{c^2}\int_0^{t^+}\!\!\int_{\mathbb{R}^3} \Big[\dot{E}\,\nabla^2\varphi + \nabla_{\mathbf{y}}E\cdot\nabla_{\mathbf{y}}\dot{\varphi} + \nabla_{\mathbf{y}}\dot{E}\cdot\nabla_{\mathbf{y}}\varphi + \nabla_{\mathbf{y}}\cdot(\dot{\varphi}\,\nabla_{\mathbf{y}}E) \\ &+ \nabla_{\mathbf{y}}\cdot(\varphi\,\nabla_{\mathbf{y}}\dot{E})\Big] Q\,\mathrm{d}\mathcal{V}(\mathbf{y})\,\mathrm{d}\tau, \end{aligned} \tag{3.66}$$

with $Q = Q(\mathbf{x}-\mathbf{y}, t-\tau)$.

It may be shown that, in the limit, as α tends to zero, Eq. 3.66 reduces to Eq. 3.16. Specifically, this may be obtained by replacing Q with its approximation $Q_{\text{A}} = G\,\delta_\alpha$ (Eq. 3.63); then, we see that the effects of viscosity are obtained essentially by replacing δ_θ with δ_α (for, the second integral in the equation above may be neglected, since it vanishes as $\alpha = \frac{2}{3}\gamma\nu$ goes to zero). The fact that $\delta_\alpha(t,r)/(1-\mathrm{e}^{-cr/\alpha})$ is a near identity (see the comments at the end of Subsection 3.5.1) implies that instead of the value on the integrand evaluated at $\tau = t-\theta$, we will have to use a suitable average value in the neighborhood of $\tau = t-\theta$ (see Ref. [1] for details).

3.5.1 The function $Q(\mathbf{x},t)$

Here, we discuss the function $Q(\mathbf{x},t)$, which is the solution of Eq. 3.62, with its boundary and initial conditions.

The function $Q(\mathbf{x},t)$ is analyzed at some length in Ref. [27], which gives an exact expression for it (also reported in Ref. [28]), as well as two convenient approximate expressions. Here, we only outline the more convenient of these two approximate expressions (for details, see Refs. [4] and [27]). The approximation consists of replacing $Q(\mathbf{x},t)$, which is defined by Eq. 3.62, with $Q_{\text{A}}(\mathbf{x},t)$, which is defined by

$$\nabla^2 Q_{\text{A}} - \frac{1}{c^2}\left(\frac{\partial}{\partial t} - \alpha\nabla^2\right)^2 Q_{\text{A}} = \delta(\mathbf{x}-\mathbf{y})\,\delta(t-\tau), \tag{3.67}$$

for which one may obtain an easier to interpret expression. Note that the factor $\alpha = \frac{2}{3}\gamma\nu$ is small.[8] Thus, the difference between $Q(\mathbf{x}, t)$ and $Q_{\text{A}}(\mathbf{x}, t)$, which is due to the term $(\alpha/c)^2\,\nabla^4 Q_{\text{A}}$, is very small. Taking the Laplace-Fourier transform of Eq. 3.67, one obtains (setting $k = \|\mathbf{k}\|$)

$$\tilde{Q}_{\text{A}}(\mathbf{k}, s) = \frac{-1}{k^2 + (s + \alpha k^2)^2/c^2}, \tag{3.68}$$

Taking the inverse Laplace transform and using $\mathfrak{L}\big[e^{-at}\sin(bt)\big] = b/[(s+a)^2 + b^2]$, one obtains

$$\mathfrak{F}\big[Q_{\text{A}}\big] = -\frac{c}{k}\,\mathrm{e}^{-\alpha k^2 t}\,\sin kct. \tag{3.69}$$

The inverse Fourier transform is given by[9]

$$Q_{\text{A}}(\mathbf{x}, t) = -\frac{c}{2\pi^2 r}\int_0^\infty \mathrm{e}^{-\alpha k^2 t}\sin kct\,\sin kr\,\mathrm{d}k. \tag{3.70}$$

Thus, using $\int_0^\infty \mathrm{e}^{-c^2u^2}\sin au\,\sin bu\,\mathrm{d}u = \sqrt{\pi}\big(\mathrm{e}^{-(a-b)^2/4c^2} - \mathrm{e}^{-(a+b)^2/4c^2}\big)/4c$, one obtains

$$Q_{\text{A}}(\mathbf{x}, t) = \frac{-1}{4\pi r}\,\frac{c\,H(t)}{\sqrt{4\pi\alpha t}}\left(\mathrm{e}^{-\frac{(ct-r)^2}{4\alpha t}} - \mathrm{e}^{-\frac{(ct+r)^2}{4\alpha t}}\right) \qquad \big(r = \|\mathbf{x}\|\big), \tag{3.71}$$

which is the desired expression for Q_{A}.

In order to continue our analysis of the function $Q_{\text{A}}(\mathbf{x}, t)$, consider the function

$$\delta_\alpha(t, r) := \frac{c\,H(t)}{\sqrt{4\pi\alpha t}}\left(\mathrm{e}^{-\frac{(ct-r)^2}{4\alpha t}} - \mathrm{e}^{-\frac{(ct+r)^2}{4\alpha t}}\right), \tag{3.72}$$

and note that, as α tends to zero, $\delta_\alpha(t, r)$ vanishes except for $t = r/c$. On the other hand, using $\int_0^\infty \mathrm{e}^{-bt - a/4t}\,t^{-1/2}\,\mathrm{d}t = \sqrt{\pi/b}\,\mathrm{e}^{-\sqrt{ab}}$ (Ref. [29], p. 1145, Eq. 17.13.31), one obtains that $\int_{-\infty}^\infty \delta_\alpha(t, r)\,\mathrm{d}t = 1 - \mathrm{e}^{-cr/\alpha}$. Thus, as α tends to zero, $\delta_\alpha(t, r)$ tends to the Dirac delta function $\delta(t - r/c)$. In other words, $\delta_\alpha(t, r)/(1 - \mathrm{e}^{-cr/\alpha})$ is a near identity. The factor $1 - \mathrm{e}^{-cr/\alpha}$ is not particularly relevant in aeroacoustics, where cr/α is large; it is important however in aerodynamics, since it assumes the value zero when $\mathbf{x} = \mathbf{y}$.

[8] Recall that for notational simplicity, we use ν. However, throughout the paper it is tacitly understood that all the variables are dimensionless. Thus, ν denotes the reciprocal of the Reynolds number, and is assumed to be small.

[9] If $\mathfrak{F}\big[f(\mathbf{x})\big]$ is only a function of $k = \|\mathbf{k}\|$, we have $\mathfrak{F}^{-1}\big[F(k)\big] = \frac{1}{2\pi^2 r}\int_0^\infty F(k)\,k\sin kr\,\mathrm{d}k$ (see, for instance, Schwartz [30], p. 204, Eqs. V,3;22 and V,3;26).

Chapter 4

Concluding remarks

In this dissertation we presented a method and the corresponding implementation to provide for a unified formulation for unsteady aerodynamics and aeroacoustics. In particular, we analyzed, from both the conceptual and the computational points of view, the methodology that steams from the application of boundary integral method to the equation modelling the phenomena under consideration.

In details, within the first issue addressed in Chapter 2, we described the complete theoretical formulation for Navier-Stokes incompressible flows and its consequent numerical formulation. The results provided through the algorithm implemented are in good agreement with other numerical and experimental data. Ultimately we achieved the primary object of this work, to provide a validation of the theoretical framework of Ref. [1].

With regards to the formulation described in Chapter 3, which represents a first step towards the complete formulation of Navier-Stokes compressible flow fields within the velocity decomposition introduced, we presented a novel reading of the source field contribution in terms of a *source surface* distribution, defining a corresponding so-called *transpiration velocity for compressible flows*. By means of this result we have obtained the pressure in the field in terms of a transfer function applied to the pressure on the boundary surface and moreover we could relate the power-spectral-density in the flow field to the same quantity evaluated on the body surface, providing a link between sets of data usually considered as independent. Again, the numerical results achieved are comforting. According to the formulation introduced, the pressure field, evaluated as a post-processing, via the suitable expression of Bernoulli theorem,[1] present a good agreement with other

[1] Specifically we refer to incompressible and compressible expressions of generalized Bernoulli theorem, see Sec-

numerical and experimental data available in literature.

In addition, preliminary work towards the application of the natural velocity decomposition for the analysis of transonic flows has been presented in Appendix A.[2]

Finally, as already mentioned, the issues addressed in Chapters 2 and 3 and in Appendix A are best seen within a context of multidisciplinary optimization. Specifically, the algorithms developed there are good candidates for aerodynamics and aeroacoustics high-level models, within the context of multi-level multi-disciplinary design optimization for the conceptual design of civil aircraft (of course, each formulation is relevant even if considered as a stand-alone). The corresponding activity performed under this doctoral program is presented in Appendix B, along with the state of the art on the development of the MDO algorithm by the Aerospace Structures and Design Group of the Mechanical and Industrial Engineering Department of the University Roma Tre, together with some analyses oriented towards aeroacoustics issues, Ref. [31], and the management of multiple modules, Ref. [32].

tions 2.3 and 3.1.

[2]This material is included as an appendix, and not in the main body of this work, simply in order to avoid confusion for the reader, that is, in order to emphasize that the natural velocity decomposition is not used for this material. Rather, this is to be considered as a first step in that direction.

Appendix A

Transonic Aerodynamics

It should be pointed out, first of all, the motivation that lead to simulate numerically transonic flow fields through a full-potential scheme solved via boundary integral formulation. First of all, we should underline that this choice has to be seen as a first necessary preliminary activity towards the inclusion of transonic analysis in the framework presented in the main body of the thesis. Indeed, the *natural velocity decomposition* might be used to evaluate the vorticity induced in the flow field due to the shock. Moreover, as already introduced in Appendix B, within the framework of *FRIDA* in which MDO analysis have been conducted, the aerodynamic models are all based on boundary integral formulations applied both to compressible and incompressible potential flows. In order to enrich this discipline through an improvement in detecting critical issues connected with transonic effects,[1] a broadening of the formulations already implemented has been conducted.

Methodologically such an analysis may be carried out using different approaches. Specifically the simulation of transonic flow, for a non viscous and non conductive fluid, is usually performed, with adequate computational resources and costs in terms of time, via computational fluid dynamics. The typical CFD models include finite difference techniques, finite volume techniques and finite element techniques. However, the problem indicated above, may be efficiently addressed also through an integral method and a simulation performed on the basis of a full-potential method solved by boundary integral equation could be effective also while addressing MDO analysis and in particular aeroelastic analysis (see Ref. [33]).

Hence, an irrotational and isentropic flow field is, if the fluid is compressible and non viscous,

[1] Such as the presence of shock waves arising on the wing span, generating a sudden and sharp variation while evaluating aerodynamic loads and inducing structural vibrations.

completely described by the full potential formulation. The convenience in such an approach is due to the possibility of evaluating a single scalar field, even though it is not possible to detect, at now, entropy and vorticity variations. It has been widely demonstrated that this inconvenience is acceptable when evaluating unsteady aerodynamic loads if the wing vibrations, in cruise, are limited and if the airfoil is thin. In this case the vorticity is bound in a thin region and the shock waves, if present, are weak.[2] In the following the theoretical formulation used in this work is briefly addressed. It should be noted that only steady transonic analysis have been performed.

A.1 Theoretical formulation

Let us consider an inviscid and non-conducting fluid and, in addition, the flow field is isentropic and irrotational. The problem addressed is, thus, formulated in terms of potential perturbation velocity φ, such that $\mathbf{v}(\mathbf{x}) = \nabla\varphi(\mathbf{x})$.

According to these hypotheses, the governing equations are the continuity equation

$$\frac{\mathrm{D}\rho}{\mathrm{D}t} + \rho\nabla\cdot\mathbf{v} = 0 \tag{A.1}$$

the Euler equation

$$\frac{\mathrm{D}\mathbf{v}}{\mathrm{D}t} = -\frac{1}{\rho}\nabla p \tag{A.2}$$

and the entropy evolution equation

$$\frac{\mathrm{D}S}{\mathrm{D}t} = 0 \tag{A.3}$$

It is known that, provided that no shock waves arise in the flow field, a flow initially isentropic and irrotational remains isentropic and quasi-potential at all times. For quasi-potential flows Eq. A.1 reads

$$\frac{\mathrm{D}\rho}{\mathrm{D}t} + \rho\nabla^2\varphi = 0 \qquad (\mathbf{x}\in\mathcal{V}/\mathcal{S}_W) \tag{A.4}$$

Using the Lagrange expression for acceleration $\mathrm{D}\mathbf{v}/\mathrm{D}t = \partial\mathbf{v}/\partial t + \frac{1}{2}\nabla v^2 + \boldsymbol{\zeta}\times\mathbf{v}$, where $\mathbf{v} = \nabla\varphi$, Eq. A.1 yields

$$\nabla\left(\frac{\partial\varphi}{\partial t} + \frac{1}{2}v^2 + h\right) = 0 \tag{A.5}$$

[2]Further details could be find in Refs. [33] and [34].

which implies that the term in parenthesis is a function of time to be obtained by the conditions at infinity. Thus, we obtain the Bernoulli theorem in the airframe:

$$\frac{\partial \varphi}{\partial t} + \frac{1}{2}v^2 + h = h_\infty \qquad (\mathbf{x} \in \mathcal{V}/\mathcal{S}_W) \tag{A.6}$$

Recalling that for isentropic flows $dh = dp/\rho$ and $p = p(\rho)$, we obtain

$$\frac{\mathrm{D}h}{\mathrm{D}t} = \frac{1}{\rho}\frac{\mathrm{D}p}{\mathrm{D}t} = \frac{1}{\rho}\frac{\mathrm{d}p}{\mathrm{d}t}\frac{\mathrm{D}\rho}{\mathrm{D}t} \tag{A.7}$$

Combining Eqs. A.7, A.6 and A.4, we obtain, in the airframe, a nonlinear wave equation[3]

$$\nabla^2\varphi = \frac{1}{a^2}\frac{\mathrm{D}_\mathrm{C}^2\varphi}{\mathrm{D}t^2} \tag{A.8}$$

where

$$a(\mathbf{x}, t) = \sqrt{\frac{\mathrm{d}p}{\mathrm{d}\rho}} \tag{A.9}$$

is the speed of sound in a point $\mathbf{x}$ at the current time t.[4]

Moreover, the speed of sound may be expressed in terms of the potential perturbation φ through the representation for ideal gases with constant specific heats. Using isentropic transformations laws and recalling that $p/p_\infty = (\rho/\rho_\infty)^\gamma$, $R = c_p - c_v$, $\gamma = c_p/c_v$ and $h = \gamma\rho/(\gamma-1)\rho$, we have

$$\frac{\rho}{\rho_\infty} = \left(\frac{h}{h_\infty}\right)^{\frac{1}{\gamma-1}} \tag{A.10}$$

Substituting in Eq. A.6 yields

$$\frac{\rho}{\rho_\infty} = \left[1 - \frac{1}{h_\infty}\left(\frac{\partial \varphi}{\partial t} + \frac{1}{2}v^2\right)\right]^{\frac{1}{\gamma-1}} \tag{A.11}$$

which is the desired relationship between density and potential perturbation. Substituting Eqs. A.9 and A.11 into Eq. A.8, isolating on the left the wave operator and equating to the sources terms,[5] one obtains

$$\nabla^2\varphi - \frac{1}{a_\infty^2}\frac{\partial^2\varphi}{\partial t^2} = \sigma \tag{A.12}$$

[3]The expression of non-linear terms is addressed in the following (see Eqs. A.11 and A.13).

[4]It should be noted that $\frac{\mathrm{D}_\mathrm{C}}{\mathrm{D}t} = \frac{\partial}{\partial t} + \mathbf{v}_\mathrm{C}\cdot\nabla$ and that it represents a time derivative following a point having constant velocity $\mathbf{v}_\mathrm{C}$ (i.e. an inertial frame of reference having velocity $\mathbf{v}_\mathrm{C} = \mathbf{v}(\mathbf{x}, t)$).

[5]For details on this approach, see Refs. [3], [34] and [36].

where

$$\sigma \;=\; \nabla\cdot\left[\left(1-\frac{\rho}{\rho_\infty}\right)\nabla\varphi\right]+\frac{\partial}{\partial t}\left(-\frac{\rho}{\rho_\infty}-\frac{1}{a_\infty^2}\frac{\partial\varphi}{\partial t}\right) \tag{A.13}$$

To complete the problem described by the above equations, we introduce the appropriate boundary conditions, which are:

- the no–slip boundary condition on the boundary surface $\mathcal{S}$

$$\mathbf{v}(\mathbf{x},t)=\frac{\partial\varphi}{\partial n}=\mathbf{v}_B(\mathbf{x},t)\qquad(\mathbf{x}\in\mathcal{S}) \tag{A.14}$$

- the boundary condition at infinity

$$\varphi\to 0\qquad(\|\mathbf{x}\|\to\infty) \tag{A.15}$$

- the boundary condition on the wake

$$\frac{\mathrm{D}_{\mathrm{W}}}{\mathrm{D}t}\Delta\varphi=0\qquad(\|\mathbf{x}\|\to\infty) \tag{A.16}$$

as well as initial conditions

$$\varphi(\mathbf{x},0)=0,\qquad\dot\varphi(\mathbf{x},0)=0 \tag{A.17}$$

In this thesis, the numerical results are limited to steady state applications (of course, in a body frame of reference in uniform translation with velocity $\mathbf{v}_B=-u_\infty\mathbf{i}$). Then, Eqs. A.12, A.13 and A.11, reduce to

$$\nabla^2\varphi-\frac{u_\infty^2}{a_\infty^2}\frac{\partial^2\varphi}{\partial x^2}=\sigma \tag{A.18}$$

where

$$\sigma=\nabla\cdot\left[\left(1-\frac{\rho}{\rho_\infty}\right)\nabla\varphi\right]-u_\infty\frac{\partial}{\partial x}\left(\frac{\rho}{\rho_\infty}+\frac{u_\infty}{a_\infty^2}\frac{\partial\varphi}{\partial x}\right) \tag{A.19}$$

$$\frac{\rho}{\rho_\infty}=\left[1-\frac{1}{h_\infty}\left(u_\infty\frac{\partial\varphi}{\partial x}+\frac{v^2}{2}\right)\right]^{1/(\gamma-1)} \tag{A.20}$$

The boundary integral representation in this case is[6]

$$E(\check{\mathbf{x}})\varphi(\check{\mathbf{x}},t)=\oint_{\check{\mathcal{S}}_{\mathrm{B}}}\left(\frac{\partial\varphi}{\partial\check{n}}\check{G}-\varphi\frac{\partial\check{G}}{\partial\check{n}}\right)\mathrm{d}\check{\mathcal{S}}(\check{\mathbf{y}})-\int_{\check{\mathcal{S}}_{\mathrm{W}}}\Delta\varphi\frac{\partial\check{G}}{\partial\check{n}}\mathrm{d}\check{\mathcal{S}}(\check{\mathbf{y}})+\int_{\check{\mathcal{V}}_{\mathrm{F}}}\sigma\check{G}\mathrm{d}\check{\mathcal{V}}(\check{\mathbf{y}}) \tag{A.21}$$

[6]The approach is methodologically equivalent to the one used in Section 2.2.3.

where $\check{}$ denotes the Prandtl-Glauert space, having coordinates $\check{x}_1 = x_1/\beta$, $\check{x}_2 = x_2$ and $\check{x}_3 = x_3$, being $\beta = \sqrt{1 - M^2}$; in addition, $\check{G} = -1/4\pi\check{r}$, with $\check{r} = \|\check{\mathbf{x}} - \check{\mathbf{y}}\|$. Since in the perturbation potential representation appears its gradient, see Eq. A.19, its evaluation should be coupled to the evaluation of the perturbation velocity.

Thus, the velocity perturbation is achieved by taking the gradient of Eq. A.21. This represents the key of this approach. The objective is to evaluate, in the physical space, the value of the perturbation velocity $\mathbf{v} = \nabla_{\mathbf{x}}\varphi(\mathbf{x})$ without using a finite different scheme. This kind of approach prevents the introduction of the so-called *artificial viscosity* or *artificial compressibility* due to the use of finite difference when evaluating the field contribution.[7]

Akin to the approach already introduced in this dissertation, Eq. A.21 is the boundary integral representation for φ in terms of φ and $\partial\varphi/\partial n$ on $\mathcal{S}_{\text{B}}$, $\Delta\varphi$ on $\mathcal{S}_{\text{W}}$ and σ in $\mathcal{V}_{\text{F}}$. To identify φ on the body contour, a limit for $\mathbf{x} \in \mathcal{V}_{\text{F}}$ tending to $\mathbf{x} \in \mathcal{S}_{\text{B}}$ is performed. The consequent boundary integral equation represents a compatibility relationship between φ and $\partial\varphi/\partial n$ on $\mathcal{S}_{\text{B}}$, $\Delta\varphi$ on $\mathcal{S}_{\text{W}}$ and σ in $\mathcal{V}_{\text{F}}$. Moreover it should be noted that, being $\sigma \neq 0$, its value may be achieved once $\mathbf{v} = \nabla_{\mathbf{x}}\varphi$ has been evaluated.

A.1.1 On the modelling of field contribution

For the sake of simplicity, in the following, the overscript $\check{}$ is dropped.

The general expression of the nonlinear contribution in Eq. A.21 is

$$\int_{\mathcal{V}_{\text{F}}} G\sigma \mathrm{d}\mathcal{V} \tag{A.22}$$

which identifies a source three dimensional distribution. For further considerations a new expression of this distribution is now introduced

$$\sigma = \nabla \cdot \mathbf{b} + u_\infty \frac{\partial \hat{b}}{\partial x} = \nabla \cdot \check{\mathbf{b}} \tag{A.23}$$

where

$$\mathbf{b} = \left(1 - \frac{\rho}{\rho_\infty}\right) \nabla\varphi \qquad \hat{b} = \left(-\frac{\rho}{\rho_\infty} - \frac{u_\infty}{a_\infty^2}\frac{\partial\varphi}{\partial x}\right) \tag{A.24}$$

[7] See Ref. [34].

and

$$\check{\mathbf{b}} = \left\{ \begin{array}{c} b_x + u_\infty \hat{b} \\ b_y \\ b_z \end{array} \right\} \tag{A.25}$$

There are two different approach to model the source term in Eq. A.21

1. the term may be directly evaluated

$$\int_{\mathcal{V}_{\mathrm{F}}} G\sigma \mathrm{d}\mathcal{V} = \int_{\mathcal{V}_{\mathrm{F}}} G\nabla_{\mathbf{y}} \cdot \check{\mathbf{b}} \mathrm{d}\mathcal{V} \tag{A.26}$$

2. the term may be integrated by parts and then evaluated

$$\int_{\mathcal{V}_{\mathrm{F}}} G\sigma \mathrm{d}\mathcal{V} = -\oint_{\mathcal{S}_{\mathrm{B}}} \mathbf{n} \cdot \check{\mathbf{b}} G d\mathcal{S} - \int_{\mathcal{V}_{\mathrm{F}}} \check{\mathbf{b}} \cdot \nabla_{\mathbf{y}} G \mathrm{d}\mathcal{V} \tag{A.27}$$

The same approach may be followed while modelling the volume integral term in the velocity equation

$$\int_{\mathcal{V}_{\mathrm{F}}} \nabla_{\mathbf{x}} G\sigma \mathrm{d}\mathcal{V} \tag{A.28}$$

1. the term may be directly evaluated

$$\int_{\mathcal{V}_{\mathrm{F}}} \nabla_{\mathbf{x}} G\sigma \mathrm{d}\mathcal{V} = \int_{\mathcal{V}_{\mathrm{F}}} \nabla_{\mathbf{x}} G\nabla_{\mathbf{y}} \cdot \check{\mathbf{b}} \mathrm{d}\mathcal{V} \tag{A.29}$$

2. the term may be integrated by parts and then evaluated

$$\int_{\mathcal{V}_{\mathrm{F}}} \nabla_{\mathbf{x}} G\sigma \mathrm{d}\mathcal{V} = -\oint_{\mathcal{S}_{\mathrm{B}}} \mathbf{n} \cdot \check{\mathbf{b}} \nabla_{\mathbf{x}} G d\mathcal{S} - \int_{\mathcal{V}_{\mathrm{F}}} \check{\mathbf{b}} \cdot \nabla_{\mathbf{x}} \nabla_{\mathbf{y}} G \mathrm{d}\mathcal{V} \tag{A.30}$$

A.2 Numerical formulation

Akin to what already presented, the boundary element method is the numerical scheme used to discretize boundary integral representation method. In this case a piece-wise constant approximation is used both for surface integral evaluation and for field ones. Dividing $\mathcal{S}_{\mathrm{B}}$ in M elements, $\mathcal{S}_m$, $\mathcal{S}_{\mathrm{W}}$ in N elements, $\mathcal{S}'_n$ and $\mathcal{V}_{\mathrm{F}}$ in Q elements, $\mathcal{V}_q$, one obtains

$$\varphi(\mathbf{x}) = \varphi(\mathbf{x}_m) \qquad \mathbf{x} \in \mathcal{S}_m \tag{A.31}$$

$$\chi(\mathbf{x}) = \chi(\mathbf{x}_m) \qquad \mathbf{x} \in \mathcal{S}_m \tag{A.32}$$

$$\Delta\varphi(\mathbf{x}) = \varphi(\mathbf{x}_n) \qquad \mathbf{x} \in \mathcal{S}'_n \tag{A.33}$$

$$\sigma(\mathbf{x}) = \varphi(\mathbf{x}_q) \qquad \mathbf{x} \in \mathcal{V}_q \tag{A.34}$$

This yields:

1. The boundary integral representation for φ with volume contribution evaluated directly

$$E_k\varphi_k = \sum_{m=1}^{M} B_{km}\chi_m + \sum_{m=1}^{M} C_{km}\varphi_m + \sum_{n=1}^{N} F_{kn}\Delta\varphi_n + \sum_{q=1}^{Q} H_{kq}\sigma_q \tag{A.35}$$

where

$$B_{km} = \int_{\mathcal{S}_m} G_k \mathrm{d}\mathcal{S} \qquad C_{km} = -\int_{\mathcal{S}_m} \frac{\partial G_k}{\partial n}\mathrm{d}\mathcal{S} \tag{A.36}$$

$$F_{kn} = -\int_{\mathcal{S}'_n} \frac{\partial G_k}{\partial n}\mathrm{d}\mathcal{S} \qquad H_{kq} = \int_{\mathcal{V}_q} G_k \mathrm{d}\mathcal{V} \tag{A.37}$$

with $G_k = G(\mathbf{x}_k, \mathbf{y})$, $\mathbf{x}_k$ being the collocation point,

2. The boundary integral representation for φ with field contribution integrated by parts

$$E_k\varphi_k = \sum_{m=1}^{M} B_{km}\check{\chi}_m + \sum_{m=1}^{M} C_{km}\varphi_m + \sum_{n=1}^{N} F_{kn}\Delta\varphi_n + \sum_{q=1}^{Q} \mathbf{h}_{kq}\cdot\check{\mathbf{b}} \tag{A.38}$$

where $\check{\chi}_m = \chi(\mathbf{x}_m) - \mathbf{n}(\mathbf{x}_m)\cdot\check{\mathbf{b}}(\mathbf{x}_m)$ and

$$B_{km} = \int_{\mathcal{S}_m} G_k \mathrm{d}\mathcal{S} \qquad C_{km} = -\int_{\mathcal{S}_m} \frac{\partial G_k}{\partial n}\mathrm{d}\mathcal{S} \tag{A.39}$$

$$F_{kn} = -\int_{\mathcal{S}_n} \frac{\partial G_k}{\partial n}\mathrm{d}\mathcal{S} \qquad \mathbf{h}_{kq} = -\int_{\mathcal{V}_q} \nabla G_k \mathrm{d}\mathcal{V} \tag{A.40}$$

The same approximation has been applied on Eqs. A.29 and A.27, yielding

1. perturbation velocity with field contribution directly evaluated

$$E_k\nabla_{\mathbf{x}}\varphi_k = \sum_{m=1}^{M} \mathbf{b}_{km}\chi_m + \sum_{m=1}^{M} \mathbf{c}_{km}\varphi_m + \sum_{n=1}^{N} \mathbf{f}_{kn}\Delta\varphi_n + \sum_{q=1}^{Q} \mathbf{h}'_{kq}\sigma_q \tag{A.41}$$

where

$$\mathbf{b}_{km} = \int_{\mathcal{S}_\mathrm{m}} \nabla_{\mathbf{x}} G_k \mathrm{d}\mathcal{S} \qquad \mathbf{c}_{km} = -\int_{\mathcal{S}_\mathrm{m}} \nabla_{\mathbf{x}} \frac{\partial G_k}{\partial n}\mathrm{d}\mathcal{S} \tag{A.42}$$

$$\mathbf{f}_{kn} = -\int_{\mathcal{S}_\mathrm{n}} \nabla_{\mathbf{x}} \frac{\partial G_k}{\partial n}\mathrm{d}\mathcal{S} \qquad \mathbf{h}'_{kq} = \int_{\mathcal{V}_\mathrm{q}} \nabla_{\mathbf{x}} G_k \mathrm{d}\mathcal{V} \tag{A.43}$$

2. The perturbation velocity with field contribution integrated by parts and then evaluated

$$E_k\nabla_{\mathbf{x}}\varphi_k = \sum_{m=1}^{M} \mathbf{b}_{km}\check{\chi}_m + \sum_{m=1}^{M} \mathbf{c}_{km}\varphi_m + \sum_{n=1}^{N} \mathbf{f}_{kn}\Delta\varphi_n + \sum_{q=1}^{Q} \mathbf{H}_{kq}\cdot\check{\mathbf{b}}_q \tag{A.44}$$

where

$$\mathbf{b}_{km} = \int_{\mathcal{S}_{\mathrm{m}}} \nabla_{\mathbf{x}} G_k \mathrm{d}\mathcal{S} \qquad \mathbf{c}_{km} = -\int_{\mathcal{S}_{\mathrm{m}}} \nabla_{\mathbf{x}} \frac{\partial G_k}{\partial n} \mathrm{d}\mathcal{S} \tag{A.45}$$

$$\mathbf{f}_{kn} = -\int_{\mathcal{S}_{\mathrm{n}}} \nabla_{\mathbf{x}} \frac{\partial G_k}{\partial n} \mathrm{d}\mathcal{S} \qquad \mathbf{H}_{kq} = \nabla_{\mathbf{x}} \int_{\mathcal{V}_{\mathrm{q}}} \nabla_{\mathbf{x}} G_k \mathrm{d}\mathcal{V} \tag{A.46}$$

It should be underlined that, to avoid singularities while evaluating field integrals, a mixed scheme has been chosen. Specifically the integrated by parts approach has been implemented, but in the case in which control point and evaluating one coincide in the field.

A.3 Numerical results

The formulation already presented has been applied to the analysis of steady two-dimensional flows in order to provide an exhaustive comparison with numerical data coming from Ref. [34]. It should be noted that two-dimensional results are obtained via the three-dimensional formulation already introduced, considering very high aspect ratio. Moreover, we should mention the steady results concerning Ref. [34] are achieved by marching in time, whereas within this approach the steady-state is imposed a priori.

A.3.1 Subcritical flows

The nonlinear potential model has been validated in a subcritical case simulating a flow around a circular cylinder at $M = 0.38$. However, as depicted in Fig. A.1, the effect of the nonlinear terms is strong. Specifically we can observe that the present method is in good agreement with the results provided by the formulation of Ref. [34], already compared with the corresponding Euler solutions, Refs. [37] and [38].[8] Moreover, a comparison with the corresponding BEM linear solution is depicted.

[8] See for comparison Ref. [34].

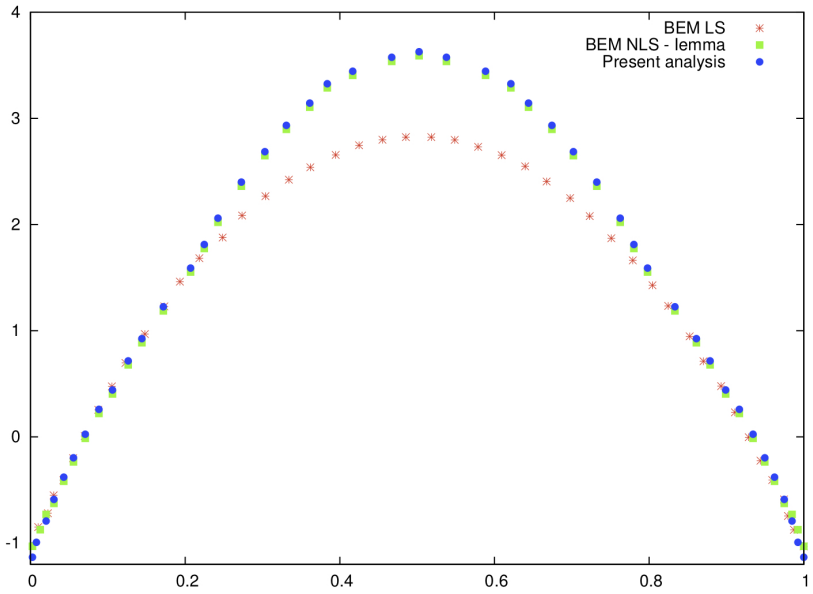

Figure A.1: Pressure coefficient along the cylinder boundary.

A.3.2 Supercritical flows

In order to show that this formulation may capture sharp shock, when they occur, in Fig. A.2 we show the pressure distribution on a cylinder at $M = 0.5$. The comparison is between the present approach, the one of Ref. [34], already compared with a finite volume full-potential solution due to Ref. [39].[9]

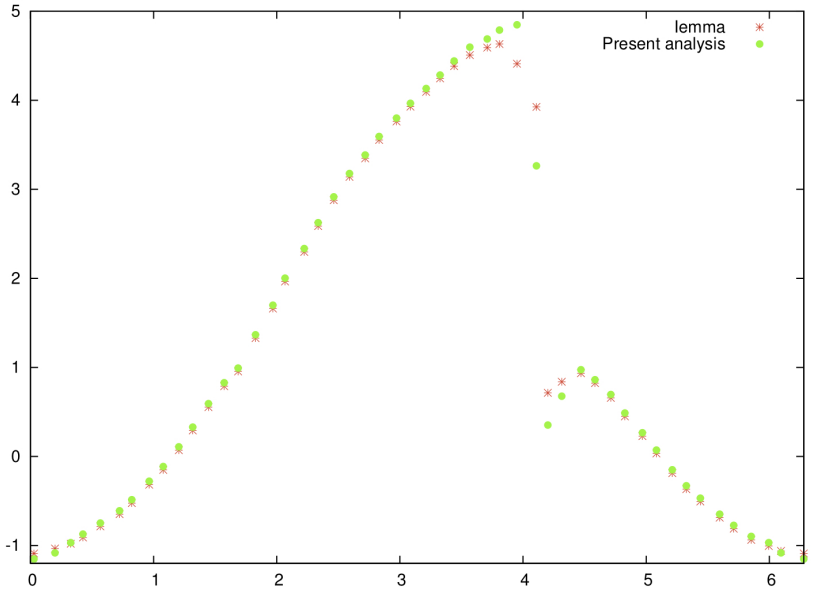

Figure A.2: Pressure coefficient along the cylinder boundary.

[9]Such a compare is provided in Ref. [34].

A.4 Comments

In this chapter we presented a transonic analysis performed through a boundary integral method. Specifically the key approach utilized is the new formulation to detect the velocity field, along with a new expression for the nonlinear terms (see Section A.1.1). The numerical results provided are obtained in two-dimensional as a limit of the three-dimensional one. They are in good agreement with the corresponding numerical data available in literature. Moreover we achieved these results without using any artificial viscosity/compressibility correction due to the new method used to evaluate the velocity field.

Such an approach appears appealing due to it is possible application in MDO context.

Appendix B

Multidisciplinary Design Optimization

We have already mentioned that the present work, specifically the issues addressed in Chapters 2 and 3, and in Appendix A may be seen within the context of an algorithm of multidisciplinary optimization for conceptual design of civil aircraft.[1] In order to illustrate this connection, in this Appendix we describe the MDO algorithm used, i.e. *FRIDA*, along with some of the results obtained, in particular in the module concerning aeroacoustics. Of particular interest is the issue of multi-level optimization, whereby models of different level of sophistication and complexity are combined, so as to achieve the accuracy of the more sophisticated models, without a major increase of the required computational time, with respect to the simpler model formulation. The corresponding activity is presented in the following. Specifically we present two analyses, one oriented towards aeroacoustics issues, Ref. [31], and the other to the management of multiple modules, Ref. [32].

B.1 Aircraft Analysis Models Used in *FRIDA*

In this section, we provide the reader an overview of the overall algorithm used for the aircraft design optimization. The analysis modules included in *FRIDA* (FRamework for Innovative Design in Aeronautics) to describe the complete mechanics of the aircraft deal with the structural dynamics, the aerodynamics, the aeroelasticity and the mechanics of flight. The models used are, whenever possible, prime-principle based so that the whole optimization algorithm can be used for the analysis of innovative configurations for which the designer can not rely on past experience.

[1] Each formulation is relevant even if considered as a stand-alone.

The theoretical models underlying the algorithms implemented are outlined in the following. The interested reader is addressed to Morino *et al.*[40], Iemma *et al.*[41], and Iemma and Diez [42].

B.1.1 Structural Analysis

The model used for the structural analysis of the wing is a three-dimensional bending-torsional beam, with structural and geometric parameters varying in the spanwise direction. These include structural element geometric dimensions (rib area, spar and skin panel thickness, etc.), wing twist, mass properties plus bending and torsional moments of inertia. Moreover, clamped boundary conditions are considered at root in order to take into account the wing-fuselage junction. Indicating with $\Psi_j(\mathbf{x})$ a set of FEM base functions, the elastic displacements can be written as

$$\mathbf{u}(\mathbf{x},t) = \sum_{j=1}^{N} u_j(t)\boldsymbol{\psi}_j(\mathbf{x}) \tag{B.1}$$

where $\mathbf{x}$ are the undisturbed spacial Cartesian coordinates, and $u_j(t)$ are the parameters - state variables - chosen to define the function $\mathbf{u}(\mathbf{x},t)$ (three displacements, two slopes and the twist angle at each node). Using the Galerkin method, *i.e.*, projecting in the direction of the base function $\boldsymbol{\psi}_j(\mathbf{x})$, one obtains

$$\mathsf{M}\ddot{\mathsf{u}} + \mathsf{K}\mathsf{u} = \mathsf{f} \tag{B.2}$$

where $\mathsf{u} = \{u_i\}$ is the state-space vector, whereas $\mathsf{f} = \{f_j\}$ is the external load vector. Eq. B.2 is used for the static analysis of the structure for vanishing inertial terms, to yield $\mathsf{K}\mathsf{u} = \mathsf{f}$ at the equilibrium. In addition, in the dynamic analysis we evaluate the approximate modes of vibration of the structure through the eigenproblem

$$-\omega_n^2 \mathsf{M}\mathsf{z}_n + \mathsf{K}\mathsf{z}_n = \mathbf{0} \tag{B.3}$$

where ω_n ($n = 1, ..., N$) denotes the n-th natural frequency, corresponding to the n-th eigenvector, $\mathsf{z}_n = \{z_{n_i}\}$, here assumed to be normalized so that the so-called generalized masses equal one. The solution of this eigenproblem is used to qualify the dynamics of the wing using a modal approach. The resulting Lagrange equations of motion are

$$\ddot{\mathsf{q}} + \Omega^2 \mathsf{q} = \mathsf{e} \tag{B.4}$$

where q denotes the Lagrangian-coordinate vector, Ω the diagonal matrix of the wing natural frequencies, and $\mathsf{e} = \{e_n\}$ the vector of the generalized forces,

$$e_n = -\oint_{S_B} p\mathbf{n} \cdot \Phi_n d\mathcal{S} \tag{B.5}$$

where Φ_n are the approximate natural modes.

B.1.2 Aerodynamics

The physical model used for aerodynamics is that of compressible quasi-potential flows, *i.e.*, flows that are potential everywhere except for the wake surface, $S_{_W}$, enriched by a boundary-layer integral model to take into account the effects of viscosity, and provide an adequate estimate of the viscous drag. Here we limit the discussion to incompressible flows - only for clarity - but compressible version is already available for the analysis. Considering the wake geometry fixed in a frame of reference connected with the wing, the velocity potential at any point $\mathbf{x} \in \mathcal{V}$, can be expressed by means of a boundary integral equation

$$\varphi(\mathbf{x}, t) = \int_{S_{_B}} \left(G\chi - \varphi \frac{\partial G}{\partial n} \right) \mathrm{d}\mathcal{S}(\mathbf{y}) - \int_{S_{_W}} \left[\Delta\varphi_{_{TE}}\right]^{\tau} \frac{\partial G}{\partial n} \mathrm{d}\mathcal{S}(\mathbf{y}) \tag{B.6}$$

where $G = -1/4\pi\|\mathbf{y} - \mathbf{x}\|$ and $[\cdot]^{\tau}$ indicated evaluation at the retarded time $t - \tau$. The above equation is completed by the boundary conditions on the body surface $S_{_B}$ (impermeability)

$$\frac{\partial \varphi}{\partial n} =: \chi = \chi_{_B} := \mathbf{v}_{_B} \cdot \mathbf{n} \quad (\mathbf{x} \in S_{_B}) \tag{B.7}$$

and on the wake $S_{_W}$ (vorticity convection in terms of velocity potential jump at the trailing edge)

$$\Delta\varphi(\mathbf{x}_{_W}, t) = \Delta\varphi(\mathbf{x}_{_{TE}}, t - \tau) \tag{B.8}$$

where τ is the convection time from $\mathbf{x}_{_{TE}}$ to $\mathbf{x}_{_W}$. The numerical solution of Eq. B.6 in the frequency domain is obtained by Laplace-transforming ($\tilde{\cdot}$ indicates Laplace transform) and applying a BEM discretization, to yield

$$\tilde{\mathsf{f}}_{\varphi} = \mathsf{E}_{_{IE}}(s)\tilde{\mathsf{f}}_{\chi} \tag{B.9}$$

The vectors $\tilde{\mathsf{f}}_{\varphi} = \{\tilde{\varphi}_j\}$, and $\tilde{\mathsf{f}}_{\chi} = \{\tilde{\chi}_j\}$ collect the values of the velocity potential, $\tilde{\varphi}$, and its normal derivative, $\tilde{\chi}$, at the centers of the surface elements, and s is the Laplace variable (see Morino [43] and Morino [44] for details).

Note that, in Eq. B.6, the boundary conditions χ can include the effect of the boundary-layer in form of a transpiration velocity. The latter is evaluated following the method presented in Morino *et al.*[45], which is not presented here for the sake of compactness. The use of a boundary layer correction allows for an estimate of the viscous contribution to the aerodynamic drag, which is important in the flight mechanics and performance analysis. The level of accuracy of such a formulation is satisfactory in civil aviation applications, since the flow is typically attached. Viscous effects are not included in the aeroelastic analysis.

B.1.3 Aeroelasticity

The aeroelastic feedback generated by the interaction between unsteady aerodynamics and structural dynamics is also taken into account in the present formulation. Under the assumption of linear unsteady aerodynamics, the relationship between the structural Lagrangian variables $\tilde{\mathsf{q}}$, and generalized forces $\tilde{\mathsf{e}}$ can be written as

$$\tilde{\mathsf{e}} = q_{_D}\, \mathsf{E}(\check{s})\, \tilde{\mathsf{q}} \tag{B.10}$$

where $\check{s} = s\ell/U_{_\infty}$ is the complex reduced frequency (*i.e.*, the dimensionless Laplace variable), $q_{_D}$ is the dynamic pressure, and the aerodynamic matrix $\mathsf{E}(\check{s})$ depends transcendentally on $\check{s}$, due to the presence of the convection and compressibility delays. In order to efficiently perform the aeroelastic analysis within the optimization procedure, a reduced order model (ROM) for $\mathsf{E}(\check{s})$ is introduced.

Specifically, following Morino *et al.*[46], the transcendental function $\mathsf{E}(\check{s})$ is approximated as

$$\mathsf{E}(\check{s}) \simeq \mathsf{E}_2\check{s}^2 + \mathsf{E}_1\check{s} + \mathsf{E}_0 + (\check{s}\mathsf{I} - \mathsf{P})^{-1}\,\mathsf{R} \tag{B.11}$$

where all the matrices on the right-hand side are evaluated by a least-square procedure starting from $\mathsf{E}(\check{s}_i)$, where $\check{s}_i$ is a suitable set of complex reduced frequencies. By doing this, the aeroelastic stability analysis can be reduced to the study of a root locus, thereby avoiding standard methods (*e.g.*, p-k method), which are somehow cumbersome and would unnecessarily complicate the optimization process (see Morino *et al.*[46] for details).

B.1.4 Flight Mechanics and Performances

The static longitudinal stability, an essential issue for aircraft, is satisfied by imposing that the derivative with respect to the angle of attack of pitch moment coefficient (evaluated with respect to the center of mass G) be less than zero: $C_{M_\alpha} < 0$ (static stability). This is performed by evaluating in the MDO process the global aerodynamic loads acting on the aircraft (evaluated via BEM) and the total mass distribution (so as to determine the location of G).

In order to evaluate fuel consumption, the mission profile considered in this work consists of: (i) take-off, (ii) climb, (iii) cruise, (iv) descent, and (v) landing. The range is computed according to the Breguet equation $R = (V_c E/c)\ln(W_i/W_f)$, where V_c is the cruise speed, c is the specific fuel consumption, $E = L/D$ is the aerodynamic efficiency (lift to drag ratio), and W_i and W_f the initial and final weights of the cruise segment, respectively. Finally, expressing the fuel consumptions for the mission segments before and during the cruise segment as fractions of the usable mission fuel weight F (indicated as k_1 and k_2, respectively), W_i and W_f can be written as: $W_i = W - k_1 F$ and $W_f = W - (k_1 + k_2)F$.

B.1.5 Aeroacoustics

The aeroacoustic modelling deserves a careful discussion. Indeed, on one hand, the prediction of the noise perceived at a specified location requires an accurate modelling of several physical phenomena. On the other hand, during a complete optimization process, each module can be called hundreds of times, and thus, a compromise between accuracy and computational efficiency is mandatory.

In this applications the noise emissions are computed using a simplified predictor which implements a noise-power-distance model build from experimental data.

B.2 Multidisciplinary design optimization oriented to noise alleviation

Within the first analysis an application of a formulation for Multidisciplinary Design Optimization for Conceptual Design (MDO-CD) of civil transportation aircraft is, however, presented. The aim of this work is to address aeroelastic issues in the context of optimal aircraft design. Specifically, the influence of the aeroelastic constraints on the optimal solutions is investigated by assuming different feasible subspaces (defined by different values of the minimum flutter/divergence speed). In other words, a sort of sensitivity analysis for the final configurations with respect to the aeroelastic limits is presented.

Moreover, different objective functions are taken into account during the optimization process.

The optimization is led for an extended range narrow body aircraft with over the wing mounted engines, which is characterized by a low environmental impact resulting in a low community noise due to the wing shielding.

Besides the alleviation effects on noise, mounting engines over the wing results in changing both aerodynamic interference and vibration dynamics of the *classical* wing system, modifying its aeroelastic characteristics, Ref. [47]. As the flutter speed decreases if the position of the engine goes behind the elastic axis, the aeroelastic constraint becomes crucial.

The optimization is performed using the analysis and optimization tool *FRIDA* (FRamework for Innovative Design in Aeronautics). The formulation implemented, Refs. [48] and [49] involves models for structures, aerodynamics, aeroelasticity, flight mechanics, propulsion and aeroacoustics. Life-cycle cost estimation is also included, Refs. [42], [48] and [50]. The main goal of the formulation is related to the assessment of innovative aircraft configurations, for which the designer cannot refers on past experience. Therefore, the algorithm used for the aircraft analysis are, whenever possible, prime-principle based. Specifically, the structural problem is solved using a finite element method (FEM), the aerodynamics is evaluated through a quasi-potential formulation for compressible flows, coupled with a boundary-layer integral model to take into account the effects of viscosity and to provide an adequate estimation of viscous drag. The aeroelastic analysis is performed by using a reduced-order model based on a finite-state approximation. The noise emissions are here evaluated by means of an empirical NPD (noise-power-distance) model enriched by a correction to take into account the wing shielding effects. A genetic algorithm coupled with a penalty function

method is finally used to find the (global) optimal solution, Ref. [51]. The multidisciplinary design optimization task is formulated as a constrained minimization problem of the type:

$$\begin{aligned} \text{minimize} \quad & f(x), \quad x \in \mathcal{A} \\ \text{subject to} \quad & h_m(x) = 0, \quad m = 1, ..., M \\ \text{and to} \quad & g_n(x) \leq 0, \quad n = 1, ..., N \end{aligned}$$

where f is the objective of the optimization task, h_m is the m-th equality constraint, g_n is the n-th inequality constraint and x is the variables (or design) vector. It may be noted that in a multidisciplinary design context, the above functions are generally evaluated by the simultaneous use of more than one discipline. In this work, the disciplines involved in the aircraft analysis are the following[2]

- structural analysis (static and dynamic);
- aerodynamic;
- aeroelasticity;
- flight mechanics;
- weights estimate and performances;
- aeroacoustics;

and the following objective functions are addressed:

$$\begin{aligned} f_1 &:= \text{structural weight} \\ f_2 &:= \text{fuel burn} \\ f_3 &:= \text{total aircraft life-cycle cost} \\ f_4 &:= \text{noise emissions} \end{aligned}$$

The feasible subspace for the variables vector is defined by the equality constraint

$$h_1(x) := W(x)/L(x) - 1 = 0 \tag{B.12}$$

[2]The models used for each discipline is briefly outlined in the followingB.1.

where W is the aircraft weight and L is the lift force, and by the inequality constraints

$$g_1(x) := \sigma(x)/\sigma_{max} - 1 \leq 0 \tag{B.13}$$

$$g_2(x) := \tau(x)/\tau_{max} - 1 \leq 0 \tag{B.14}$$

$$g_3(x) := U_{f,min}/U_f(x) - 1 \leq 0 \tag{B.15}$$

$$g_4(x) := U_{d,min}/U_d(x) - 1 \leq 0 \tag{B.16}$$

where σ is the normal stress arising in the structure, τ is the shear stress and U_f and U_d are the flutter and divergence speed respectively. In this work, the design variables pertain the wing system such as span, root and tip chord, root and tip thickness ratio, root and tip built-in angle of attack, sweep angle, panels and spars thickness, number of stringers, etc.

In the following, the optimization results of an extended range narrow body aircraft with over the wing mounted engines are shown. To the aim of this analysis, the engines are considered as concentrated masses (no aerodynamic effects are taken into account).

The aircraft category main features are outlined in Table B.1.

number of seats	160
payload, kg	18,000
max. range, nm	5,000
cruise Mach no.	0.80
number of engines	2
max thrust per engine, lb	30,000
engine weight, kg	3,000
engine placement	over the wing

Table B.1: Design configuration.

As mentioned above, four different objective functions are considered (wing structural weight, fuel burn, life-cycle cost, noise) and four separated single objective optimization tasks are performed. Specifically, noise emissions are evaluated while the aircraft is approaching in clean wing configuration (no high-lift devices used). The optimization procedure pertains only the wing system. The variables used during the minimization task are shown in Table B.2, whereas the relative feasible

subspaces are indicated in Tables B.3 and B.4. The two subspaces differ in the definition of the aeroelastic constraints (minimum flutter and divergence speed).

variable	lower b.	upper b.
span, m	20.00	60.00
root chord, m	5.00	10.00
tip chord, m	0.50	5.50
root t/c	0.10	0.20
tip t/c	0.04	0.10
root panel thickness, mm	0.5	10.00
tip panel thickness, mm	0.5	10.00
root spar thickness, mm	1.0	100.00
tip spar thickness, mm	1.0	100.00
root no. of stringers	12	40
tip no. of stringers	4	20
root built-in angle of attack, deg	0.00	8.00
tip built-in angle of attack, deg	0.00	8.00
sweep angle, deg	0.00	50.00

Table B.2: Variables vector.

Maximum normal stress constraint	$\sigma \leq 400$ MPa
Maximum shear stress constraint	$\tau \leq 400$ MPa
Flutter speed constraint	$U_F \geq 350$ m/s
Divergence speed constraint	$U_D \geq 350$ m/s

Table B.3: Design constraints for feasible subspace #1.

Maximum normal stress constraint	$\sigma \leq 400$ MPa
Maximum shear stress constraint	$\tau \leq 400$ MPa
Flutter speed constraint	$U_F \geq 250$ m/s
Divergence speed constraint	$U_D \geq 250$ m/s

Table B.4: Design constraints for feasible subspace #2.

The results for subspace #1 are summarized in Table B.5,[3] whereas the final configurations are depicted in Figures B.1-B.4.

It may be noted how the optimization tasks aimed at sustainability issues such as fuel burn and noise emissions go both towards the aeroelastic constraint limit for flutter speed.

Similar optimization procedures are then conducted in the feasible subset #2 characterized by more relaxed aeroelastic limits. The results for subspace #2 are shown in Table B.6 (again, bold face indicates the relevant objectives) with the relative final configurations depicted in Figures B.5-B.6. Figures B.7 and B.8 show the convergence history of the genetic algorithm for minimum fuel burn and minimum noise, moving the analysis in the different subspaces. It is worth noting that the adoption of more relaxed aeroelastic constrains allows for final solutions characterized by lower fuel burn and lower noise.

[3]Bold face indicates the relevant objectives.

	str. weight	fuel burn	LCC	noise
span, m	20.00	38.76	27.2	60.00
root chord, m	5.00	5.00	5.00	5.00
tip chord, m	3.00	0.50	0.50	0.71
root t/c	0.13	0.10	0.10	0.10
tip t/c	0.04	0.04	0.04	0.04
root panel thickness, mm	0.50	3.30	0.60	3.47
tip panel thickness, mm	0.50	5.76	0.51	0.91
root spar thickness, mm	1.00	6.50	1.39	2.55
tip spar thickness, mm	1.00	2.73	1.27	1.05
root no. of stringers	12	14	12	12
tip no. of stringers	4	4	4	4
root built-in angle of attack, deg	7.19	4.00	6.00	6.28
tip built-in angle of attack, deg	7.02	7.01	5.94	8.00
sweep angle, deg	6.85	39.06	19.48	11.63
wing structural weight, kg	**8,071**	13,219	**8,834**	14,031
fuel burn (5,000 nm), kg	24,287	**15,207**	**16,169**	39,843
Noise at 500 ft, SEL[dB]	94	91	92	**90**
aerodynamic efficiency (cruise, $M_\infty = 0.8$)	12.27	21.60	18.28	22.92
aerodynamic efficiency (approach, $M_\infty = 0.3$)	12.95	21.43	18.72	35.04
max. normal stress, MPa	100.05	179.67	125.37	308.50
max. shear stress, Mpa	387.14	89.98	399.75	272.83
futter speed, m/s	> 400.00	358.00	> 400.00	351.00
divergence speed	> 400.00	> 400.00	> 400.00	> 400.00

Table B.5: Optimized parameters for feasible subspace #1.

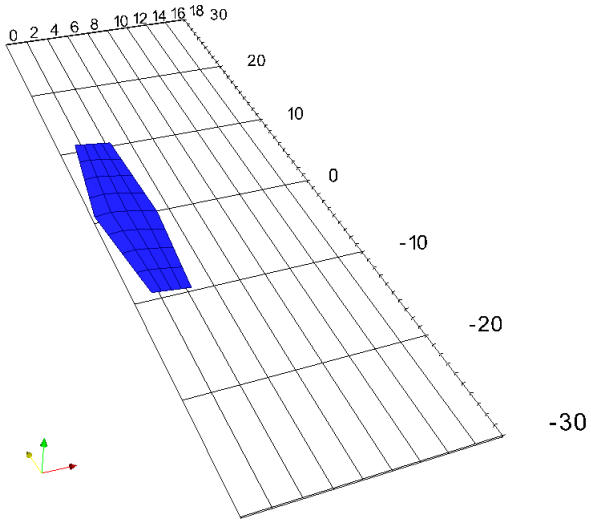

Figure B.1: Minimum wing structural weight solution for feasible subspace #1.

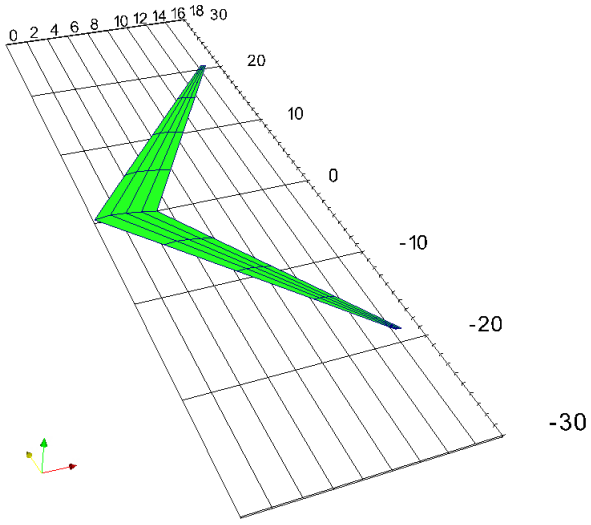

Figure B.2: Minimum fuel burn solution for feasible subspace #1.

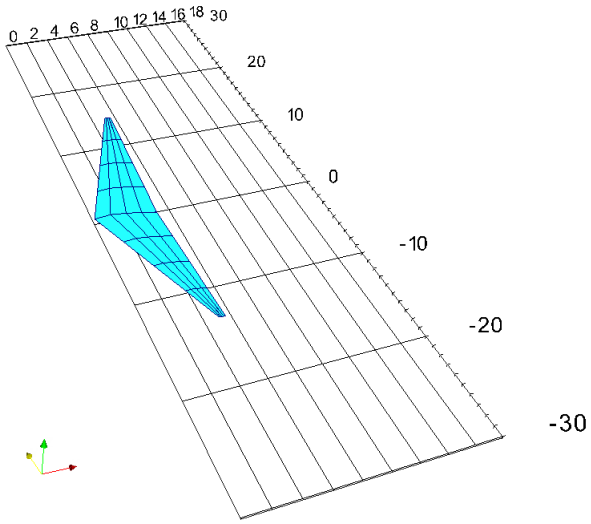

Figure B.3: Minimum life-cycle cost solution for feasible subspace #1.

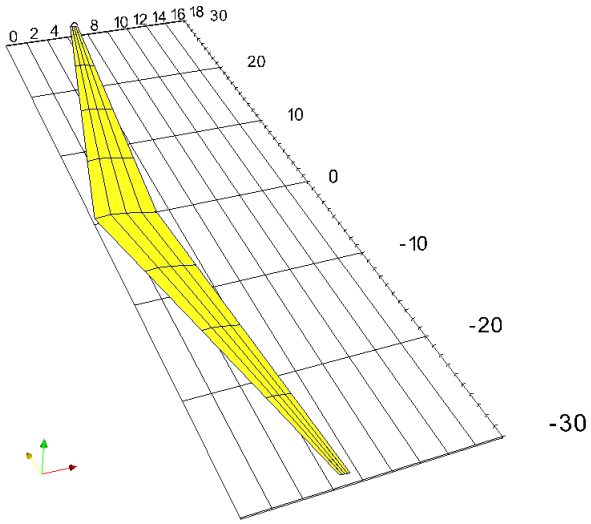

Figure B.4: Minimum noise solution for feasible subspace #1.

	fuel burn	noise
span, m	40.06	59,98
root chord, m	5.00	5.00
tip chord, m	0.50	0.68
root t/c	0.10	0.10
tip t/c	0.04	0.04
root panel thickness, mm	1.57	0.87
tip panel thickness, mm	2.15	1.82
root spar thickness, mm	1.80	1.22
tip spar thickness, mm	3.02	1.84
root no. of stringers	13	12
tip no. of stringers	5	4
root built-in angle of attack, deg	4.25	6.38
tip built-in angle of attack, deg	5.50	8.00
sweep angle, deg	37.49	10.97
wing structural weight, kg	12,122	12,733
fuel burn (5,000 nm), kg	**14,092**	40,509
Noise at 500 ft, SEL[dB]	90	**88**
aerodynamic efficiency (cruise, $M_\infty = 0.8$)	21.29	22.61
aerodynamic efficiency (approach, $M_\infty = 0.3$)	21.27	37.05
max. normal stress, MPa	214.28	385.50
max. shear stress, Mpa	205.77	382.34
futter speed, m/s	252.00	250.00
divergence speed	> 400.00	> 400.00

Table B.6: Optimized parameters for feasible subspace #2 (min. fuel burn and noise only).

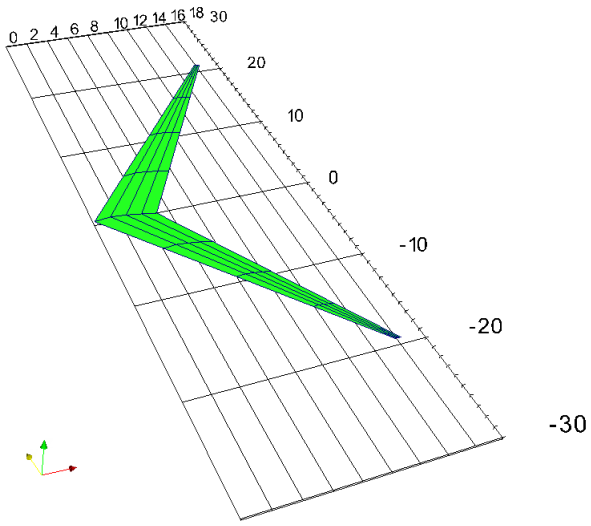

Figure B.5: Minimum fuel burn solution for feasible subspace #2.

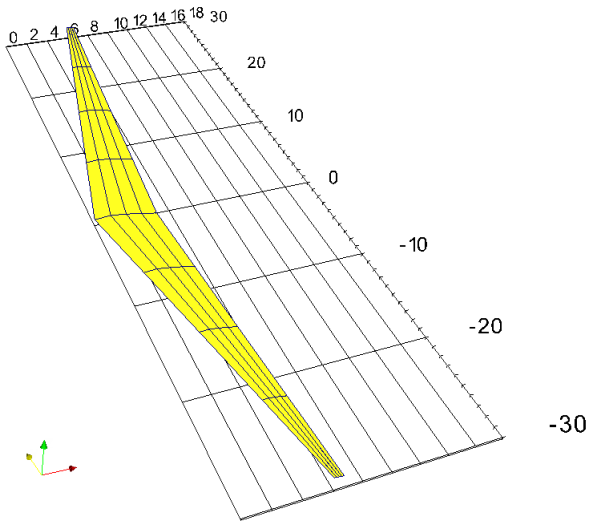

Figure B.6: Minimum noise solution for feasible subspace #2.

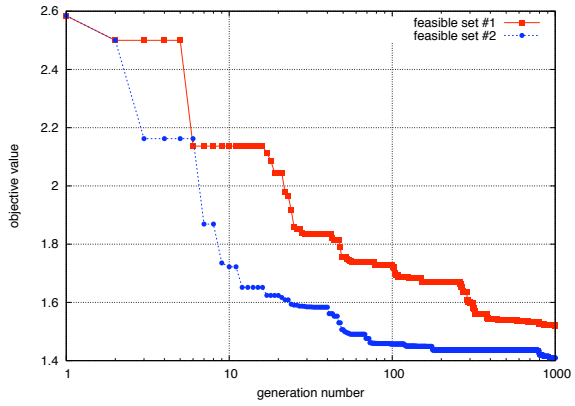

Figure B.7: Genetic algorithm convergence for the minimization of the fuel burn.

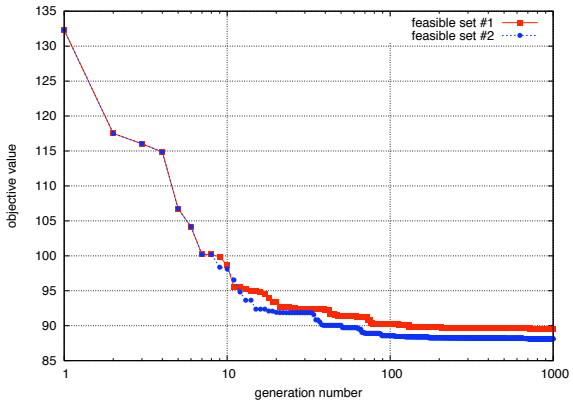

Figure B.8: Genetic algorithm convergence for the minimization of the noise.

B.3 A multi-fidelity formulation for multidisciplinary design optimization

Within the second work some preliminary results of a formulation for MDO for conceptual design of civil transportation aircraft are presented, specifically the formulation has been applied to the optimal design of a low environmental impact aircraft. The attention is focused on the use of multi-fidelity models to characterize all the relevant disciplines involved in the design process (Ref. [32]).

As a traditional multidisciplinary optimization process requires high computational resources and high costs in terms of time - each analysis module can be recalled hundreds of time during each optimization task - the use of multi-fidelity models can drastically reduce both the resources and the time required for the design process coupling

- high accuracy of high fidelity models;
- low computational costs of low-fidelity ones.

The models devote to integrated design comprise the following disciplines[4]

- static and dynamic structural analysis (modal analysis and stress analysis via FEM);
- steady and unsteady aerodynamic (BEM + viscous correction);
- aeroelasticity;
- flight mechanics;
- aeroacoustics;
- performances analysis.

It is worth underlining that the high-fidelity models are, whenever possible, *prime-principle based*, Ref. [52]. The whole analysis may be hence applied on innovative configurations for which the designer can not rely on past experience. The process of constrained minimization can be formalized as follows

$$\min_{\mathbf{x}} f(\mathbf{x}), \qquad \mathbf{x} \in D \tag{B.17}$$

[4]The models used for each discipline is briefly outlined in Section B.1.

(where f represents the objective function, $\mathbf{x}$ the design variables), with inequality constraints

$$g_n(\mathbf{x}) < 0, \;\; n = 1, .., N \tag{B.18}$$

and equality constraints

$$h_m(\mathbf{x}) = 0, \;\; m = 1, .., M \tag{B.19}$$

The objective function $f(\mathbf{x})$ can be modelled as

$$f(\mathbf{x}) := \sum_{k=1}^{K} \eta_k f_k(\mathbf{x}) \tag{B.20}$$

where f_k may describe different features, as structural weight, fuel burn, noise emission, ... and η_k are the relative weights, whereas the constraints the final layout has to satisfy, can be for example: normal stress $\sigma < \sigma_{max}$, or tangential stress $\tau < \tau_{max}$, or flutter speed $u < u_f$ or, however centering (balancing) $C_{M_\alpha} < 0$.

To resolve this kind of problem an *Approximation Model Management Optimization* has been employed. A first-order approximation, Ref. [53], of the high-fidelity model is based on the low-fidelity one, by imposing

$$a_c(\mathbf{x}_c) = f_{HI}(\mathbf{x}_c) \tag{B.21}$$

$$\nabla a_c(\mathbf{x}_c) = \nabla f_{HI}(\mathbf{x}_c) \tag{B.22}$$

The resulting model is assumed as a good approximation for the high-fidelity function within a *trust region* in which the minimization is performed.

A β-correlation is, then, introduced. Its definition reads

$$\beta(\mathbf{x}) = \frac{f_{HI}(\mathbf{x})}{f_{LO}(\mathbf{x})} \tag{B.23}$$

and a first-order Taylor expansion of $\beta(\mathbf{x})$

$$\beta_c(\mathbf{x}) = \beta(\mathbf{x}_c) + \nabla^T \beta(\mathbf{x}_c)(\mathbf{x} - \mathbf{x}_c) \tag{B.24}$$

is performed, thus it is possible to build the approximated model

$$a_c(\mathbf{x}) = \beta_c(\mathbf{x}) f_{LO}(\mathbf{x}) \tag{B.25}$$

An enlargement of the *trust region* is performed if during the current iteration there has been improvements otherwise its dimension is reduced. The approximation procedure is iterated until

convergence, Refs. [53] and [54], thus the minimization process is stopped when the following condition is not verified

$$x_{m_i} \in \partial Tr \tag{B.26}$$

As reference value a *figure of merit* ρ_c, is used,

$$\rho_c = \frac{f_{HI}(\mathbf{x}_c) - f_{HI}(\mathbf{x}_c + \mathbf{s}_c)}{f_{HI}(\mathbf{x}_c) - a_c(\mathbf{x}_c + \mathbf{s}_c)} \tag{B.27}$$

$\mathbf{s}_c$ is a the local variable in the *trust region*. It represents the improvement obtained by the use of the approximated model with respect to the ones obtained using the high-fidelity one.

Within this application, the optimization of a wing system is performed. The design variables are represented by

$$\mathbf{x} = \{A, c_r, c_t, s_r, s_t\}^T \tag{B.28}$$

where A is the wing span, c_r the root chord, c_t the tip chord, s_r the root thickness spar and s_t the tip thickness spar.

The constraints imposed are of structural nature

$$\sigma < \sigma_{max} \qquad \text{where} \quad \sigma_{max} = 120[MPa] \tag{B.29}$$

$$\tau < \tau_{max} \qquad \text{where} \quad \tau_{max} = 80[MPa] \tag{B.30}$$

and of aeroelastic nature

$$u_{div} \geq u_{div_{min}} \qquad u_{div} = \text{ divergence speed} \tag{B.31}$$

$$u_f \geq u_{f_{min}} \qquad u_f \text{ flutter speed} \tag{B.32}$$

Hence the whole analysis is performed resolving the structural problem by a finite element model with a fine mesh for the high fidelity problem and a coarse one for the low fidelity model. The high fidelity aerodynamics is evaluated via a quasi potential formulation in the high fidelity configuration whereas the low fidelity model used is an incompressible potential formulation.

The following Figs. B.9 and B.10 depict the meshes used to solve the aerodynamic problem. Within each iteration the constrained minimization problem is solved using a sequential quadratic programming algorithm, Ref. [57]. The results, compared with those obtained by a traditional high-fidelity optimization process, show excellent agreement in terms of final solution and present a relevant abatement of computational costs [Figs. B.11, B.12, B.13 and Tab. B.7].

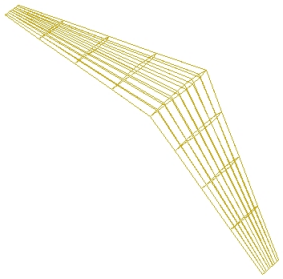

Figure B.9: BEM mesh - High-fidelity model

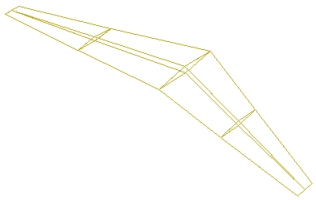

Figure B.10: BEM mesh - Low-fidelity model

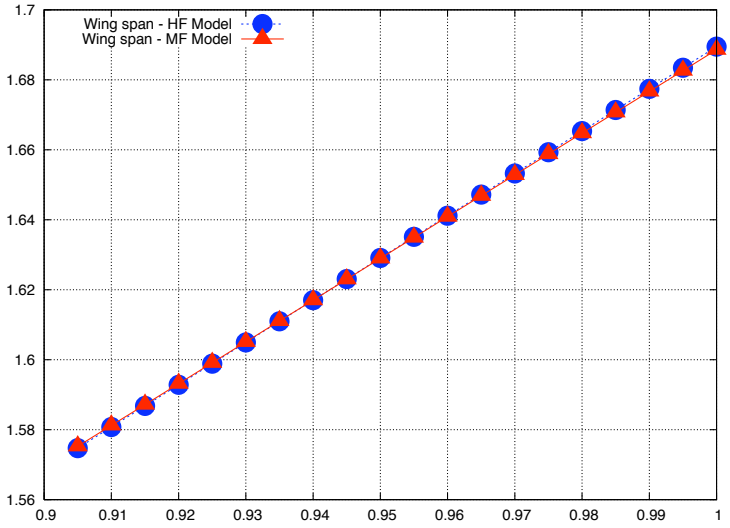

Figure B.11: Wing span - A.

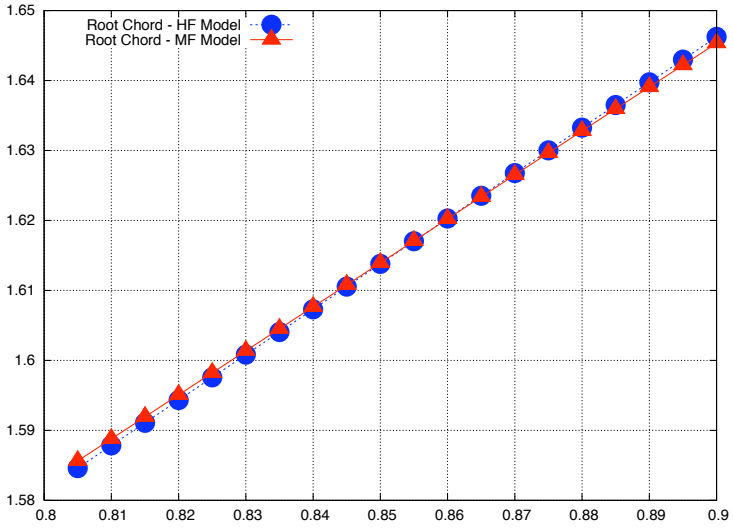

Figure B.12: Root chord - c_r

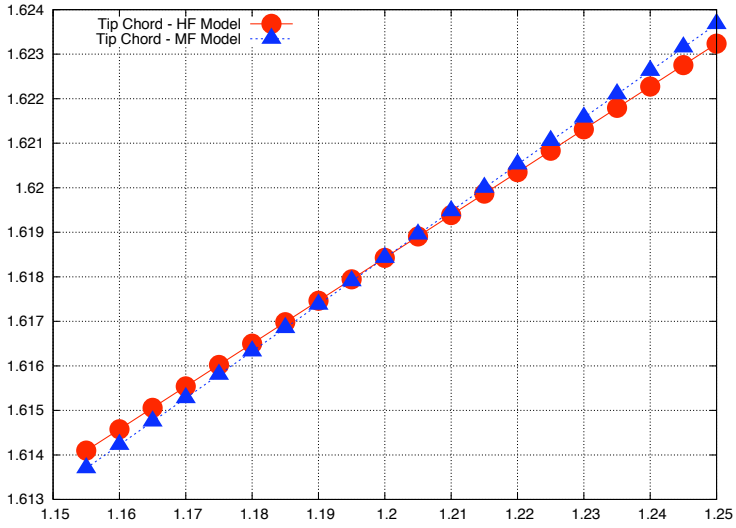

Figure B.13: Tip chord - c_t

$FEM_{HI}\ n = 20, FEM_{LO}\ n = 6$; $BEM_{HI}\ (8,4,4), BEM_{LO}\ (2,2,2)$		
	High-fidelity Model	Approximated Model
A	0.824	0.824
c_r	0.304	0.299
c_t	0.400	0.400
s_r	0.182	0.182
s_t	0.182	0.182
$f_{HI}(\mathbf{x}_{ott})$	1.070	1.068
σ	0.978	0.999
τ	0.613	0.656
n calls f_{HI}	47	28
$\%$ reduction in high-fidelity calls =47$\%$		

Table B.7: Multi-fidelity approach - concluding results.

Bibliography

[1] Morino, L., "A Primitive-Variable Boundary Integral Formulation Unifying Aeroacoustics and Aerodynamics, and a Natural velocity Decomposition for Vortical Fields," International Journal of Aeroacoustics, Vol.10, no. 2&3 , pp. 295-400, 2011.

[2] Morino, L., "A General Theory of Compressible Potential Aerodynamics," NASA CR-2464, 1974.

[3] Morino, L., Tseng, K., "A General Integral Formulation for Unsteady Compressible Potential Flows with Applications to Airplane and Rotors," in P.K. Banerjee and L. Morino (eds.), *Boundary Element Methods in Nonlinear Fluid Dynamics, Vol. 6 of Developments in Boundary Element Methods*, Elsevier Applied Science, London, UK, pp. 183–246, 1990.

[4] Morino, L., "Is There a Difference Between Aeroacoustics and Aerodynamics? An Aeroelastician's Viewpoint," AIAA Journal, Vol. 41, No. 7, pp. 1209–1223, 2003.

[5] Morino, L., Bernardini, G., Gennaretti, M., "A Boundary Element Method for the Aerodynamic Analysis of Aircraft in Arbitrary Motions," Computational Mechanics, Vol. 32, No. 4–6, pp. 301–311, 2003.

[6] Morino, L., Bernardini, G., Gennaretti, M., "A Boundary Element Method for Aerodynamics and Aeroacoustics of Bodies in Arbitrary Motions," International Journal of Aeroacoustics, Vol. 2, No. 2, pp. 129–156, 2003.

[7] Serrin, J., "Mathematical Principles of Classical Fluid Mechanics," in S. Flügge (Ed.), *Encyclopedia of Physics, VIII/1*, Springer–Verlag, Berlin, pp. 125-263, 1959.

[8] Morino, L., “Helmholtz Decomposition Revisited: Vorticity Generation and Trailing Edge Condition, Part 1: Incompressible Flows,” Computational Mechanics, Vol. 1, No. 1, pp. 65-90, 1986.

[9] Morino, L., “Helmholtz and Poincaré Potential–Vorticity Decompositions for the Analysis of Unsteady Compressible Viscous Flows," in P.K. Banerjee and L. Morino (eds.), *Boundary Element Methods in Nonlinear Fluid Dynamics, Vol. 6 of Developments in Boundary Element Methods*, Elsevier Applied Science, London, UK, pp. 1–54, 1990.

[10] Morino, L., Salvatore, F., Gennaretti, M., “A New Velocity Decomposition for Viscous Flows: Lighthill’s Equivalent–Source Method Revisited,” Computer Methods in Applied Mechanics and Engineering, Vol. 173, No. 3–4, pp. 317–336, 1999.

[11] Morino, L., and Bernardini, G., “On the Vorticity Generated Sound for Moving Surfaces,” Computational Mechanics, Vol. 28, No. 3–4, pp. 311–316, 2002.

[12] Morino, L., Bernardini, G., Caputi-Gennaro, G., “A vorticity formulation for computational fluid dynamic and aeroelastic analyses of viscous flows,” Journal of Fluids and Structures, Vol. 25, pp. 1282–1298, 2009.

[13] Lighthill, M.J., “On Displacement Thickness,” Journal of Fluid Mechanics, Vol. 4, pp. 383-392, 1958.

[14] Lighthill, M.J., “On Sound Generated Aerodynamically," *Philosophical Transactions of the Royal Society*, London, Series A11, pp. 564–587, 1952.

[15] Dennis, S.C.R., Chang, G.Z., "Numerical solutions for steady flow past a circular cylinder at Reynolds numbers up to 100," Journal of Fluid Mechanics 42, pp. 471Ð489, 1970.

[16] Fornberg, B., "A numerical study of steady viscous flow past a circular cylinder," Journal of Fluid Mechanics 98, pp. 819Ð855, 1980.

[17] Cossu, C., Morino, L., "A vorticity-only formulation and a low-order asymptotic expansion solution near Hopf bifurcation," Computational Mechanics 20, pp.229Ð241, 1997.

[18] Noack, B.R., Eckelmann, H., "A low-dimensional Galerkin method for the three-dimensional flow around a circular cylinder, " Physics of Fluids 6, pp. 124Ð143, 1994.

[19] Thom, A., "Flow past circular cylinders at low speeds," Proceedings of the Royal Society A 141, pp. 651Ð669, 1933.

[20] Grove, A.S., Shair, F.H., Petersen, E.E., Acrivos, A., "An experimental investigation of the steady separated flow past a circular cylinder," Journal of Fluid Mechanics 19, pp. 60Ð80, 1964.

[21] Cossu, C., "Analisi di stabilitĹ lineare e non-lineare del flusso viscoso intorno ad un cilindro circolare," Ph.D. Dissertation, Dipartimento di Ingegneria Aerospaziale, UniversitĹ degli Studi di Roma La Sapienza, Roma, Italy, 1997.

[22] Morino, L., Leotardi, C., Camussi, R., "Power-spectral-density transfer function from boundary-pressure to field-pressure," AIAA/CEAS Aeroacoustic Conference, Stockholm, AIAA Paper 2010-3993, 2010.

[23] Morino, L., Caputi Gennaro, G., Camussi, R., Iemma, U., “On the vorticity generated sound: a transpiration-velocity/power-spectral-density approach,” AIAA Paper 2007-3400, 13th AIAA/CEAS Aeroacoustics Conference, Roma, Italy, May 21–23, 2007.

[24] Caputi Gennaro, G., Camussi, R., Iemma, U., Morino, L., “Power-Spectral-Density Boundary-to-Field Transfer Function,” 14th AIAA/CEAS Aeroacoustics Conference, Vancouver, Canada, AIAA Paper 2008-3002, 2008.

[25] Lighthill, M.J., “On Displacement Thickness,” J. Fluid Mechanics, Vol. 4, pp. 383-392, 1958.

[26] Jacob, M.C., Grilliat, J., Camussi, R., Caputi–Gennaro, G. (2007) “Tip leakage experiment - Part one: aerodynamic and acoustic measurements,” 13th AIAA/CEAS Aeroacoustics Conference, Rome, Italy, May 21–23, Paper AIAA–2007–3684, 2007.

[27] Piva, R., Morino, L., “Vector Green’s Function Method for Unsteady Navier–Stokes Equations,” Meccanica, Vol. 22, pp. 76–85, 1987.

[28] Piva, R., Morino, L., “A Boundary Integral Formulation in Primitive Variable for Unsteady Viscous Flows,” in P.K. Banerjee and L. Morino (eds.), *Boundary Element Methods in Nonlinear Fluid Dynamics, Vol. 6 of Developments in Boundary Element Methods*, Elsevier Applied Science, London, UK, pp. 117–150, 1990.

[29] Gradshteyn, I.S., Ryzhik, I.M., *Tables of Integrals, Series, and Products*, A. Jeffrey (ed.), 5th edition, Academic Press, Boston, MA, 1994.

[30] Schwartz, L., *Mathematics for the Physical Sciences*, Addison-Wesley, Reading, MA, 1966.

[31] Diez, M., Leotardi, C., Iemma, U., "Aeroelastic Issues in Multidisciplinary Design optimization of Aircraft Configurations, ", IFASD 2009-004, Seattle, July 2009.

[32] Diez, M., Burghignoli, L., Leotardi, C., Sargentini, A., "A Multi-Fidelity Formulation for Multidisciplinary Design Optimization of Aircraft Configurations," 5th European Congress of Computational Methods in Applied Science and Engineering, ECCOMAS, 2008.

[33] Iemma, U., Gennaretti, M., "A Reduced-Order Model For Linearized Transonic Fixed-Wing Aeroelasticity," Journal of Fluids and Structures, Vol 21, Issue 3, p.243-255, 2005.

[34] Iemma, U., and Morino, L., "Steady Two-Dimensional Analysis Using a Boundary Integral Equation Method," Journal of Fluids and Structures, Vol. 11, 1997.

[35] Morino, L., Tseng, K., “A General Theory for Compressible Potential Flows with Application to Aeroplanes and Rotor,” In Boundary Elements Method in Nonlinear Fluid Dynamics, Eds. Elsevier Apllied Scince, London, pp. 183-245, 1990 .

[36] Tseng, K.,“Application of the Green’s Function Method for 2- and 3-Dimensional Steady Transonic Flows,” AIAA Journal, 1984.

[37] Lerat, A., Sides, J., "Implicit transonic calculations without artificial viscosity or upwinding. In Numerical Simulation of Compressible Euler Flows," (eds A. Dervieux, B. Van Leer, J. Periaux & A. Rizzi), GAMM Workshop, pp. 227-250, Braunschweig, Vieweg & Sohn, 1986.

[38] Dadone, A. "Computation of transonic steady flows using a modified lambda formulation. In Numerical Simulation of Compressible Euler Flows, " (eds A. Dervieux, B. Van Leer, J. Periaux & A. Rizzi), GAMM Workshop, pp. 122-137, Braunschweig: Vieweg & Sohn, 1986.

[39] Salas, M. D., "Recent developments in transonic Euler flow over a circular cylinder," NASA Technical Memorandum 83282, Langley Research Center, Hampton, Virginia, U.S.A, 1982.

[40] Morino, L., Bernardini, G., and Mastroddi, F., "First-principle based dynamic aircraft modeling for MDO," Invited Lecture International Conference on Computational Experimental Engineering and Sciences, ICCES'03, Corfu, Greece, 2003.

[41] Iemma, U., Diez, M., and Morino, L., "Community noise impact on the conceptual design of innovative aircraft configurations," AIAA- Paper 2005-2982, 11-th AIAA/CEAS Aeroacoustic Conference, Monterey, USA, 2005.

[42] Iemma, U. and Diez, M., "Optimal life-cycle-costs design of new large aircraft including the cost of community noise," Invited Lecture International Conference on Computational Experimental Engineering and Sciences, ICCES'05, Chennai, India, 2005.

[43] Morino, L., Bernardini, G., Mastroddi, F., "Multi-Disciplinary Optimization for the Conceptual Design of Innovative Aircraft Configurations," Computer Modeling in Engineering and Sciences, Vol. 13, No. 1, pp. 1–18, 2006.

[44] Morino, L., " Boundary integral equations in aerodynamics," Appl. Mech. Rev., 46, 445-466, 1993.

[45] Morino, L., Salvatore, F., and Gennaretti, M., " A velocity decomposition for viscous flows: Lighthill equivalent-source method revisited," Boundary Integral Methods for Nonlinear Problems, 161-166, 1997.

[46] Morino, L., Mastroddi, F., Troia, R.D., et al., "Matrix fraction approach for finite-state aerodynamic modeling," AIAA Journal, Vol.33, pp. 703-711, 1995.

[47] Fujino, M., Oyama, H., and Omotani, H., "Flutter characteristics of an over-the-wing engine mount buisness-jet configuration," Paper no 2003-1942, 44-th AIAA/ASME/ASCE/AHS Structures, Structural Dynamics and material Conference, 7-10 April 2003, Norfolk, Virginia, 2003.

[48] Iemma, U. and Diez, M., "Optimal conceptual design of aircraft including community noise prediction," AIAA Paper 2006-2621, 12-th AIAA/CEAS Aeroacoustic Conference, Cambridge, Massachusetts, 2006.

[49] Diez, M., Iemma, U., and Marchese, V., "A sound-matching-based approach for aircraft noise annoyance alleviation via MDO," AIAA Paper 2007-3667, 13-th AIAA/CEAS Aeroacoustic Conference Rome Italy, 2007.

[50] Morino, L., Bernardini, G., De Gregorio, D., et al., "Life-cycle cost multidisciplinary optimization for Prandtl-plane," Proceedings of the 2004 International Conference on Computational and Experimental Engineering and Sciences, pp. 26-29, 2004.

[51] E.Goldberg, D., "Genetic Algorithms in Search, Optimization, and Machine Learning," Addison-Wesley Pub. Co, 1989.

[52] Iemma, U., Diez, M., "Optimal Conceptual Design of Aircraft Including Community Noise Prediction," AIAA Paper 2006-2621, Twelfth AIAA/CEAS Aeroacoustic Conference, Cambridge, Massachussets, 2006.

[53] Alexandrov, N.M., Lewis, M., "An overview of first-order model for engineering optimization," Optimization and Engineering, 2, pp.413-430, 2001.

[54] Alexandrov, N.M., "Robustness properties of a trust region framework for managing approximation in engineering optimization," AIAA Paper 96-4112, Sept. 1996.

[55] Haftka, R.T., "Combining global and local approximation," AIAA Journal, Vol.29, pp.1523-1525, 1991.

[56] Moré, J.J., "Recent Development in Algorithms and Software for Trust Region Methods," Mathematical Programming, The State of Art, Springler-Verlag, Berlin Editions, Bonn 1983.

[57] Gill, P.E., Murray, W., Wright, M.H., "Practical Optimization," London Academic Press, 1981.

List of Figures

List of Tables